



University
of Glasgow

Loland, Olaf (1978) A vibration method for integrity monitoring of fixed offshore steel platforms. PhD thesis

<http://theses.gla.ac.uk/6191/>

Copyright and moral rights for this thesis are retained by the author

A copy can be downloaded for personal non-commercial research or study, without prior permission or charge

This thesis cannot be reproduced or quoted extensively from without first obtaining permission in writing from the Author

The content must not be changed in any way or sold commercially in any format or medium without the formal permission of the Author

When referring to this work, full bibliographic details including the author, title, awarding institution and date of the thesis must be given.

A VIBRATION METHOD FOR INTEGRITY MONITORING
OF FIXED OFFSHORE STEEL PLATFORMS

VOLUME ONE

Olaf Loland B.Sc.

DEPARTMENT OF MECHANICAL ENGINEERING
UNIVERSITY OF GLASGOW

THESIS SUBMITTED FOR THE DEGREE

OF

DOCTOR OF PHILOSOPHY

OCTOBER 1978

ACKNOWLEDGEMENTS

The writer is grateful for the facilities made available by the University of Glasgow and in particular to Professor J.D. Robson in whose department the work was carried out. The writer's thanks are also due to his supervisor Dr. A.C. Mackenzie for his enthusiasm and many helpful suggestions when was most needed. The writer also wishes to express his gratitude to Dr. R.D. Begg and Dr. C.J. Dodds; their valuable help will not be forgotten.

In addition the writer is indebted to the following people:

- Dr. D.K. Brown for an introduction to the University's computing facilities.
- Dr. G.K.S. Browning and the staff of the University's computing service.
- The staff of the Mechanical Engineering workshop and in particular Mr. H.C. Cunningham who constructed the model structures with speed and accuracy.
- Mr. N.S. Miller and the staff at the Naval Architecture Experiment Tank.
- Det norske Veritas and in particular Mr. P. Dahl for making available data of a full scale structure.
- General Radio Corporation and in particular Mr. G. Roriston for making available a Time Series Analyser.
- Miss C. Lawson whose skill in typing the thesis is evident.

CONTENTS

SUMMARY	1
CHAPTER 1: INTRODUCTION	4
CHAPTER 2: PRELIMINARY COMPUTATIONS AND EXPERIMENTS ON SIMPLE STRUCTURES	10
2.1 INTRODUCTION	10
2.2 CANTILEVER BEAM STRUCTURE	10
2.2.1 Description of structure	10
2.2.2 Method of computing dynamic response	11
2.2.3 Computed results for dynamic response and comparison with analytical results	30
2.2.4 Computed results with point mass at tip and comparison with analytical results	32
2.2.5 Computed results with shaker at tip	34
2.2.6 Method of measuring dynamic response	36
2.2.7 Measured dynamic response with shaker at tip ..	42
2.2.8 Comparison of measured and computed responses with shaker at tip	44
2.3 PLANE FRAME STRUCTURE	47
2.3.1 Description of plane frame	47
2.3.2 Frame beam element model	47
2.3.3 Computed static response	48
2.3.4 Measured static response	49
2.3.5 Comparison of measured and computed static responses	49
2.3.6 Computed dynamic response	50
2.3.7 Measured dynamic response	53

2.3.8 Computed and measured dynamic responses in water	56
2.3.9 Comparison of computed and measured dynamic responses	59
CHAPTER 3: SELECTION OF FULL SCALE PLATFORM AND COMPUTED RESULTS ...	61
3.1 INTRODUCTION	61
3.2 DESCRIPTION OF PLATFORM	62
3.3 COMPUTED RESULTS	64
3.4 DISCUSSION	65
CHAPTER 4: MODEL PLATFORM DESIGN AND COMPUTED RESULTS	69
4.1 INTRODUCTION	69
4.2 DESIGN OF MODEL PLATFORM	70
4.3 BEAM ELEMENT MODEL	75
4.4 COMPUTED RESULTS	79
4.5 DISCUSSION OF COMPUTED NORMAL MODES	82
4.5.1 Sway modes	82
4.5.2 Torsion modes	84
4.5.3 Other global modes	86
4.5.4 Ovalising modes	88
4.6 DISCUSSION OF NORMAL MODE SENSITIVITY TO MEMBER SEVERANCE	90
4.6.1 Sway and torsion modes	90
4.6.2 Ovalising and other global modes	93
4.6.3 Deck load changes	94
4.6.4 Support stiffness changes	95
4.6.5 The shear structure	96

CHAPTER 5: EXPERIMENTS ON MODEL PLATFORM	99
5.1 INTRODUCTION	99
5.2 EXPERIMENTAL RESULTS	100
5.2.1 Method of test	100
5.2.2 Determination of natural frequencies and mode shapes	100
5.2.3 Removal of members	103
5.3 DISCUSSION OF MEASURED AND COMPUTED NATURAL FREQUENCIES AND MODE SHAPES, AND THE EFFECT OF MEMBER REMOVAL	105
5.3.1 Fundamental mode group	105
5.3.2 Second mode group	107
5.3.3 Third mode group	109
5.3.4 Ovalising and other global modes	113
5.4 RANDOM VIBRATION	114
5.4.1 Introduction	114
5.4.2 Frequency analysis of random vibration ..	115
5.4.3 Basic equations and computational approach	115
5.4.4 Results	120
Conclusions	125
References	126
Appendix: PRACTICAL IMPLEMENTATION OF THE MEHTOD	131

SUMMARY

Up to a decade ago fixed offshore platforms in the Gulf of Mexico were inspected below the water line only after extreme loading from hurricanes or ship collisions. However, increased investment in new platforms has led to oil companies introducing regular inspection routines, and some countries have laid down regulations for instrumentation and inspection of offshore installations, to ensure safe operation and a feedback of data to designers.

The conventional techniques used for inspection of offshore structures include:

- (a) visual inspection by divers and use of underwater television with video and sound recording;
- (b) magnetic particle and ultrasonic crack detection methods.

These all require diver access, and are feasible in moderate water depths and in areas with long and predictable periods of calm weather. Neither of these conditions is met in the northern North Sea.

There is a demand for inspection methods which will monitor the performance of platforms under any weather conditions, and, in particular under storm conditions. The methods must give unambiguous warning about failures which could endanger the installations. Furthermore, they should depend on only a small number of transducers all positioned above the waterline for easy access and maintenance.

The purpose of this work was to investigate a method of detecting damage from changes in the natural frequencies of a structure. The main objective was to investigate what changes in natural frequencies would occur when a primary load-carrying member became detached from a typical fixed offshore platform. The platform design was a four-leg, K-braced platform for which approximate dimensions were available, and which operated in 70 metres of water. A 1/20th scale model was also designed and the structural analysis programme ICES STRUDL II used to compute the natural frequencies and mode shapes of both the full scale and model platforms.

Before STRUDL II was applied to the quite complex offshore platform, analyses were carried out on two simple structures to gain experience in using the programme. Natural frequencies and mode shapes were computed and compared with measured values and with analytical solutions where applicable. This preliminary work also gave experience in dynamic response testing.

The sensitivity of the natural frequencies of the platform was investigated by removing a single diagonal in one K-panel, and again computing the natural frequencies of the structure. The brace was then replaced and the computations were repeated with other single braces removed in turn. The reductions in the frequencies with each member removed could then be calculated. There were large changes in some of the modes and the pattern of the frequency reductions gave an indication of the location of the failure.

The computational study was repeated for the model platform and frequency reductions similar to those for the full scale platform were found. The model platform was built and sinusoidal force excitation was applied to determine its natural frequencies and mode shapes. Comparison of computed and measured frequencies was generally good. Two K-braces in different planes and at different elevations were severed and repaired in turn; the changes in natural frequencies compared well with the computed predictions.

In the third stages of the project a dedicated Time Series Analyser became available and a number of tests were carried out with random excitation. The results for frequencies and mode shapes were in good agreement with those obtained with sinusoidal excitation. This demonstrated the feasibility of obtaining natural frequencies and mode shapes from response to **random** excitation.

It was concluded for the project that changes in natural frequencies could provide a viable method of detecting gross damage in offshore structures.

CHAPTER 1

INTRODUCTION

Offshore oil exploration and production have developed over three decades, from platforms in 6 metres of water to the recently launched Forties field platforms in 120 metre water depths [1,2,3].

Experience and technology are being extrapolated to develop a new generation of deep water platforms and designs for fixed drilling and production platforms for 400 metres of water are on the drawing-board [4].

The North Sea is a hostile environment where structures suffer high corrosion rates and where there are frequent storms with waves up to 20 metres and hundred year waves of 24 metres to 30 metres.

The danger of structures suffering fatigue damage below the water line from the repeated loading is much greater than in other offshore areas such as the Gulf of Mexico and the Persian Gulf. Failures which have occurred on structures in the North Sea [5] have highlighted the need for regular checks on structural integrity.

Mobile exploration units such as drillships, jack-ups and submersibles can normally be drydocked and inspected by conventional means. However, fixed deep water platforms require a different approach.

Up to a decade ago fixed offshore platforms in the Gulf of Mexico were only inspected below the water line after extreme loading conditions produced, for example, by hurricanes or ship collisions. However, increased investment in new platforms has led oil companies to introduce regular inspection routines and some

countries have laid down regulations for instrumentation of offshore installations to ensure safe operation and a feedback of data to designers [6].

The conventional techniques used for inspection of offshore structures include:

- (a) visual inspection by divers and use of underwater television with video and sound recording;
- (b) magnetic particle and ultrasonic crack detection methods.

These all require diver access, and are thus most feasible in moderate water depths and in areas where weather conditions are calm for long and predictable periods. Neither of these conditions is met in the northern North Sea.

There is a demand for inspection methods which will monitor the performance of platforms under any weather conditions, and, in particular, under storm conditions. The methods must give unambiguous warning about failures which could endanger the installations. Furthermore, they should depend on only a small number of transducers all positioned above the waterline for easy access and maintenance.

An ultrasonic pulse-echo system has been designed and tested in the laboratory for continuously monitoring structural welds on an offshore platform in Cook Inlet, Alaska [7]. The system was designed for a five year life and 144 transducers were installed at the construction site. They monitored 80 areas above and below water level and included interior and exterior surfaces. The in-service performance has not yet been published.

Other techniques which, it has been suggested, might be developed into useful monitoring systems include;

- (a) measurements of attitude and position of the platform;
- (b) witness systems such as conducting wires or small low pressurised tubes which will sever when a member breaks;
- (c) strain gauges in areas of anticipated weakness;
- (d) automatic television monitoring;
- (e) acoustic emission;
- (f) dynamic response monitoring.

Of these the dynamic response method is probably the most promising technique for total monitoring of the general integrity of the structure.

Measurements of vibratory responses have been employed for some time in the field of machinery testing and maintenance [8].

One of the earliest references to the possible use of dynamic response measurements for monitoring the integrity of offshore structures was made by Blumberg [9]. He suggested that changes in natural frequencies might be a good indicator of the integrity of offshore structures and conducted a series of measurements on three bottom supported structures, with the purpose of checking theoretically calculated natural frequencies. Natural and artificial methods of excitation were employed to excite fundamental sway and torsion modes. The results were found to agree well with the theoretical frequencies.

More recently Tiedemann [10] has examined the whole problem of offshore surveying and inspection and concludes that the cost of

doing meaningful surveys with present day techniques has become too high. He calls for practical and reliable low cost techniques which will enable an operator to indulge in realistic surveying schedules and suggests the monitoring of natural frequency changes as a possible new surveying technique for offshore structures.

Hudson (11) has done extensive measurements on tall buildings before and after they were subjected to earthquake tremors. He reports in many cases significant changes in their natural period of vibrations; in one particular case, Los Angeles buildings were found to have period changes of as much as 35% after an earthquake tremor.

The first objective of the present work was to investigate what changes in natural frequencies might occur when a primary load-carrying member became detached from a typical fixed offshore platform. The platform design was a four-leg, K-braced platform for which approximate dimensions were made available, and which operated in 70 metres of water. Large changes in natural frequency were found, particularly in the higher modes (12, 13), and the concept of frequency monitoring was explored further, including the possibility that the position of a failure might be determined from the changes in frequency response. This involved a thorough study of the modes of vibrations of the platform (14).

Advantages and disadvantages of the method, including operational problems are discussed in the papers included in the appendix.

In 1972/73 when the work was started there was, to the best of the author's knowledge, no published paper which specifically dealt with the applications to offshore structures of the frequency response method of monitoring. When the project was at an advanced stage the author became aware of a similar, parallel study by Vandiver [15]. This study concentrated on changes in the fundamental frequencies only; the present study includes changes in the higher frequencies.

To investigate the sensitivity of natural frequencies to structural failures in the chosen platform both a full scale computational model and a 1/20th scale model were used. For the computations the structural analyses programme ICES STRUDL II [16], available to University of Glasgow users at the Edinburgh Regional Computing Centre, was used. It is well suited for dynamic eigenvalue analysis, having facilities such as static condensation of degrees of freedom which can be considered redundant in a dynamic analysis, and two methods:- "Iteration" [17] or "Tridiagonalisation" [18] - for computing natural frequencies (eigenvalues) and mode shapes (eigenvectors).

The heart of the computational study was the sensitivity of the natural frequencies in particular, and the mode shapes, to changes of the elements in the matrices describing the inertia and stiffness properties of the structure. These matrices are readily available from the STRUDL pre-processor, and normally these matrices are processed by chosen eigenvalue algorithm to yield a predetermined number of eigenvalues and eigenvectors. The sensitivity of computed natural frequencies and mode shapes to

changes in inertia and/or stiffness matrices can then be computed in two ways, either by performing another eigenvalue computation based on modified matrices, or, if the changes are sufficiently small, by a perturbation analysis [19, 20].

In view of the possibility that there might be large changes in natural frequencies, it was decided in the first instance to recompute natural frequencies after each structural change.

Before an attempt was made to apply STRUDL II to the quite complex offshore platform, it was thought prudent to gain experience in its use on two simple structures including a simple cantilever. Natural frequencies and mode shapes were computed and compared with analytical solutions where applicable, and with measured values. This preliminary work gave confidence in the use of STRUDL II and experience in dynamic response testing.

CHAPTER 2
PRELIMINARY COMPUTATIONS AND EXPERIMENTS
ON SIMPLE STRUCTURES

2.1 INTRODUCTION

The simple structures investigated were:

- (a) A uniform cantilever beam with and without tip mass;
- (b) A six member plane frame.

The cantilever beam was chosen because it is a simple model of offshore oil platforms and is often used by designers and research-workers to estimate the fundamental sway and torsion frequencies of such structures [9]. The plane frame was modelled as a simple panel of a typical jacket structure.

The dynamic analysis of the cantilever structure contains many of the features of the analysis of more complex structures. Hence the opportunity is taken in this chapter to describe the essential steps of the method of analysis and to define many of the terms that are used throughout the thesis.

2.2. CANTILEVER BEAM STRUCTURE

2.2.1 Description of Structure

The choice of physical dimensions of the cantilever beam was in no way related to the dimensions of an offshore platform, but the beam was made to a convenient size from rolled hollow steel section available from stock, Figure 2.1. It was 1.5 m long with a square cross-section 63.5 x 63.5 x 3.2 mm, and the total uniformly distributed mass was 8.8 kg.

The beam was inserted into a machined base plate 390 x 450 x 51mm and welded to both sides of the plate. Four 25.4 mm diameter bolts were used to fix the base plate to a pad in a reinforced concrete strengthened floor to give an approximately encastred end condition. A smaller plate 235 x 235 x 24 mm was welded in the same way to the other end of the beam to accept a shaker assembly. A Ling Dynamic System electromagnetic shaker was used and is shown with its mounting fixture in Figure 2.2. The assembly mass was 23.6kg.

To prevent unwanted out-of-plane vibration the beam was supported by a tensioned wire in a plane perpendicular to the required plane of vibration. The wire was attached to the shaker support plate and was long enough, about 1 m on each side of the cantilever beam, not to interfere with the in-plane vibration.

2.2.2 Method of computing dynamic response

The steps in the matrix structural analysis and the implementation on STRUDL II are conveniently studied with the cantilever beam as an example (Figure 2.1 and 2.3).

The analysis technique can be roughly divided into the following:

- (a) structural idealisation;
- (b) computation of beam element matrices;
- (c) assembly of global matrices;
- (d) condensation of global stiffness matrix;
- (e) computation of natural frequencies and mode-shapes;
- (f) computation of frequency response function.

(a) Structural idealisation

This was accomplished by reducing the cantilever beam to an

assembly of discrete structural elements of equal length. The uniform cantilever beam is in itself a discrete structural element and no sub-division is necessary for a static analysis. However, as the main object of the analysis was to compute the first three sway modes of vibration a sub-division was required.

The least number of lateral dynamic degrees of freedom necessary to compute these modes for example is three. For the cantilever beam this gives a three beam element assembly. It has been observed by Archer [21] that if only lateral dynamic degrees of freedom are used, then the number of beam elements should exceed the number of natural frequencies computed by one to obtain an accuracy satisfactory for most engineering purposes, i.e. about $\pm 10\%$.

Considerable improvement in accuracy of the computed modes can be expected if rotational dynamic degrees of freedom are included, Archer [21]. However, the problem size in terms of matrix elements is proportional to the square of the degrees of freedom used in the analysis. This often leads to omission of the rotational dynamic degrees of freedom.

(b) Computation of beam element matrices

In matrix form the differential equations for the dynamic response of an undamped, constrained linear elastic structure subjected to time varying forces $\underline{P}(t)$ is

$$M \ddot{\underline{U}} + K_R \underline{U} = \underline{P}(t) \dots\dots\dots(2.1)$$

where \underline{U} are the chosen dynamic degrees of freedom and K_R and M are the appropriate stiffness and mass matrices respectively. These global matrices are assembled from the matrices of the individual members.

Stiffness Matrix

The stiffness matrix of the beam element relates end force and moment vector \underline{S} to the corresponding displacement vector \underline{U} (Figure 2.3) i.e.

$$\underline{S} = k \underline{U} \dots\dots\dots(2.2)$$

For in-plane deformation of a beam element of uniform cross-section and linear elastic material, the terms in the symmetric matrix k are as follows.

$$k = \begin{bmatrix} \frac{EA}{l} & & & & & & \\ 0 & \frac{12EI}{l^3} & & & & & \\ 0 & \frac{6EI}{l^2} & \frac{4EI}{l^2} & & & & \\ -\frac{EA}{l} & 0 & 0 & \frac{EA}{l} & & & \\ 0 & \frac{-12EI}{l^3} & \frac{-6EI}{l^2} & 0 & \frac{12EI}{l^3} & & \\ 0 & \frac{6EI}{l^2} & \frac{2EI}{l} & 0 & \frac{-6EI}{l^2} & \frac{4EI}{l} & \end{bmatrix} \dots\dots(2.3)$$

The elements in column one are derived by obtaining the forces \underline{S} to produce displacement u_1 with all other displacements zero. Similarly for the other columns. These forces can be determined through the equations of virtual work.

$$\int_0^l \frac{M}{R} dx + F e - \sum s_i u_i = 0 \dots\dots\dots(2.4)$$

where the bending moment M, axial force F and end force vectors s_i are the equilibrium set, and curvature R^{-1} , axial deformation e and end displacement vectors u_i are an appropriate compatible deformation set.

M and F may be expressed in terms of the end displacements as follows.

For a uniform beam subject to end forces and moments only the lateral displacements v is cubic in x and easily expressed in terms of the associated end displacements by

$$v = \left[\frac{2}{l^3} (u_2 - u_5) + \frac{1}{l^2} (u_3 + u_6) \right] x^3 + \left[\frac{3}{l^2} (u_5 - u_2) - \frac{1}{l} (2u_3 + u_6) \right] x^2 + u_3 x + u_2 \dots\dots\dots(2.5)$$

with associated curvature

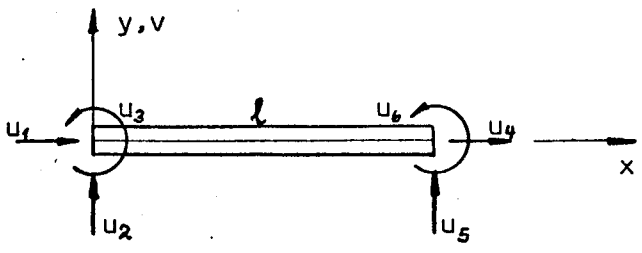
$$\frac{d^2 v}{dx^2} = \frac{1}{R} \dots\dots\dots(2.6)$$

Thus:

$$M = \frac{EI}{R} = EI \left(6 \left[\frac{2}{l^3} (u_2 - u_5) + \frac{1}{l^2} (u_3 + u_6) \right] x + 2 \left[\frac{3}{l^2} (u_5 - u_2) - \frac{1}{l} (2u_3 + u_6) \right] \right) \dots\dots\dots(2.7)$$

The axial force F is

$$F = \frac{EA}{l} (u_4 - u_1) \dots\dots\dots(2.8)$$



For the elements in the second row of the matrix (2.3), for example, the relevant values of M and F are those with $u_1 = u_3 = u_4 = u_5 = u_6 = 0$; $u_2 \neq 0$, i.e.

$$\left. \begin{aligned} M &= EI \left[\frac{12}{l^3} x - \frac{6}{l^2} \right] u_2 \\ F &= 0 \end{aligned} \right\} \dots\dots\dots(2.9)$$

To evaluate element $k_{23} = k_{32}$,

operate on these values of M and F with a deformation set $u_1 =$

$u_2 = u_4 = u_5 = u_6 = 0$; $u_3 \neq 0$ and

$$\frac{1}{R} = \left[\frac{6}{l^2} x - \frac{4}{l} \right] u_3 \dots\dots\dots(2.10)$$

The equation of virtual work Equation 2.4 then gives with

Equations 2.9 and 2.10

$$\int_0^l EI \left(\frac{12}{l^3} x - \frac{6}{l^2} \right) u_2 \left(\frac{6}{l^2} x - \frac{4}{l} \right) u_3 dx - s_3 u_3 = 0 \dots\dots(2.11)$$

$$s_3 = \frac{6EI}{l^2} u_2 \dots\dots\dots(2.12)$$

and

$$k_{32} = \frac{s_3}{u_2} = \frac{6EI}{l^2} \dots\dots\dots(2.13)$$

Similarly for the other stiffness coefficients.

These stiffness coefficients were derived with no regard to shear deformation; based on the assumption that the ratio of radius or gyration of cross-section to element length is small compared to unity. The specific figure for the cantilever beam elements used here was 0.065. STRUDL II will include shear-deformation if the effective cross-sectional shear area is specified.

The derivation of the stiffness matrix for a three dimensional beam element follows from the previous results and is extensively treated by Przemieniecki [22].

Mass Matrix

The elastic property of the beam element is expressed exactly within the framework of Engineers' theory of bending by the stiffness matrix. The inertia property however, as described by the mass matrix, will only be an approximation which generally is adequate for engineering purposes. STRUOL II offers two techniques for representing the inertia property:

- (a) lumped mass;
- (b) consistent mass.

The lumped mass condensation is the simplest way to include the inertial properties of the beam element. The translational and rotational inertias are represented by concentrated masses at the joints; these masses are calculated by assuming that one half of the beam element moves as a rigid body. Thus, the concentrated translational mass becomes half the beam element distributed mass,

$$m_{ii} = \frac{1}{2} \rho A l \dots\dots\dots(2.14)$$

and the concentrated rotational mass is the mass moment of inertia of a beam element of length $l/2$ rotating about one end.

$$m_{jj} = \frac{1}{2} \rho A l \left[\frac{l^2}{48} + \frac{l^2}{16} \right] = \frac{\rho A l^3}{24} \dots\dots\dots(2.15)$$

STRUOL allows the numerical factor in Equation (2.15) to be changed to any value the user might think suitable; to allow for the fact that the motion is not rigid body rotation about a node.

The assumption used to calculate the lumped masses excludes dynamic coupling between the element ends, and the mass matrix is diagonal

$$[m_{ij}] = \frac{1}{2} \rho A l \begin{bmatrix} 1 & & & & & & \\ & 1 & & & & & \\ & & \text{Symmetric} & & & & \\ & & & \frac{l^2}{12} & & & \\ & & & & 1 & & \\ & & & & & 1 & \\ & & & & & & \frac{l^2}{12} \end{bmatrix} \dots\dots\dots(2.16)$$

This diagonal form of the lumped mass matrix results in shorter computer solution time than when consistent mass matrix is used. However, it has been shown by Archer [21] that consistent mass condensation, when applied to simple beam vibration problems, results in significant improvement in accuracy.

To obtain the consistent mass matrix it is assumed that under dynamic loading the displacements and accelerations of the beam element are related to the end displacements and accelerations by the same functions which relate $v(x)$ and $u(x)$ to the end displacements under static loading. The transverse acceleration $\ddot{v}(x)$ is thus given from Equation 2.5 by

$$\begin{aligned}
\dot{v} = & \left[\frac{2}{l^3} (\ddot{u}_2 - \ddot{u}_5) + \frac{1}{l^2} (\ddot{u}_3 + \ddot{u}_6) \right] x^3 \\
& + \left[\frac{3}{l^2} (\ddot{u}_5 - \ddot{u}_2) - \frac{1}{l} (2\ddot{u}_3 + \ddot{u}_6) \right] x^2 \\
& + \ddot{u}_3 x + \ddot{u}_2 \dots\dots\dots(2.17)
\end{aligned}$$

Associated with a transverse displacement v is the longitudinal displacement u_y which can be calculated from

$$u_y = -y \frac{\partial v}{\partial x} \dots\dots\dots(2.18)$$

and the coupled longitudinal acceleration \ddot{u}_y is from Equation (2.18)

$$\begin{aligned}
\ddot{u}_y = & -y \left[3 \left[\frac{2}{l^3} (\ddot{u}_2 - \ddot{u}_5) + \frac{1}{l^2} (\ddot{u}_3 + \ddot{u}_6) \right] x^2 \right. \\
& \left. + 2 \left[\frac{3}{l^2} (\ddot{u}_5 - \ddot{u}_2) - \frac{1}{l} (2\ddot{u}_3 + \ddot{u}_6) \right] x + \ddot{u}_3 \right] \dots\dots\dots(2.19)
\end{aligned}$$

The acceleration from a purely longitudinal displacement u_x is

$$\ddot{u}_x = (\ddot{u}_4 - \ddot{u}_1) \frac{x}{l} + \ddot{u}_1 \dots\dots\dots(2.20)$$

The distributed inertia forces $\rho A \dot{v}$, $\rho A \ddot{u}_y$ and $\rho A \ddot{u}_x$ (where ρA is the mass per unit length) are replaced by a statically equivalent set of end forces and moments. This is done by equating the work done by the distributed inertia forces and moments to that done by equivalent end forces and moments for any virtual set of compatible deformations. The following consistent-mass matrix results.

$$\begin{aligned}
 [m_{ij}] &= \frac{eAl}{420} \begin{bmatrix} 140 & & & & & & \\ 0 & 156 & & & & & \\ 0 & 22l & 4l^2 & & & & \\ 70 & 0 & 0 & 140 & & & \\ 0 & 54 & 13l & 0 & 156 & & \\ 0 & -13l & -3l^2 & 0 & -22l & 4l^2 & \\ & & & & & & \end{bmatrix} \\
 &+ \frac{eAl}{30} \left(\frac{r}{l}\right)^2 \begin{bmatrix} 0 & & & & & & \\ 0 & 36 & & & & & \\ 0 & 3l & 4l^2 & & & & \\ 0 & 0 & 0 & 0 & & & \\ 0 & -36 & -3l & 0 & 36 & & \\ 0 & 3l & -l^2 & 0 & -3l & 4l^2 & \\ & & & & & & \end{bmatrix} \dots\dots\dots(2.21)
 \end{aligned}$$

The matrix (2.21) consists of two terms; the elements of the first term represent translational inertia while the rotatory inertia is represented by the second term. The elements in column j are the end forces and moments associated with end acceleration \ddot{u}_j and all other end accelerations zero. Mass-coefficient m_{32} for example is obtained from

$$\int_0^l \left(eA \left(2 \frac{x^3}{l^3} - 3 \frac{x^2}{l^2} + 1 \right) \ddot{u}_2 \right) \left(\frac{x^3}{l^2} - 2 \frac{x^2}{l} + x \right) u_3 \, dx$$

$$+ \int_0^l \left(eA \left(6 \frac{x^2}{l^3} - 6 \frac{x}{l^2} \right) (-y) \ddot{u}_2 \right) \left(3 \frac{x^2}{l^2} - 4 \frac{x}{l} + 1 \right) (-y) u_3 \, dx$$

$$= s_3 u_3 \dots \dots \dots (2.22)$$

giving

$$\frac{22}{420} eAl^2 \ddot{u}_2 + \frac{3}{30} eAl^2 \left(\frac{r}{l} \right)^2 \ddot{u}_2 = s_3 \dots \dots \dots (2.23)$$

or

$$m_{32} = eAl^2 \left(\frac{22}{420} + \frac{3}{30} \left(\frac{r}{l} \right)^2 \right) \dots \dots \dots (2.24)$$

where r is the radius of gyration of the beam element cross-section.

From the basic assumption of static deformations of the beam element under a dynamic loading it becomes apparent that the beam element length should be chosen such that its fundamental clamped-clamped frequency is high compared to the structural frequencies which are to be computed.

The beam elements of a structure should have their fundamental clamped-clamped frequencies as close as possible to obtain global stiffness and mass matrices where the numerical value of the elements are as similar as possible in the respective matrices. To this effect Archer [21] states as a "rule of thumb", that a clamped-clamped frequency of the beam elements should be of the same order of magnitude.

Distributed rotary inertia is proportional to the square of the ratio of the radius of gyration of the beam cross-section to beam element length $\left(\frac{r}{l} \right)^2$ (matrix 2.21), and can be assumed negligible

for ratios of $r/\rho \ll 1$ STRUDL includes rotatory inertia automatically for all ratios of r/ρ , when the consistent mass option is used.

(c) Assembly of Global Matrices

STRUDL utilises the matrix displacement method, which assumes joint displacements and rotations are unknown and externally applied loads are known quantities. The system equations are based on force equilibrium at the joints with each equation representing equilibrium in one of the global directions, i.e.

$$\underline{\bar{S}} = K \underline{\bar{U}} \quad \dots\dots\dots(2.25)$$

where $\underline{\bar{S}}$ and $\underline{\bar{U}}$ are the external force and displacement vectors at the joints respectively in the global directions and K is the global stiffness matrix.

Before a global stiffness matrix can be constructed from the beam element matrices a transformation of the beam element matrices from local to global co-ordinates must take place. From the joint co-ordinates of each element the direction cosines are computed and a transformation matrix constructed for each beam element; consider the (i)th element,

$$\underline{S}^{(i)} = T^{(i)} \underline{\bar{S}}^{(i)} \quad \dots\dots\dots(2.26)$$

and

$$\underline{U}^{(i)} = T^{(i)} \underline{\bar{U}}^{(i)} \quad \dots\dots\dots(2.27)$$

The transformation matrix $T^{(i)}$ is the same for both forces and displacements. If Equations (2.26) and (2.27) are substituted into the matrix equation of element i (Equation 2.2) then it follows that,

$$\underline{\bar{S}}^{(i)} = \underline{T}^{(i)-1} \underline{k}^{(i)} \underline{T}^{(i)} \underline{\bar{U}}^{(i)} \dots\dots\dots(2.28)$$

The transformation matrix however is orthogonal, i.e. $\underline{T}^{-1} = \underline{T}^T$, and

$$\underline{\bar{K}}^{(i)} = \underline{T}^{(i)T} \underline{k}^{(i)} \underline{T}^{(i)} \dots\dots\dots(2.29)$$

With all beam element matrices calculated for global co-ordinates the principle of force equilibrium at the joints is employed to construct the global stiffness matrix. Force equilibrium implies that stiffness co-efficients can be added together. The element positions in the global stiffness matrix to which a stiffness co-efficient or co-efficients are placed are determined by the numbering sequence of the joints.

For the cantilever beam the global axes are chosen such that they coincide with the local axes of the beam elements. This makes the direction cosine equal to unity and the global matrix can be assembled directly from the beam element matrices.

The global stiffness matrix is reduced when the displacement boundary conditions are applied; these usually prescribe certain joint displacements to be zero and this removes the associated columns and rows in the global matrix. The final matrix \underline{K}_R relates joint displacements and rotations to external loads in the form,

$$\underline{\bar{S}} = \underline{K}_R \underline{\bar{U}} \dots\dots\dots(2.30)$$

and the solution of this set of equations to static loads is accomplished in principle by inverting the non-singular stiffness matrix to yield

$$\underline{\bar{U}} = K_R^{-1} \underline{\bar{S}} \dots\dots\dots(2.31)$$

Back substitutions of the computed joint displacements and rotations $\underline{\bar{U}}$ then enables local beam element displacements, deformations and reactions to be calculated.

The assembly of the global consistent-mass matrix follows steps outlined for the global stiffness matrix. However, when lumped mass is used, no transformation is required as this formulation is independent of frame of reference.

A naturally lumped mass, for example the shaker, is modelled as a concentrated inertia attached to a joint; and its mass is added to the corresponding diagonal element of the global mass matrix.

(d) Condensation of Global Stiffness Matrix

The global stiffness matrix K_R of Equation (2.30) relates all external loads $\underline{\bar{S}}$ to their corresponding displacements $\underline{\bar{U}}$. If the load vector $\underline{\bar{S}}$ has a number of zeros and only the displacements corresponding to points of non-zero applied loads in the structure are of interest, then a reduction of the matrix K_R is possible. This is particularly relevant in a dynamic analysis, when the effect of certain inertial loads can be considered negligible.

Static condensation is implemented on STRUDL II and is an exact static condensation technique as can be seen from the following simple derivation.

The force displacement Equation (2.30) is re-arranged and partitioned as follows,

$$\begin{bmatrix} \bar{S}_x \\ \bar{S}_y \end{bmatrix} = \begin{bmatrix} K_{xx} & K_{xy} \\ K_{yx} & K_{yy} \end{bmatrix} \begin{bmatrix} \bar{U}_x \\ \bar{U}_y \end{bmatrix} \dots\dots\dots(2.32)$$

When $\bar{S}_y = 0$, \bar{U}_y can be expressed as

$$\bar{U}_y = -K_{yy}^{-1} K_{yx} \bar{U}_x \dots\dots\dots(2.33)$$

if $|K_{yy}| \neq 0$. Equation (2.33) is then substituted into Equations (2.32) with the following results,

$$\bar{S}_x = (K_{xx} - K_{xy} K_{yy}^{-1} K_{yx}) \bar{U}_x \dots\dots\dots(2.34)$$

which yields the condensed stiffness matrix K_c

$$K_c = (K_{xx} - K_{xy} K_{yy}^{-1} K_{yx}) \dots\dots\dots(2.35)$$

The use of static condensation combined with intelligent assumptions about inertial loads which may be neglected can reduce the dynamic eigenvalue/eigenvector problem considerably.

The effect of excluding certain inertial loads becomes clear from computations on the cantilever beam.

(e) Computation of Natural Frequencies and Mode Shapes

The assembled stiffness and mass matrices representing the cantilever beam give rise to an algebraic eigenvalue problem.

$$K \underline{U} = \Omega^2 M \underline{U} \quad \dots\dots\dots(2.36)$$

where Ω is the angular natural frequency of the structure in any one of its natural modes. STRUDL has two algorithms implemented for computations of natural frequencies and mode shapes.

- (i) Householders Q-R Method;
- (ii) Matrix decomposition and iteration.

(i) Householders Q-R Method

Householders Q-R method [18] tridiagonalises the dynamic matrix

$$M^{-\frac{1}{2}} K M^{-\frac{1}{2}} \quad \dots\dots\dots(2.37)$$

and thus computes the natural frequencies and mode shapes of this matrix by means of Sturm sequence property and inverse iteration, respectively. The basic disadvantages of the technique is that it must tridiagonalise the dynamic matrix even if only a few natural frequencies are required and the computational time increases as a function of n^3 where n is the number of dynamic degrees of freedom.

(ii) Matrix Decomposition and Iteration

Equation (2.36) can be written in the form

$$D \underline{U} = \frac{1}{\Omega^2} \underline{U} \quad \dots\dots\dots(2.38)$$

in which

$$D = K^{-1} M \quad \dots\dots\dots(2.39)$$

The lowest natural frequency ω_1 and corresponding mode shape can be obtained by iteration of Equation (2.38), and convergence to higher modes can be achieved by iteration and use of the orthogonality property of normal modes. Decomposition is used to avoid inversion of the stiffness matrix of Equation (2.39).

The solution time for the Iteration technique [17] depends basically on the accuracy and the number of modes which are to be extracted from the matrix problem and the time may increase significantly if two or more natural frequencies are very close together. The accuracy of the Iteration technique [17] is claimed to compare favourably with the Householder technique and certainly good enough for engineering purposes.

The conclusion is that if only relatively few natural frequencies are required from a large dynamic problem then the Iteration technique should be used. This is very much the situation in the analyses of offshore platforms and the Iteration technique described in references [16, 17] was employed exclusively in all the computations which follow.

(f) Computation of Frequency Response Function

The equation of motion in matrix form for an undamped constrained structure subjected to time dependent exciting forces $\underline{P}(t)$ is given by Equation (2.1)

$$M \ddot{\underline{U}} + K_R \underline{U} = \underline{P}(t) \quad \dots\dots\dots(2.1)$$

This set of differential equations is in general difficult to solve because of coupling through non-zero off-diagonal coefficients

in the stiffness and mass matrices. The classical normal mode technique however, offers a way of uncoupling the equations, provided natural frequencies and mode shapes are known. The displacements \underline{U} of an idealised structure can be expressed as a linear combination of the mode shapes with a time-dependent multiplier for each mode

$$\underline{U} = \theta \underline{\xi} \dots\dots\dots(2.40)$$

Equation (2.40) may be substituted into Equation (2.1) and according to the theorem of orthogonal modes [22] premultiplied by θ^T

$$\theta^T M \theta \ddot{\underline{\xi}} + \theta^T K \theta \underline{\xi} = \theta^T \underline{P}(t) \dots\dots(2.41)$$

The matrix products $\theta^T M \theta$ and $\theta^T K \theta$ are known as the generalised mass M_G and stiffness K_G matrices respectively. They are both diagonal with the effect of uncoupling the differential equations. The product $\theta^T \underline{P}(t)$ is termed the generalised force matrix \underline{P}_G . The solution of Equation (2.41) for free harmonic vibration is

$$(- M_G \Omega^2 + K_G) \underline{\xi} = 0 \dots\dots\dots(2.42)$$

from which it is found that

$$K_G = M_G \Omega^2 \dots\dots\dots(2.43)$$

and Equation (2.41) can be written

$$M_G \ddot{\underline{\xi}} + M_G \Omega^2 \underline{\xi} = \underline{P}_G \dots\dots\dots(2.44)$$

Equation (2.44) does not include damping, but if linear viscous damping is assumed, the equation of motion is

$$M \ddot{\underline{U}} + C \dot{\underline{U}} + K \underline{U} = \underline{P}(t) \dots\dots\dots(2.45)$$

The generalised damping matrix follows from the previous derivations

$$C_G = \theta^T C \theta \quad \dots\dots\dots(2.46)$$

Damping is not necessarily an inherent property of the system like stiffness and mass, and the value is found by experiment rather than by calculation. The Matrix C_G is therefore not in general diagonal, but can be made so by making the assumption that the damping in each mode of vibration is similar to that of a single degree of freedom system. The critical damping in a single degree of freedom system is

$$c_{crit} = 2m\omega \quad \dots\dots\dots(2.47)$$

and the ratio of actual damping to critical damping is defined as

$$\eta_r = \frac{c_r}{c_{crit}} \quad \dots\dots\dots(2.48)$$

hence

$$c_r = 2\eta_r m\omega \quad \dots\dots\dots(2.49)$$

and in matrix form

$$C = 2\eta M\Omega \quad \dots\dots\dots(2.50)$$

η and Ω are both diagonal matrices and the mass matrix is made diagonal through pre and post-multiplying with θ^T and θ respectively. This is obtained if Equation (2.50) is substituted into Equation (2.46).

$$C_G = 2\eta \theta^T M \theta \Omega = 2\eta M_G \Omega \quad \dots\dots\dots(2.51)$$

This generalised damping matrix is diagonal, because the damping was chosen proportional to the mass matrix. Equation (2.44) can now

be written

$$M_G \ddot{\underline{\xi}} + 2\eta_{M_G} \Omega \dot{\underline{\xi}} + M_G \Omega^2 \underline{\xi} = \underline{P}_G \quad \dots\dots\dots(2.52)$$

This set of differential equation is uncoupled and the equations for the r^{th} mode multiplier ξ_r is

$$(M_G \ddot{\xi}_r + 2\eta_{M_G} \dot{\xi}_r + M_G \omega_r^2 \xi_r) = P_{G_r} \quad \dots\dots\dots(2.53)$$

If harmonic excitation is assumed at the j^{th} degree of freedom and all the other exciting forces equal zero then the time dependent multiplier ξ_r is

$$\xi_r = \frac{\theta_{jr} P_j(\omega, t)}{M_G (\omega_r^2 - \omega^2 + i 2\eta_r \omega_r \omega)} \quad \dots\dots\dots(2.54)$$

and the response at u_i follows from Equation (2.40)

$$u_i(\omega, t) = \sum_{r=1}^n \frac{\theta_{ir} \theta_{jr} P_j(\omega, t)}{M_{G_r} (\omega_r^2 - \omega^2 + i 2\eta_r \omega_r \omega)} \quad \dots\dots\dots(2.55)$$

The displacement response at the i^{th} degree of freedom to a harmonic force of unit peak amplitude at the j^{th} degree of freedom,

$j = (1, 2, \dots, i, \dots, n)$, is defined as the displacement receptance.

$$\mathcal{L}(i\omega)_{ij} = \sum_{r=1}^n \frac{\theta_{ir} \theta_{jr}}{M_{G_r} \omega_r^2 \left(1 - \frac{\omega^2}{\omega_r^2} + i 2\eta_r \frac{\omega}{\omega_r}\right)} \quad \dots\dots\dots(2.56)$$

The acceleration receptance $\ddot{\mathcal{L}}_{ij}$ is obtained from the second time derivation of Equation (2.56).

$$\ddot{L}_{ij} = -\omega^2 L_{ij} \dots\dots\dots(2.57)$$

where ω is the frequency of the exciting force.

2.2.3 Computed Results for Dynamic Response and Comparison with Analytical Results

It was decided that for the present purpose it was sufficient to compute the first three sway modes of vibrations and the cantilever was modelled as a four beam element structure. Lateral and rotational dynamic degrees of freedom were employed together with lumped and consistent mass condensation. The natural frequencies of these four beam element models and the percentage difference from analytical frequencies are given in Table 2.1.

The tabulated frequencies show clearly that consistent mass condensation is superior to lumped mass condensation for this simple cantilever beam. The computed results for the consistent mass model with lateral and rotational degrees of freedom agreed almost exactly with the analytical model, for example, the difference being -0.25% in the third mode.

If the rotational accelerations of the beam elements are assumed to be negligible then it follows that the dynamic moments at the joints, arising from distributed linear and rotatory motion, can be ignored. This is done by removing the appropriate rows and columns from the global consistent mass matrix and a static condensation of the global stiffness matrix will follow to eliminate rotational degrees of freedom. This approach was applied to the cantilever beam, and the accuracy of the consistent mass model with only lateral

dynamic degrees of freedom was good; an error of +6.04% in the third mode is acceptable for engineering purposes.

In the lumped mass model it is evident from Table 2.1 that the translational inertia has been over estimated, all three computed frequencies being lower than the analytical value, the maximum difference being -13.8% in the third mode. Introducing mass moment of inertia at the joints leads to an increased negative error in all modes, as can be expected.

The solution times for the four models increased with the complexity of the models. For example, an increase of 17% in C.P.U. time gave an improvement of about 13. % in the third natural frequency.

Computed mode shapes, normalised to unit displacement at the beam tip, are plotted in Figure 2.3. It was noticed that the second mode shape was computed 180 degrees out of phase with the analytical mode shape calculated from the equation ,

$$\theta(x)_2 = \cosh\left(\frac{4.694x}{l}\right) - \cos\left(\frac{4.694x}{l}\right) - 1.018 \left[\sinh\left(\frac{4.694x}{l}\right) - \sin\left(\frac{4.694x}{l}\right) \right] \dots$$

.....(2.58)

for a cantilever beam, and tabulated by Bishop [23].

Such an inversion is of no significance in the present work. The accuracy of the mode shapes was expected to be consistent with the trend of the frequency Table 2.1. This is confirmed by Table 2.2 which was compiled for the fundamental mode to show percent difference in computed and analytical mode shapes. The mode shape of the consistent mass model with lateral and rotational dynamic degrees of freedom agreed almost exactly, and the errors in the remaining

models are less than 2%.

A computer programme was written to compute and plot receptances. Figure 2.4 shows the acceleration receptance $|\ddot{x}_{77}|$ at the cantilever tip plotted from analytical and computed normal modes. The computed normal modes used were those from the consistent mass model with lateral and rotational dynamic degrees of freedom. As expected the two receptances agree almost exactly. From the plot, which is on a logarithmic amplitude-scale, it becomes apparent that the cantilever develops a "node" at the tip for two frequencies, 137 Hz and 454 Hz. The "node" is a result of the transition from one mode to the next. The modal damping ratio was given the value of 0.5% in all modes. This is a rather high damping figure for a steel cantilever beam, but 0.5% gives a dynamic magnification of 100 which is a convenient figure. Dynamic magnification is related to the damping ratio by

$$Q_r = \frac{1}{2\zeta_r} \dots\dots\dots(2.59)$$

2.2.4 Computed Results with Point Mass at Tip and Comparison with Analytical Results

The cantilever beam problem with a translational point inertia at the tip has an analytical solution. The equation governing the natural frequency is [24]

$$1 + \frac{1}{\cosh \lambda_r l \cos \lambda_r l} - \gamma \lambda_r l (\tan \lambda_r l - \tanh \lambda_r l) = 0 \dots\dots(2.60)$$

where γ is the ratio of the point mass to the total distributed

mass, Figure 2.5,

$$\gamma = \frac{M}{\rho A l} \dots\dots\dots(2.61)$$

For the present purposes mass ratios γ of 2 and 5 were chosen, and Equation (2.60) solved for the first three natural frequencies. Tables 2.3 and 2.4 give the frequencies for the mass ratios $\gamma = 2$ and $\gamma = 5$ respectively. The beam element computation was then carried out for the two lumped-mass and two consistent-mass models and the result for $\gamma = 2$ and $\gamma = 5$ are included in Tables 2.3 and 2.4 respectively. These tables show that the consistent mass condensation with lateral and rotational dynamic degrees of freedom gives the best results, the error in the third frequency being 0.05% for $\gamma = 2$ and $\gamma = 5$. The lumped mass models without rotational dynamic degrees of freedom show remarkably small errors, for example -2.27% ($\gamma = 2$) and 2.01% ($\gamma = 5$) in the third frequency. This is in contrast with errors calculated for the cantilever beam without point mass. It may also be noted that the accuracy improved slightly for increasing mass ratio γ . These observations point to the fact that when the system is dominated by a lumped mass greater than the distributed mass of the beam, the choice of mass condensation technique becomes irrelevant with respect to accuracy.

The computed mode shapes were found to be virtually the same for the two mass ratios and are plotted in Figure 2.5. In the second and third modes there is very little translation at the beam tip and these mode shapes are similar to those for a clamped/pinned beam. The acceleration response $|\ddot{x}_3|$ at $x_3 = \frac{1}{2}l$ for excitation

at $X_7 = \ell$ was also computed for the two mass ratios and is plotted in Figure 2.6. The plots show clearly the effect of an increased mass ratio on the amplitude and the natural frequency of the response for a given excitation. The response amplitude in all modes was reduced by more than 50%. The reduction in natural frequencies was greatest in the fundamental mode - 34.6% - with only 1.62% and 0.56% in the second and third modes respectively.

2.2.5 Computed Results with Shaker at Tip

The final extension to the cantilever beam was a dynamic model of the shaker and its support, Figure 2.2. The shaker and support might be treated as a single unit of mass in using Rayleigh's formula [23], for example, to estimate the fundamental frequency

$$f = \frac{1}{2\pi} \sqrt{\frac{k}{M + 0.236 \rho A \ell}} \quad \dots\dots\dots(2.62)$$

where k is the stiffness at the beam tip, M is the lumped shaker assembly mass and $\rho A \ell$ the total distributed beam mass. The fundamental frequency calculated from Equation (2.62) was

$$f = \frac{1}{2\pi} \sqrt{\frac{82370.}{33.2 + 0.236 \times 8.88}} = 7.69 \text{ Hz} \quad \dots\dots(2.63)$$

However, this model might not be good enough for computing higher modes as there is a significant spacing between the shaker and its support base, and a node may occur between the two masses in the second and third modes. A dynamic model for the cantilever beam was therefore taken to consist of two lumped masses (shaker and support base) connected by a beam element, Figure 2.7. This connecting

element has a tapered cross-sectional shape, but, as a first approximation the dimensions of the cross section at two thirds distance from the base was used to calculate equivalent cross-sectional properties, Figure 2.7. The mass m_1 in Figure 2.7 is the inertia of the shaker only, and its mass moment of inertia was calculated from formula for a cylinder

$$J_1 = \frac{m_1}{12} (a_1^2 + 3b_1^2) \dots\dots\dots(2.64)$$

The mass m_2 is the total inertia of the shaker support and base plate with mass moment of inertia calculated from formula for a plate

$$J_2 = \frac{m_2}{12} (a_2^2 + b_2^2) \dots\dots\dots(2.65)$$

To investigate the effect of increasing the number of elements, it was decided to compute the normal modes for two different models: a five beam and a nine beam element model, Figure 2.8. The nine beam element model was derived from the five element model by halving the length of the elements of the uniform cantilever. A check on the convergence of the computed frequencies would then indicate if further sub-division was required.

The results in Table 2.5 show clearly that no further sub-division is necessary if consistent inertia with lateral and rotational dynamic degrees of freedom are used. In the other three cases further sub-division is expected to improve the values for the second and third natural frequencies. Computed normalised mode shapes for the five beam element models are plotted in Figure 2.8. Both the second and third mode shapes have a node between the shaker and the support base

and in the third mode the second node is located at a distance 1.12 m from the cantilever base.

2.2.6 Method of Measuring Dynamic Response

A generalised block diagram of the equipment used to record the acceleration response of the cantilever beam to sinusoidal force excitation is shown in Figure 2.9. The main components are:

- (a) Signal generator with correlator or amplitude regulator;
- (b) Power amplifier;
- (c) Electro-magnetic shaker;
- (d) Accelerometers and pre-amplifiers;
- (e) Signal amplifiers;
- (f) Switch box, digital frequency meter, oscilloscopes, and recorders.

Similar equipment was used in all the experimental work reported in this thesis.

(a) Signal Generator

To generate the excitation signal at discrete frequencies a Solartron Digital Transfer Function Analyser JM 1600 A (TFA) was used. This unit has a frequency range from 10^{-5} Hz to 159.9 Hz with an accuracy of $\pm 0.05\%$ of the frequency setting. Frequencies can be dialled in steps of 0.01 Hz in the range from 1 Hz to 15.99 Hz and in steps of 0.1 Hz in the range from 10 Hz to 159.9 Hz. The voltage amplitude range is 10 volts RMS with measuring resolution of 0.1% of full scale and accuracy of $\pm 0.5\%$ of reading. The amplitude and phase angle of the signal is displayed digitally in cartesian,

polar or log polar form. This display also serves the correlator unit, which computes the amplitude and phase angle of the response signal relative to the generator signal. The result, displayed in polar form, gives the amplitude to three digits (0.1%) with an accuracy of $\pm 0.5\%$ of reading. The phase angle has a four digit display (360° or $0'$) and is accurate to $\pm 1^\circ$ at $0.1 \times$ full scale amplitude.

The Transfer Function Analyser (TFA) is a unit for measuring response amplitude and phase angle at discrete frequencies. Recording a complete frequency response, however, is a slow process. To overcome this problem, the alternative sweep sine technique was also employed. A Brüel & Kjaer Beat Frequency Oscillator Type 1017 together with a Level Recorder Type 2305 was available.

The Beat Frequency Oscillator (BFO) consists of a sine-wave generator for the frequency range 2 Hz to 2K Hz on a logarithmic frequency scale. Voltage amplitudes up to 12 volts can be obtained and the output displayed on an analogue meter calibrated in RMS values of sinusoidal voltage with an accuracy of $\pm 1\%$ of full scale deflection. The output frequency from the BFO can be remotely controlled via a mechanical drive which is linked up with the Level Recorder drive by a flexible shaft. The output speed (rpm) of the Level Recorder drive-shaft has ten different settings which enables very low logarithmic sweep rates to be used for lightly damped structures. The Level Recorder was equipped to record AC signal amplitude variations of maximum 50 db on rolled paper of 100 mm writing width. The speed of the recording paper can be adjusted

to compress or expand the record, and paper with pre-printed frequency scales can be used. When the Level Recorder is used to sweep the frequency in conjunction with the BFO, it may be necessary to control the amplitude of the output voltage, driving the power-amplifier in order to keep constant the force amplitude over the frequency sweep range. This is achieved when an acceleration control signal is fed back from the shaker armature mass to the signal regulator unit which is an integral part of the BFO unit. The regulator has a dynamic range of 45 db for a change of 2 db in the control signal. In other words, if the structure under test requires a voltage change from the BFO of less than 45 db over the sweep frequency range, full regulation can be achieved. The frequency response of the regulator unit is within ± 0.5 db. Successful regulation of the force input to the structure under frequency sweep test depends on the dynamic characteristics of the power-amplifier and shaker unit.

(b) Power Amplifier

The function of the power-amplifier is to raise the power level of the signal derived from the signal generator to a level sufficient to operate the shaker; this in turn excites the structure under test.

The basic requirements of the power-amplifier are high input and low output-impedance within specified frequency limits. A high input impedance makes the amplifier easily matched with any signal generator. The ratio of load to source impedance should in general be as high as possible. On the output side, the shaker is considered

a load on the amplifier, and this impedance ratio should be unity.

Harmonic and intermodular distortion are relevant performance data when testing lightly damped structures. Harmonic distortion is harmonic frequencies at the output of the amplifier when a sinusoidal voltage is applied at the input. Intermodulation is the modulation of the components of a complex signal by each other, producing signals of frequencies equal to the sums and differences of integral multiples of the components of the original complex signal.

The amplifier used for the cantilever experiment was designed and made by the Engineering Laboratories. It is a constant gain, AC coupled power-amplifier rated for approximately 40 watts but, because of its AC coupling, it was found to be not suitable for low frequency excitations (7. Hz). For subsequent work a CROWN DC-300A power amplifier was used. This is a unit with good performance in most aspects of signal amplification. The input sensitivity is 1.75 volts with input impedance varying between $100\text{ K}\Omega$ and $10\text{ K}\Omega$ at minimum gain and maximum gain respectively. The frequency response is within ± 0.1 db from DC to 20K Hz, and the output impedance is less than 0.01Ω 140^o up to 200 Hz. The amplifier will work on a completely reactive load; for a resistive load of 1Ω the maximum output power is 100 watts RMS.

(c) Electro-Magnetic Shaker

The function of the shaker is to convert electric power into mechanical power. The shaker has two main parts: a permanent magnet and a moving mass/coil assembly (armature) suspended by a

spring, Figure 2.10. When a current is passed through the moving armature coil of the shaker, the armature will follow the waveform of the current in magnitude and direction.

If the shaker assembly is made an integral part of the structure under test, the exciting force can be derived from the acceleration of the armature mass. This principle of dynamic force generation is used for all experiments described in this work. It has the advantage that no auxiliary structure need be constructed to react forces. The force generated was deduced from the acceleration measured by an accelerometer attached to the armature platform. A sinusoidal force of 137 Newtons is the maximum rating when natural cooling is used. The shaker has an operating frequency range from 5 Hz to 9K Hz. The force/frequency response is not linear, Figure 2.11. In the region from 5 Hz to 30 Hz the response increases by approximately 12 db/octave exhibiting a resonant peak between 30 Hz and 40 Hz. The response drops by 5 db in the range 40 Hz to 100 Hz, from which frequency it can be considered flat.

(d) Accelerometers and Pre-Amplifiers

The vibrations induced by the electro-magnetic shaker were measured by piezoelectric accelerometers with magnetic bases for mounting on the steel structure, Figure 2.12. The basic accelerometer consists of two piezoelectric discs on which is resting a mass, Figure 2.12. When the accelerometer is subjected to vibration the mass will apply a force proportional to the acceleration on the piezoelectric discs. Due to the piezoelectric effect a variable voltage will develop between the two discs. The particular accel-

erometer used was a Brüel & Kjaer Type 4338. The nominal specifications for this accelerometer are; voltage sensitivity 90 mv/g, transverse sensitivity $< 3\%$, output impedance $> 20000 \text{ M}\Omega$, mounted resonance 12K Hz and weight 60 grammes. A 2.5 grammes accelerometer Type 4344 was also used for measurements on light structural members. The particulars for this accelerometer are; voltage sensitivity 2.7 mv/g, transverse sensitivity $< 3\%$, mounted resonance 131K Hz and output impedance $> 20000 \text{ M}\Omega$

Piezoelectric accelerometers have very high output impedance ($> 20000 \text{ M}\Omega$) and an impedance converter (pre-amplifier) is required in order to operate the transducer without loss of sensitivity. A voltage pre-amplifier is basically an amplifier with high input and low output impedance, and it should be as close as possible to the accelerometer, so as to keep the capacitance and resistance of the connecting cable small.

The voltage pre-amplifiers used were designed and made by the Electronic Workshop. The circuit consists basically of a semi-conductor with unit feedback. Power is obtained from two 9 volt batteries, which together with the circuitry are assembled in a small diecast box.

The frequency response of the pre-amplifier is nominally flat.

(e) Signal Amplifiers

The pre-amplifiers were designed with unit voltage gain. This may at first seem not right, but the pre-amplifier is positioned close to the accelerometer, and in some cases attached to the vibrating structure. Hence the size and weight are important design

parameters. The signal amplification as such was therefore performed by separate amplifiers connected to the pre-amplifiers with 70 Ω co-axial cable.

The signal-amplifier design is based on the 741 operational amplifier. A ten-turn potentiometer gives infinitely variable gain between 30 and 300. The frequency response is flat and the lower -3 db frequency is 1 Hz, determined by a blocking capacitor, which was included to eliminate pre-amplifier DC off-set. The input impedance is $\approx 2K\Omega$ and the unit is powered by two 9 volt PP9 batteries.

(f) Switch Box, Digital Frequency Meter, Oscilloscope, and Recorders.

The switch box was designed with two six way one pole switches to enable any two of six input signals to be monitored and/or recorded. Signals were displayed on two Solartron Schlumberger Oscilloscopes. A Racal SA520 digital frequency meter was used to measure signal frequency. The meter frequency range is from 2 Hz to 30K Hz; it displays frequency to the nearest integer frequency with an accuracy ± 1 count \pm internal crystal stability. In addition period measurements are included to enable low frequency signals to be measured with very high accuracy.

A Brüel & Kjaer Level Recorder was used to record the envelope of the structural response. This unit is described under point (a). Complete time histories were recorded on a Ultra-Violet Recorder.

2.2.7 Measured Dynamic Response with Shaker at Tip

Natural frequencies and mode shapes were first measured using discrete frequency excitation. The input force was the same at

each frequency and the acceleration response was recorded on both sides of the resonant peaks.

Figure 2.13 is a plot of the response in the region of the second sway mode. It shows clearly that the mode is lightly damped and that the natural frequency was between 104-105 Hz. Another estimate of the natural frequency was obtained from the phase angle plot, Figure 2.14.

The phase shift of 90° between response and force at resonance was used to locate the natural frequency again between 104-105 Hz. From these two plots Figures 2.13 and 2.14 the second natural frequency was estimated to be 104.48 Hz.

The dynamic magnification was extracted from the phase angle plot Figure 2.14 by considering the frequency bandwidth at the half-power points, which were at 45° on each side of the resonant phase angle point (90°). The dynamic magnification was then calculated from the expression

$$Q_r = f_r / \Delta f \quad \dots\dots\dots(2.66)$$

where f_r is the natural frequency and Δf is the half-power point bandwidth. This in turn gave the modal damping ratio

$$\eta_2 = \frac{1}{2Q_2} \quad \dots\dots\dots(2.59)$$

For this second sway mode the value of Q_2 was estimated to be $104.5/0.25 = 418$ or $\eta_2 = 0.12\%$.

The third mode was examined in the same way and results are plotted in Figures 2.15 and 2.16. The measured natural frequency

was 255.55Hz and the value of Q_3 was 182 giving a modal damping ratio of 0.28%.

Because of the unfavourable frequency response characteristics of the power amplifier and shaker at the lower frequencies, it was not possible to use this method to determine the response of the beam at the fundamental frequency. Instead the fundamental mode was excited manually by simply pulling the cantilever at shaker level from its natural position and then releasing.

The resulting oscillation was recorded on an Ultra-Violet recorder and the natural frequency measured from the record to be 7.33 Hz. The logarithmic decrement δ was calculated by measuring the amplitude ratio for 22 cycles.

$$\delta_1 = \frac{\ln 1.14}{22} \dots\dots\dots(2.67)$$

which gives a modal damping ratio of

$$\eta_1 = \frac{\delta_1}{2\pi} 100 = 0.095\% \dots\dots\dots(2.68)$$

which is a Q_1 of 527.

2.2.8 Comparison of Measured and Computed Responses with Shaker at Tip

The measured natural frequencies are compared with the computed values for both the 5 and 9 element models in Tables 2.6 and 2.7. The fundamental natural frequency was measured to be 7.33 Hz and the Rayleigh formula Equation (2.63) for a one degree of freedom model predicted a fundamental natural frequency of 7.69 Hz. This is an error

of 4.9% which is considered acceptable for engineering purposes.

All the beam element models gave fundamental frequencies with good accuracy. Errors of about 1.4% or less are indicated in Tables 2.6 and 2.7.

The second natural frequency was found at 104.5 Hz, and was computed with good accuracy from the models with lateral and rotational dynamic degrees of freedom. Errors varying from -2.4% to -1.2% are indicated by Tables 2.6 and 2.7.

The models without rotational dynamic degrees of freedom show errors of 14.7% to 18.6%. From these results it appears that the choice of mass condensation technique is irrelevant, but that inertia forces and moments associated with rotations are not negligible in this second mode.

The third natural frequency was measured at 255.55Hz and the qualitative performance of the beam element models is similar to the second mode. Models with lateral and rotational dynamic degrees of freedom show errors up to +3.3%, and without rotational dynamic degrees of freedom errors of 30% to 40%.

Computed and Measured mode shapes are in good agreement, Figures 2.8 and 2.17. The second and third modes both have a node between the shaker and its support. The position of the second node measured on the cantilever in the third mode is 1.105 m from the base of the cantilever and is very close to the computed node position measured on Figure 2.8.

Experimental modal damping ratios were used to compute the lateral acceleration receptance $|\ddot{u}_{39}|$ at a position 0.75 m from

the cantilever base, Figure 2.18.

Sweep sine testing should have produced a similar plot for the same frequency range. However, the frequency response of the exciter system plotted in Figure 2.11 made this impossible. The acceleration response was therefore recorded from about 90 Hz and Figure 2.19 shows the measured acceleration response where the second and third natural frequencies are easily identified.

2.3 PLANE FRAME STRUCTURE

2.3.1 Description of plane frame

The plane frame is shown in Figure 2.20. It may be thought of as a single panel or substructure of a K-braced jacket. It was chosen because its dynamic response would be more complex than that of the cantilever beam structure, but still much simpler than that of a K-braced platform. The frame was constructed from square hollow sections; the two legs had the same dimensions as the cantilever beam of the previous study. The spacing of the legs was fixed by the pitch of fixing plates in the re-inforced concrete strength floor. The two horizontal beams were spaced to give the K-braces an angle of approximately 45° .

The foundation plates were thinner than in the cantilever beam, and were bolted to the floor foundations, with washers between the plates and the floor, to give approximately encastred fixing. The shaker assembly was fixed to a plate on one leg.

2.3.2 Frame beam element model

It was intended that the normal mode computation would give the first five or six global and local modes. Global modes were regarded as those in which all structural members suffer appreciable displacement; in local modes only one member or small group of members deform significantly.

To model the frame it was decided that each member should be subdivided into at least three beam elements. A member modelled by three beam elements can describe member deformations such as an approximate $3/2$ period sine wave, which was expected to occur in

higher modes. The beam element model is shown in Figure 2.21. The shaker system was modelled in the way described for the cantilever beam structure (Chapter 2, Section 2.5).

The base plates were idealised as beams (Figure 2.20 and 2.21) and each plate was modelled as an assembly of two beam elements with a joint between them to which a leg of the frame was attached. Rather than attempt to model the bolting constraints of the base plates accurately it was decided to study two extreme conditions:

- (a) The bolts providing simple support;
- (b) The bolts providing encastré support.

These two idealised models are included in Figure 2.21.

2.3.3 Computed static response

As a preliminary to the dynamic response computations, the stiffness of the frame with a horizontal load applied at joint 20X was used to calculate a force/displacement coefficient for both encastré and simply supported constraints. For encastré conditions the stiffness $k_{20X,21X}$ was 11.05 KN/mm with a reduction of 24.1% for simply supported condition.

An estimate was also made of the maximum load that might safely be applied to the frame in an experiment to check the computed stiffness. The K-braces were the critical members, and 37.7 KN was estimated to be the maximum compressive load which these members could safely withstand. This was reached at an applied load of 40 KN. Based on this rough estimate the applied load was limited to 30 KN.

2.3.4 Measured static response

A diagram of the force/displacement experiment is shown in Figure 2.22. A simple two member structure constructed from square hollow sections was used to react the force of the hydraulic ram. A clock gauge mounted on another frame recorded displacement at joint 21X, the resolution of the gauge being 0.01 mm. The force transmitted through the clock gauge was very small and deformation of the support frame would not lead to significant error in displacement measurement. The hydraulic ram was activated by a hand pump equipped with a pressure gauge calibrated in force units for different rams. A calibration check gave the following relation between gauge readings F_m in tons and the transmitted force F_A in KN

$$F_A = 8.7F_m + 2 \dots\dots\dots(2.69)$$

The force was increased in steps of 0.5 tons up to 3.5 tons and the displacement at joint 21X plotted, Figure 2.23. A straight line was drawn to give the best fit to the experimental points, and the gradient of the line was measured from the plot to be 10.2 KN/mm .

2.3.5 Comparison of computed and measured static responses

The assumption about the end constraints of the base plates gave satisfactory results. With encastré support plates the frame stiffness $k_{20X,21X}$ was overestimated by 8.3%, and for simply supported ends underestimated by 17.8%, making the assumptions of encastré support of the baseplates more realistic than the assumption of simple support.

From these results the chosen beam element model was considered sufficiently accurate for a stiffness computation and the only other point which might cause concern was the joint stiffness. In the computer model the joints are assumed rigid and this results in a stiffer frame. However, it was beyond the scope of this work to study the frame in such detail. Further, it was considered that the assumption about joint stiffness would have a smaller effect on the stiffness $k_{20X,21X}$ than the assumption about base plate fixing.

2.3.6 Computed dynamic response

The first five vibration modes were computed for the two support conditions of the static analysis. Consistent mass condensation was used for the beams with two translational and one rotational dynamic degrees of freedom at each joint.

The shaker and support were modelled as lumped masses. Static condensation was used to eliminate horizontal dynamic degrees of freedom at the leg bases, joints 5X and 6X Figure 2.21. The dynamic model had thus 64 degree of freedom or 2 less than the static model.

The natural frequencies are given in Table 2.8 and the percent reduction in going from encastré to simply supported end conditions in the base plates included. The first natural frequency for encastré supports was found to be 41.21Hz and the corresponding mode shape is plotted and tabulated in Figure 2.24 and Table 2.9. This plot showed that the frame was basically vibrating as a one degree of freedom system, where the shaker/support inertias constituted

the major part of the moving mass, with the frame acting as the spring element. The mode shape clearly involved rotations of the legs at the base plates and the rotational stiffness of these plates would affect the natural frequency and mode shape. When the support conditions were changed from encastré to simply supported, the natural frequency was reduced by 5.1%.

The second natural frequency was predicted at 67.60Hz for the condition with encastré base plate ends, with a reduction of 6.5% for the simply supported configuration. The mode shape is plotted and tabulated in Figure 2.25 and Table 2.10. It was dominated by lateral movement of the upper horizontal beam. The shape of the beam approximated a half period sine wave.

In the third mode at 73.21Hz the K-braces vibrated in an approximately clamped-clamped fundamental mode with other members conforming to this deformation, Figure 2.26 and Table 2.11. The mode did not involve significant deformation of the base plates and hence was relatively insensitive to base stiffness changes. A reduction in frequency of only 1.1% was noted.

The fourth mode was a local mode with the K-braces vibrating out of phase in an approximate clamped-clamped mode at 78.08Hz, (Figure 2.27) and with very little other deformation. The fundamental frequency of a clamped-clamped beam, 77.50Hz, was close to the measured value. There was only 0.24% reduction in going from encastré to simply supported conditions.

The fifth mode was another global mode in which the frame was translating horizontally with legs bending in phase to approximately

half period sine waves; remaining members deformed in sympathy with considerable displacements, Figure 2.28. The computed natural frequency was 96.12Hz with a reduction of 4.2% in going from encastré to simply supported base plates; this reduction was accounted for by the change in rotational stiffness of the base plates.

In Figure 2.29 the receptance at joint 23 in the global Y-direction, denoted 23Y, is plotted for the two support conditions and for a dynamic magnification of 100. Joint 23Y was chosen because all modes appeared to be represented at that station. The modal displacement at joint 26X, the point of excitation, was very small in the fourth mode and consequently made this mode difficult to excite.

The computed receptance Figure 2.29 give a good indication of four natural frequencies, but the fourth mode can easily be overlooked in an experiment with excitation at joint 26X.

A change of support conditions from encastré to simply supported not only changed the vibration frequencies but also the mode shapes; this was apparent from the receptance plot, Figure 2.29, and Tables 2.9 to 2.13.

The amplitude response at the second natural frequency was reduced to approximately one third of its original value; at the third natural frequency, the response was increased by a factor of two, when the base supports were encastré.

The receptance calculation also provided an estimate of the force required to excite the frame to a measurable level.

2.3.7 Measured dynamic response

The dynamic response was measured with the equipment described in section 2.6, and a block-diagram of the measurement set-up is shown in Figure 2.9. It was decided that measurements should also be taken with the frame submerged in water in order to check the accuracy of the beam element model with added virtual mass, and the damping effect of water. To perform this experiment a relatively massive support for the frame had to be constructed, Figure 2.30. It consisted of a heavy I-beam with two plates welded to the I-beam to accept the base plates of the test frame, which was bolted to this foundation. The I-beam was constructed with four legs to avoid submerging the shaker during experiments conducted at the Naval Architecture Experiment Tank.

The sweep sine equipment was set to give a constant force amplitude of 10 Newtons peak and the response was recorded from 30Hz to approximately 100Hz. The sweep time was long, 46 minutes, but this was necessary to avoid transients in the response when the excitation frequency went through a natural frequency.

An accelerometer with a magnetic base was positioned at joint 23Y to measure vibrations in the y-direction. The acceleration response is shown in Figure 2.31. Three major peaks were located immediately from the plot and these were at 39.9Hz, 69.7Hz and 92.7Hz. An investigation of the mode shapes at these particular frequencies gave good agreement with the computed modes, 1, 2 and 5 at 41.21Hz, 67.60Hz and 96.12Hz respectively. The natural frequencies of modes 3 and 4 were not easily determined from this

plot, Figure 2.31. However, the response showed two peaks at 79.1Hz and 84.6Hz and three more frequencies at which the response indicated that a resonance was present in the frame.

To clarify the response a very light accelerometer (2.5 grammes mass) was attached to joint 18, Figure 2.21, on a K-brace to measure transverse vibration. The sweep test was then repeated for the frequency range 65Hz to 95Hz approximately, Figure 2.32.

Two peaks at 75.8Hz and 79.1Hz gave the most distinct response and the measured mode shapes confirmed that these modes were similar to the computed third and fourth modes.

The response was also recorded on the other K-brace at joint 19, Figure 2.21, confirming the two peaks at 75.8Hz and 79.1Hz, Figure 2.33.

The response plot at joint 23Y, Figure 2.31, also revealed unexpected peaks at 30.9Hz, 43.7Hz and 84.7Hz. The first peak was found at a frequency which was one-third of the fifth natural frequency. This indicated the presence of a third harmonic in the excitation. The amount was not measured, but as a result of low modal damping it was enough to make the frame respond distinctly. Similar explanations could account for the peaks at 43.7Hz and 84.7Hz.

The response immediately after the fourth natural frequency showed peaks and valleys which were thought to be out-of-plane resonances. This was not confirmed, being beyond the scope of the experiment.

The damping in each mode was measured by tuning the excitation frequency to a natural frequency; when the response was considered steady, the excitation was discontinued and the ensuing response recorded on an Ultra-Violet recorder.

The dynamic magnification Q_r was then calculated from the expression

$$Q_r = \frac{\pi t f_r}{\ln \left(\frac{\ddot{x}_0}{\ddot{x}_n} \right)} \dots\dots\dots(2.70)$$

where $\frac{\ddot{x}_0}{\ddot{x}_n}$ is the ratio of the decaying acceleration response, t is the time elapsed between \ddot{x}_0 and \ddot{x}_n and f_r is the natural frequency of the r th mode. The dynamic magnification in the first, second and fifth mode was measured at joint 23Y and was found to be 59, 92 and 346 respectively. The third and fourth modes were mainly vibrations of the K-braces, and consequently measurements were made at joints 18 and 19. From several measurements in the third mode, the dynamic magnification Q was found to vary from 250 to 295 at joint 18 and from 320 to 385 at joint 19. In the fourth mode, Q 's of 706 and 739 were measured at joints 18 and 19 respectively.

2.3.8 Computed and measured dynamic responses in water

It would not be right to terminate the frame research without an experiment in water.

The vibration of structures in water is still a topic of discussion. Problems such as amplitude and frequency dependence of the liquid mass with the added complication when the vibrations take place relatively near the water surface are being investigated by research-workers [25]. It was beyond the scope of this work to study these aspects and consequently constant liquid mass was used.

A table of added-liquid-mass values for some two-dimensional geometric shapes in unsteady motion is given in Figure

2.34. For a beam of square section the distributed liquid mass is

$$m_L = 1.51 \rho_w \pi a^2 \dots\dots\dots(2.71)$$

and for a long flat plate

$$m_L = \rho_w \pi a^2 \dots\dots\dots(2.72)$$

where ρ_w is the density of water and $2a$ is the dimension of the side of the square, or the length of the plate.

STRU DL was not programmed to calculate added-liquid-mass, but it was included by calculating an effective density from the relation

$$\rho = \frac{m_{st} + m_L}{A} \dots\dots\dots(2.73)$$

where m_{st} is the distributed mass of the beam and A the cross-sectional area. The liquid mass of the base plates was also calculated in the same way. In the beam element model, liquid mass was added to all beam elements excluding the shaker and its support plate. This corresponded to the submerged position of the frame

where the water surface was just below the top of the legs in order not to flood these.

The first five natural frequencies were computed for encastré supports, Tables 2.9 to 2.14. The fundamental changed least, a reduction of 5.1% was calculated, while the other four changed by as much as 16% to 20%.

The difference in reduction between the fundamental and the four other frequencies can be understood when the mode shapes are considered. In the fundamental mode considerable displacements took place above the water line (shaker/support), whereas in the four other modes displacements took place mainly in parts of the structure which were submerged.

Addition of liquid mass was not expected to produce any new modes of vibration, and only small changes in the mode shapes were calculated compared with mode shapes in air, Tables 2.9 to 2.13. The coordinate of maximum displacement remained the same for all modes, except for the fourth mode shape. Here it moved from one K-brace (joint 14Y) to the other K-brace (joint 15Y) in air and water respectively.

In the experiment with the frame in water accelerometers were positioned at joints 18 and 23 as in the experiment in air. Figure 2.35 shows the response at joint 23Y. The fundamental natural frequency was found at 37.9Hz which gave a computational error of +3.2%, Table 2.14.

The second mode was predicted at 54.1Hz, and the recording showed two peaks in that region. The first peak appeared at 52.7Hz

and the other at 58.4Hz. It was not possible to determine with confidence which peak was associated with the computed second mode. However, from recordings at joint 18 and 23, Figures 2.35 and 2.36, the peak at 58.4Hz appeared as the most predominant response and it was assumed to be the second mode as predicted by the beam element model, giving an error in natural frequency of -7.4%.

The third and fourth modes were modes with strong vibration of the K-braces. This was clear from the two recordings, Figures 2.35 and 2.36, which showed an increase in vibration amplitude of about an order of magnitude between joints 18 and 23. Both frequencies compared well with the computed frequencies, with the third natural frequency measured at 63.4Hz, and the fourth at 67.4Hz, which gave errors of -3.9% and -3.6% relative to the computed natural frequencies.

A significant peak was also found at 72.9Hz. This frequency could be claimed to be the fourth mode. However, the error -10.8% relative to the computed fourth natural frequency at 65Hz was found to be too big considering what was measured and computed for the frame in air.

The fifth natural frequency was measured at 78.3Hz and an error of -2.6% calculated.

A summary containing five computed and seven measured natural frequencies was prepared in Table 2.14 together with their respective measured dynamic magnification factor Q.

2.3.9 Comparison of measured and computed dynamic responses

The measured and computed natural frequencies are summarised in Table 2.15. The fundamental natural frequency was found at 39.9Hz, which gave errors of 3.3% and -2% for encastré and simple base constraints respectively. These errors were reasonable both in magnitude and sign because they implied that the correct base plate constraint stiffnesses were between the two limits used.

The theoretical frequency response at joint 23Y was computed with measured Q-factors for a peak force of 10 N acting at joint 26X and plotted on logarithmic scales, Figure 2.37. From the plot the response amplitude was roughly 1.09g and .95g for encastré and simple supports respectively. The measured response amplitude was 1.88g, Figure 2.31. Thus the amplitude at the fundamental natural frequency was underestimated by 42% and 49.5%.

The second natural frequency was computed to within -3% and -9.3% for encastré and simple supports respectively. The response amplitude was sensitive to changes in the base plate constraints and it decreased from 1.58g to .5g when the supports were changed from encastré to simple. The measured response amplitude was 1.33g at 69.7Hz.

Mode three was basically a local mode and it was computed with errors in natural frequency of -3.4% and -4.5% for encastré and simple supports respectively. The theoretical amplitude increased from 0.5g to 1.41g when the base conditions changed from encastré to simple. The agreement with the measured amplitude at joint 23Y was rather poor, as the frame developed a node close to joint 23.

From the computed mode shape, Table 2.11, this node was predicted between joints 20 and 22.

The fourth mode was also a local mode and it was virtually insensitive to the base conditions. It was computed with errors of -1.3% and -1.5% for encastré and simple supports. The theoretical amplitude increased from .075g to .316g for encastré and simple supports respectively. The measured amplitude was found between these limits and it was .084g.

The fifth natural frequency was computed with errors of 3.7% and -0.7% for encastré and simple supports, with the magnitude increasing from 2.51g to 3.98g. The measured magnitude at the natural frequency was 2g and less than the theoretical values.

SELECTION OF FULL SCALE PLATFORM AND COMPUTED RESULTS3.1 INTRODUCTION

The platforms associated with production in offshore gas or oil fields are usually fixed platforms of which there are two main types:

- (a) steel platforms fixed to the seabed by piles;
- (b) concrete gravity platforms with large cellular bases which are flooded to keep them in position on the seabed.

The platforms are designed to last the production life of the field, which may be as much as thirty years, and any serious structural failure requiring shut-down of a platform would have serious economic implications; a catastrophic failure could also cause serious pollution. It is essential that methods be devised to detect serious structural failure at the earliest possible stage. The present investigation is concerned with the detection of such failures in members of fixed steel platforms.

Fixed steel platforms are constructed in two main parts, the jacket and the deck structure. The jacket consists of at least 3, and sometimes as many as 24, legs connected by horizontal and diagonal braces; the legs and bracing members are usually circular tubes.

In some jackets, the piles are driven through the legs and welded to the top of the jacket; in others they are driven through guides outside the legs and cut off above the mud line (skirt piles). The piles may extend 50 m or more into the seabed to give sufficient resistance to the shear force and overturning moment produced by the largest expected wave (100 year wave).

The deck structure is fabricated from tubular members, structural I-beams and flat plates; it is lifted into position and welded to the piles/jacket once piling is completed. Finally prefabricated modules containing machinery and accommodation units are installed on the deck structure.

3.2 DESCRIPTION OF PLATFORM

Before a particular platform configuration was chosen different aspects of jacket type platforms were considered. Platforms with three, four, six, and eight legs with diagonal, K- and/or X- bracing all appeared to be in common use in offshore gas and oil fields. However, for a limited research project of this nature it was necessary to select a reasonably simple structure, and a four-leg platform with K-bracing was chosen.

It was also realised that such a platform could not be designed by the author as this was a major task in itself and a number of companies and institutions in Norway, which might have a design of a suitable structure, were approached. Det norske Veritas (DnV) made available a design of a structure which had been used in checks on their computer programmes.

The platform was a conventional jacket-type structure, Figure 3.1, with piles through the legs and a 2-level superstructure. It was designed for a water depth of 70 m, and a 100 year wave of 24 m with a period of 15 secs. The cross-section of the jacket at mud line was 34 x 40 m and the taper angle 7 degrees.

The tubular legs had outside diameter (O/D) 1.14 m and wall-

thickness (W.T.) 0.0127 m and the piles were 1.07 m O/D. The 22 mm gap between leg and pile was filled with grout and this was assumed to give shear connection for the two to act as a composite beam. The jacket had five levels of K-bracing and the cross-sectional dimensions of the tubular braces varied from 0.66 x 0.016 m at the mud line to 0.46 x 0.0127 m in the splash-zone. The dimensions of the six horizontal levels of rhombic bracing reduced from 0.38 x 0.0127 m at the mud line to 0.36 x 0.0127 m above the water line.

The deck structure was greatly simplified in the computational model. It was taken as two decks of equal area 12.2 x 18.3 m, spaced apart vertically by 6.1 m and constructed of structural I-beams. The four legs were tubular members of 1.067 m O/D and 0.044 m W.T.

Tubular K-braces were used to stiffen the deck structure in the vertical plane, and the lower deck was 19.5 m above mean water level.

A table of joint numbers and X-Z-Y coordinates used in the computation is given in Table 3.1. The vertical axis of the structure was labelled Y and was equi-distant from all four legs. The origin was taken at the mean water level: thus the mud line was at elevation -70.104 m and the upper deck at elevation +25.527 m. There was a total of 88 joints.

To model the stiffness of the piles in the seabed the piles were assumed to be discontinued at elevation -77.1 m and replaced by a set of stiffness coefficients which were calculated by DnV and are given in Table 3.2. The angles θ_1 , θ_2 and θ_3 rotate the axis system of the support joints to agree with the pile/leg axis system.

Thus KFX was the axial stiffness of the piles and KFY and KFZ the lateral stiffness. The rotational stiffness was denoted by KMY and KMZ. The piles were assumed to have no torsional stiffness, hence $KMX = 0$

The structure had 208 members; these are listed in Table 3.3 and the cross-sectional properties are given in Table 3.4. For the purpose of a normal mode analysis the self-weight of the members with added liquid mass of water where applicable were worked out by DnV and lumped to the corner joints on seven levels, Figure 3.1A.

This was a great simplification of the actual mass distribution, but was considered sufficient to compute the fundamental modes with good accuracy. Higher global modes, however, cannot be computed with the same accuracy from this model, but as the object of the computation was to study changes in frequencies associated with changes in stiffness rather than absolute values of frequencies, this model was considered adequate. The lumped masses with their respective joints are given in Table 3.5. All of these masses were given dynamic degrees of freedom in the X and Z directions.

3.3 COMPUTED RESULTS

Natural frequencies and mode shapes were computed for the complete jacket structure, and then with a single diagonal in one K-panel removed. This brace was then replaced and the computation repeated with another brace removed: five were removed from each of two perpendicular faces of the jacket. The members removed are shown in Figure 3.1A .

Nine normal modes were computed: three sway modes in the XY and ZY planes and three torsion modes. The computed natural frequencies for the undamaged structure and with the ten members removed in turn are given in Tables 3.6 and 3.7. The percentage reductions in frequency associated with the removal of each member are also shown.

The computed mode shapes are contained in Tables 3.8 to 3.16 which give the normalised X and Z displacement of each of the joints to which masses were lumped.

3.4 DISCUSSION

The mode shapes of a space frame such as an offshore platform are complex. However, a simplified picture can be obtained if the displacements of an imaginary vertical centre line of the structure (the Y-axis in Figure 3.1) are plotted for the XY and ZY planes separately. Figure 3.2 shows the mode shapes of the undamaged platform for the first three sway modes in the ZY plane plotted from the computed mode shapes given in Tables 3.8, 3.12 and 3.15. The associated natural frequencies were 0.4, 1.385 and 3.015 Hz in the ratios 1 : 3.46 : 7.54.

In the fundamental mode the lateral normalised displacements of the jacket increased nearly linearly between level -51.8 m and level +6.1 m just above the waterline. There was then a sharp increase between elevations +6.1 m and +19.4 m due to the absence of K-bracing between the top of the jacket (el. +6.1 m) and the lower deck (el. +19.4 m); this is a common feature of offshore platforms in which jacket and deck structure are mated offshore.

In the second mode the lateral displacement remained almost constant from the -51.8 m level to sea level. Between sea level and the lower deck the displacements were in antiphase with considerable relative magnitude.

In the third mode, the displacements between the -51.8 m level and the lower deck level followed an approximate sine wave with nodes close to elevations -35 m and +19.4 m. The normalised displacements of the decks in the second and third modes were small compared to those in the fundamental mode.

The first three torsion modes were also obtained from the computed modal displacements in Tables 3.10, 3.13 and 3.16 by plotting the normalised rotation at each level. Figure 3.3 shows that these mode shapes are very similar to the sway mode shapes. This is not surprising since in a largely shear structure such as this a torsion mode can be regarded as approximately a combination of two sway modes with opposite sides of the jacket moving in antiphase. The torsion frequencies were 0.579, 1.466 and 3.681 Hz for the fundamental, second and third modes respectively in the ratios 1 : 2.53 : 6.36

The frequency tables computed for the damaged platform showed some interesting results; firstly in magnitude of the frequency changes and secondly in their distribution. Table 3.6 shows a reduction of almost 32% in the frequency of the second sway mode in the YZ plane when a K-brace between the mudline elevation -70.1 m and elevation -64.8 m (member 85) was removed. Removal of the same brace also reduced the fundamental sway frequency by 2.8% and the

third by 7.7%. The sway frequencies in the perpendicular XY plane were virtually unchanged, as member 85 does not contribute significantly to the sway stiffness in that plane. The sensitivity of all three torsion modes to removal of the member was small compared with that of the second sway mode, and the changes in torsion frequencies lay between the changes in sway frequencies in the two principal directions.

Table 3.6 also shows that removal of member 101 between elevation -19.8 m and -35. m has a maximum effect on the third Z sway mode, reducing its frequency by about 26.0% compared with 2.3% in the fundamental mode and 3.6% in the second. There were negligible frequency changes in the other principal direction. The biggest change in torsion frequencies was 2.2% in the third mode.

When member 117 in the splash-zone (el. +6.1 m, -6.1 m) was removed there was a drop of 8.0% in the fundamental frequency, 4.7% in the second, and 0.6% in the third. The trend in the torsion modes was similar with changes of 6.2% in the fundamental, 0.45% in the second, and 0.19% in the third.

Thus the frequency Table 3.6 shows that significant reductions in the natural frequencies occur when a K-brace is made inactive, and the pattern of changes gives an indication of the location of an inactive member.

Table 3.7 was compiled for 5 members removed in turn from the wider face of the structure. It shows a pattern of frequency changes similar to those of Table 3.6 but the percent changes were generally smaller. An extract from Tables 3.6 and 3.7 of maximum percent

changes is given below.

MODE	MEMBER	% REDUCTION SWAY Z	MEMBER	% REDUCTION SWAY X
1	117	8.0	114	8.5
3	109	20.1	106	16.1
3	101	25.6	98	23.0
3	93	19.7	90	18.8
2	85	31.8	82	25.2

The large changes in the second and third sway frequencies were not fully understood at this stage of the investigation. There was also some doubt about the beam element model which was a considerable simplification of the actual structure with only horizontal, translational dynamic degrees of freedom of the corner joints. It was decided that the next stage of the investigation would be the design and construction of a model platform for computational and experimental verification of the frequency tables.

CHAPTER 4MODEL PLATFORM DESIGN AND COMPUTED RESULTS4.1 INTRODUCTION

The normal mode calculations for the full scale platform were sufficiently encouraging to justify further work on a structure which might be constructed in the laboratory. The object of work in this chapter was thus:

- (a) to design a scaled down model having dynamic properties similar to those of the full scale structure;
- (b) to compute global and local normal modes up to the third torsion mode;
- (c) to compute normal modes with a number of structural changes;
- (d) to assess whether the frequency shifts were sufficient to warrant the construction and testing of a model platform.

4.2 DESIGN OF MODEL PLATFORM

The first constraint put on the model platform design was space available in the laboratory. Firstly, the height was limited to about 5 m to allow the structure to be erected and to allow enough work space between the ceiling and the platform deck. Secondly, existing anchor pads were to be used to bolt the structure to the concrete floor. These were at 1.07 m spacing and the base dimensions of the structure were to be confined to two pitch lengths (2.14 m x 2.14 m). Thirdly, consideration had to be given to the dynamic response of the electromagnetic shaker system available for testing the structure. It had a poor force/frequency response at low frequencies and thus the fundamental frequency of the structure had to be high enough to allow constant force input testing to be carried out from the fundamental frequency to the third torsion frequency. To achieve this the platform structure had to be designed such that its fundamental frequency was in the range 10 Hz to 15 Hz.

If the geometry of a structure is scaled exactly the natural frequencies will scale in proportion to the linear scaling factor. The full scale platform was about 100 m high including the deck sections, and thus, to give a model about 5 m high, 20 was used as the scaling factor.

This factor was used for all the basic member lengths in the jacket and if it had also been used for the cross-section dimensions of all members, and for all deck details, the fundamental sway frequency of the model would have been

$$20 \times 0.4 = 8 \text{ Hz} \dots\dots\dots(4.1)$$

However, this was not possible because of limitations in the available steel sections.

To estimate the fundamental sway frequency of a model made from the available steel, the model was considered as a single degree of freedom system with the mass concentrated at the deck. Thus the frequency was given by

$$f = \frac{1}{2\pi} \sqrt{\frac{k}{m}} \dots\dots\dots(4.2)$$

where k was the stiffness, and m the mass at the deck level. The mass was taken to be 250 kg which was $(1/20)^3$ of the deck mass of the full scale structure. The stiffness k was scaled from the full size structure by two approximate methods in which the structure was considered as

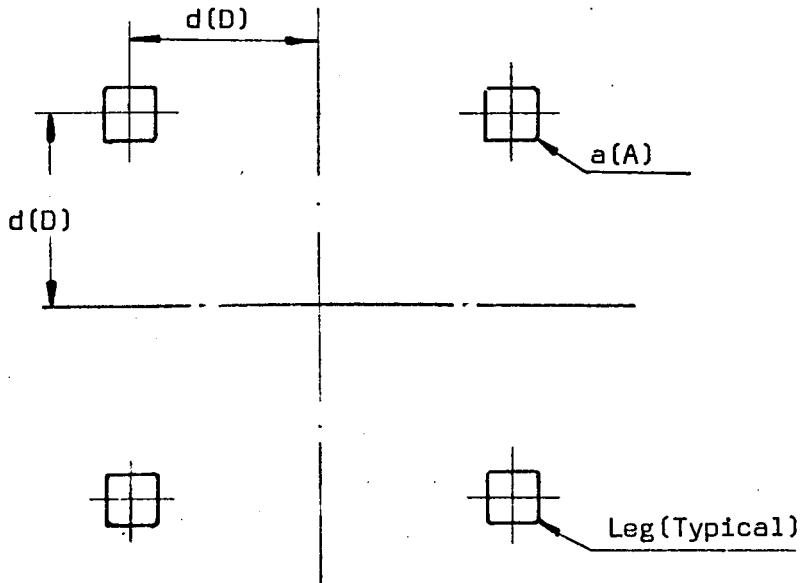
- (a) a cantilever fixed at its lower end;
- (b) pin-jointed

(a) Cantilever Estimate

$$k = \frac{W}{\delta} = \frac{3EI}{L^3} \dots\dots\dots(4.3)$$

where δ is the displacement at the deck caused by load W, and the second moment of area I was obtained from

$$I = 4ad^2 \dots\dots\dots(4.4)$$



Thus the ratio of stiffness of model (k) and full scale structure (K) was given by

$$\frac{k}{K} = \frac{ad^2}{AD^2} \left(\frac{L}{\ell}\right)^3 \dots\dots\dots(4.5)$$

with $L/\ell = D/d = 20$, and $A/a = 163$ (available steel), equation (4.5) gives

$$k = 0.123K \dots\dots\dots(4.6)$$

The stiffness of the full scale structure at deck level was 17500 KN/m and thus with equation (4.2)

$$f = \frac{1}{2\pi} \sqrt{\frac{0.123 \times 1.75 \text{ E7}}{250}} = 14.8 \text{ Hz} \dots\dots(4.7)$$

(b) Pin-jointed

If the two structures are considered as pin-jointed the distribution of forces will be the same in both of them if the ratio $\frac{L/EA}{\ell/Ea}$ is the same for all members. The value of L/ℓ was constant, but, with the steel available for the model A/a varied from about 163 in the main legs to less than 140 in some of the bracing members. If an average value of 150 is assumed the ratio of stiffness is

$$\frac{k}{K} = \frac{a}{A} \times \frac{L}{\ell} = \frac{20}{150} = 0.133 \dots\dots(4.8)$$

which compares well with the cantilever estimate.

These approximate calculations did not take into account scaling of the unbraced section of the platform between jacket and deck. More detailed calculations which did take it into account did not indicate large differences from the stiffness ratios already

calculated. The estimate of natural frequency from Equation (4.7) is within the desired range 10 to 15 Hz, but the fundamental frequency of the model could be adjusted by changing the deck mass and/or the support stiffness. The ratio of natural frequencies could also be adjusted to some extent by such mass change if this was found to be necessary.

The jacket design was based on these relatively simple calculations, and a drawing of the jacket is shown in Figure 4.1. All the members were of square cross section tube rather than circular as this greatly simplified fitting of the joints. A square cross section tube has the same I value about any axis through its centroid so it was unlikely that the use of square tube would lead to any significant difference in dynamic response. The legs were 63.5 x 63.5 x 4 mm and all bracing members were 25.4 x 25.4 x 3.2 mm section except those near the top of the structure deck marked A in Figure 4.1 - which were from 19 x 19 x 2. mm section. All joints were welded to an acceptable standard and the dimensions of the finished jacket were checked and found to agree well with design dimensions. The final overall dimensions were 1.8 x 1.5 m at the base, 0.9 x 0.5 m at the top, and the height without decks and base plates was 4.476 m.

A base plate shown in Figure 4.2 was designed to anchor the structure to the floor and at the same time to give some flexibility in the vertical direction. Vertical deflection was made possible by spacer washers fitted between the plates and the floor at each bolt location. The lay-out of the four base plates on the floor is shown in Figure 4.3.

The deck structure shown in Figure 4.2 was fabricated from 63.5 x 63.5 x 4 mm square hollow section and consisted of two main frames of dimension 1.8 x 1 m spaced by 0.31 m. The vertical bracing was also square hollow section 25.4 x 25.4 x 3.2 mm. Fixing pads were welded to the lower deck frame in three different positions to accept shaker assemblies. The mass of the deck structure with two shaker assemblies was approximately 260 kg and it was welded to the top of the jacket legs as shown in Figure 4.3. The total mass of the model was 500 kg and the total height 4.9 m.

4.3 BEAM ELEMENT MODEL

An isometric drawing of the structure is given in Figure 4.4. It shows the numbering of the jacket joints and of the leg joints at the decks. The joint coordinates for jacket and decks are listed in Table 4.1, the Y coordinates being measured from the waterline. Numbers 1 to 4 were given to the four support joints, and numbers 5 to 52 to real joints of the jacket; no intermediate (imaginary) joints were created as the number of real joints was considered sufficient to describe the required number of higher global modes and local modes involving groups of members. Joint numbers 53 to 103 were used for deck coordinates and four of these 51 joints (67, 68, 71, 72) were at the interface with the jacket. Two joints (82 and 90) were located between the decks at the centroids of the two shaker masses. The remaining 45 joints were used to describe the geometry of the decks.

Member incidences are given in Table 4.2, and a member is defined by the numbers of its two end joints. Member numbers 1 to 28 were allocated to the legs, 29 to 140 to the jacket braces, and 141 to 244 to deck members. The length of each member is also indicated.

Member properties and material constants are listed in Table 4.3 and estimated values of force and moment coefficients for the support plates are given in Table 4.4. These were estimated by assuming the support plate to be a simple cantilever. Thus

$$KFY = \frac{W}{\delta} = \frac{3EI}{l^3} \dots\dots\dots(4.9)$$

and

$$KMZ = \frac{M}{\theta} = \frac{EI}{l} \dots\dots\dots(4.10)$$

where l was the distance between the floor fixing bolt nearest to the jacket leg, and the centre line of the jacket leg. The I value was calculated from the cross-sectional dimensions without deduction for holes. Thus the estimate of KFY was

$$KFY = \frac{3 \times 2.1 E11 \times 0.48 \times 0.0245^3}{0.152^3 \times 12} = 117.6 E6 (N/M) \dots(4.11)$$

and similarly

$$KMZ = \frac{2.1 E11 \times 0.48 \times 0.0254^3}{0.152 \times 12} = 905.6 E3 (Nm/rad) \dots(4.12)$$

As the direction of KMZ thus calculated was not parallel with a global axis it was necessary to calculate an angle of rotation for each support joint. The definitions of support joint angles θ_1 , θ_2 and θ_3 were given in Chapter 3, Figure 3.1B.

The model structure (jacket and decks) consisted of 103 joints which were equivalent to 618 dynamic degrees of freedom. A problem of this size could not be run without major interruption of normal services to other computer users and a considerable reduction in dynamic degrees of freedom was necessary.

The first class of inertia forces considered to be of secondary importance were those associated with rotation of joints, and, through static condensation, all rotational dynamic degrees of freedom were eliminated.

It was also decided that no translational inertia need be allocated to the four support joints. A listing of dynamic degrees of freedom and the method of mass condensation (lumping) used is given in Table 4.5. All the joints of the jacket were given two

horizontal (X and Z) dynamic degrees of freedom and the leg joints, including the four which interface with the deck, were also given a vertical (Y) dynamic degree of freedom. The vertical inertia associated with all brace joints such as 9 to 12 in Table 4.5 were not considered large enough to retain. It was not likely that interesting local modes would be lost as a result of this decision. The jacket was thus modelled by 124 dynamic degrees of freedom as compared to 288 (joints 5 to 52) without reduction. Consistent mass condensation (lumping) was used at all joints of the jacket. A substantial reduction in degrees of freedom was also applied to the two decks. Figure 4.5 shows those joints which were completely eliminated, those which had only horizontal degrees of freedom, and those for which three translational degrees of freedom were retained. The final number of dynamic degrees of freedom for the whole structure was 215.

Lumped (concentrated) mass condensation (lumping) was used at all joints of the decks, and the mass of eliminated joints was distributed to nearby joints. As an example, the mass of joint 57 was divided into three equal parts and added to joints 59, 67 and 69. Figure 4.5 shows that no vertical dynamic degrees of freedom were retained for the top deck, and the vertical inertias of this deck were therefore added to the joints of the lower deck. As an example, the inertia of joint 74 was added to the vertical inertia of joint 54.

The shaker assembly was modelled as two concentrated masses linked by a massless beam element as explained in Chapter 2,

Section 2.5. Two shaker assemblies were used, and Figure 4.5 indicates that these were attached to joints 69 and 70 on the lower deck. Joints 82 and 90 were introduced to carry the mass of the shakers, and these joints were located at 0.171 m above the lower deck.

4.4 COMPUTED RESULTS

Natural frequencies and mode shapes were computed for the complete model platform and then with a single diagonal member in one panel removed. The member was then replaced and the computation repeated with another member removed. In all, seven members were removed; five from one of the faces parallel to the Z axis, one from a face parallel to the X axis, and one horizontal brace at level 5. The members removed are shown in Figure 4.4.

Twenty normal modes were computed; three sway modes in the XY and ZY planes, three torsion modes, one vertical mode, four modes characterised by different deck movements and six local modes. The computed natural frequencies for the undamaged structure and with seven members removed and replaced in turn are given in Tables 4.6 to 4.9. Table 4.6 lists results for the first six sway modes and first three torsion modes with the five members in a face parallel to the Z axis removed and replaced in turn. Results for the eleven remaining modes are given in Table 4.7. Tables 4.8 and 4.9 give the corresponding results for members 135 and 118.

The computed mode shapes for the undamaged structure are contained in Tables 4.10 to 4.18 for the first six sway modes and the first three torsion modes. Only the displacements at the main leg joints of each level are given and these were normalised by dividing by the maximum X, Y or Z displacement of that mode. The joints at which this maximum displacement occurred are indicated and often did not occur at corner joints. The six local mode shapes are contained in Tables

4.19 to 4.24, and the remaining five mode shapes in Tables 4.25 to 4.29.

Only reduced sets of mode shapes were tabulated for the simulated damage conditions. For the removal of five members in a face parallel to the global Z axis only the first three sway modes in the Z direction were tabulated, and for member 135 removed only the first three sway modes in the X direction. A summary of these tabulated results is given below

MEMBER NO. REMOVED	MODE IDENTIFICATION	TABLE NO.
84	Z,1; Z,2; Z,3	4.30 to 4.32
92	Z,1; Z,2; Z,3	4.33 to 4.35
100	Z,1; Z,2; Z,3	4.36 to 4.38
104	Z,1; Z,2, Z,3	4.39 to 4.41
102	Z,1; Z,2; Z,3	4.42 to 4.44
135	X,1; X,2; X,3	4.45 to 4.47

No modes were tabulated for member 118 removed because the computed frequency changes were too small to be of any significance.

The sensitivity of the natural frequencies to increases in deck mass was also studied and Table 4.48 lists the natural frequencies for the first six sway modes and first three torsion modes with increases in deck mass of 5% and 100%. The frequencies for the other eleven modes are given in Table 4.49. Important mode shapes were tabulated for the two deck load conditions and they are listed below with the relevant table number.

DECK MASS INCREASED BY	MODE IDENTIFICATION	TABLE NO.
5% (12.8 kg)	Sway Z,1	4.50
5%	Sway X,1	4.51
100% (256 kg)	Sway Z,1; X,1	4.52, 4.53
100%	Torsion 1	4.54
100%	Sway Z,2; X,2	4.55, 4.56
100%	Torsion 2	4.57
100%	Sway Z,3; X,3	4.58, 4.59
100%	*Torsion 3	4.60

* Very distorted, may not be a proper torsion mode

Finally, the effect on the natural frequencies of two support changes were computed, and the results for rigid supports and a 10% reduction in the vertical support stiffness are listed in Table 4.61 for the first six sway and three torsion modes. Natural frequencies for the eleven remaining modes are given in Table 4.62. Mode shapes were not tabulated for either of these changes.

4.5 DISCUSSION OF COMPUTED NORMAL MODES

The beam element model of the scaled down structure was more detailed than that of the full scale structure and this gave rise to a number of modes not obtained in the full scale computation. Eleven additional modes were found between the first fundamental sway mode and third torsion mode to give a total of twenty modes. All the mode shapes were tabulated in a way which emphasised important characteristics, and only a reduced set of joints and their normalised X, Y and Z modal displacements were listed.

4.5.1 Sway Modes

Table 4.10 was compiled from the first computed normal mode at 15.07Hz and included the normalised X, Y and Z modal displacements of the legs from level 2 to level 7. The displacements of level 8 and 9 were obtained from the deck legs which were extensions of the jacket legs. No vertical (Y) displacements were available for level 9 as these degrees of freedom were not included in the dynamic model. From the displacements the mode was interpreted as the fundamental sway mode in the Z-direction with the maximum displacement at joints 73 and 74 of level 9. From the Z displacements it was clear that the mode shape also contained some rotation, but that the major movement was horizontal translation in the Z-direction. The rotation was caused by the mass asymmetry of the lower deck with one shaker offset along the X-axis. The mean displacements were also normalised by taking the maximum value as unity.

The other five sway modes were tabulated in the same way and Table 4.11 contains the fundamental sway mode in the X-direction. The frequency was 16.46 Hz and the mode shape was symmetric about the XY plane. The mean mode shapes of the fundamental modes of the model platform and the full scale platform were not significantly different; both structures showed a considerable increase in displacement between level 7 and level 8 because of the lack of shear bracing between these levels. The ratios of the fundamental frequencies of the two platforms (model/full scale) were 37.7 and 38.6 in the Z- and X-directions respectively. These were about 1.8% and 11.2% higher than estimates based on Equation (4.7).

The second normal mode in the Z-direction was at 62.59 Hz (Table 4.13) and the frequency ratio of model/full scale platform was 45.2, or 20% higher than the fundamental ratio. The maximum displacement occurred at level 5 and the mode shape contained some rotation. The deck structure and jacket were 180 degrees out of phase and the node plane was between levels 7 and 8.

The second normal mode in the X-direction was at 64.48 Hz (Table 4.14) and the frequency ratio model/full scale was 47, or 22% higher than the fundamental ratio. The maximum displacement occurred at level 6 and the mode shape was symmetric about the XY plane with the node plane again between levels 7 and 8. It was noticed here that the order of the second modes of the model platform was reversed from that of the full scale platform (Table 3.6)

The third sway mode in the Z-direction occurred at 136.02 Hz (Table 4.16) and the model/full scale frequency ratio of 45 was

similar to that of the second modes. The maximum displacement was at level 7, and the mode was not symmetric about the ZY plane. There were two 180 degree phase changes, between levels 4 and 5 and levels 8 and 9. Finally, the third sway mode in the X-direction was at 143.89 Hz (Table 4.17), and the frequency ratio of model/full scale was 46 and again similar to the other second and third modes. Maximum displacement occurred at level 7 and the mode was symmetric about the XY plane. The two node planes were between levels 4 and 5 and levels 7 and 8. In both third modes the upper node plane was very close to level 8, above it for the mode in Z-direction (Table 4.16) and below it for the mode in the X-direction (Table 4.17).

The frequency ratios for the second and third sway modes were all about 20% higher than the ratios for the fundamental frequencies, probably due mainly to the rigid lateral supports used in the model platform. Differences in mass distribution between model and full scale may be a further reason.

The normalised mean mode shapes for the three sway modes in the Z-direction were plotted and given in Figure 4.6. A comparison with the mode shapes for the full scale structure plotted in Figure 3.2 revealed no important difference between the first and second mode shapes. In the third mode the model structure exhibited considerably more displacement at level 9.

4.5.2 Torsion Modes

The first torsion mode shape is contained in Table 4.12 and the layout of the table was similar to the table of sway modes except for the calculation of the mean mode shape. The angle of rotation at each level was calculated from the relative displacement of opposite faces and

normalised to give the results shown in the second last column of Table 4.12. From this a normalised mean rotation was calculated and is listed in the last column of Table 4.12.

The natural frequency of the first torsion mode was 19.45 Hz and the frequency ratio of model/full scale platform was 33.6 or about 11% less than the ratios for the two fundamental sway frequencies. It can be seen from the second last column that the rotation calculated from X and Z displacements were within about 5% of the mean values. The offset of the centre of twist along the x axis, apparent from the tabulated displacements, is due to the mass of the offset shaker assembly. The rotation increased significantly between levels 7 and 8. This was also found for the full scale platform and the fundamental sway modes, and was caused by the lack of shear bracing in this section of the structures.

The second torsion mode was at 81.44 Hz (Table 4.15), the frequency ratio model/full scale was 55.6, or about 50% higher than the ratio for the fundamental sway frequencies, and the node plane was below but close to level 8. Difference in mass distribution of the decks in model and full scale, which had all masses lumped to leg joints, may account for the increased frequency ratio model/full scale in this mode.

The third torsion mode occurred at 169.1 Hz (Table 4.18) and the model/full scale frequency ratio of 46 was 22% higher than the ratio for the fundamental sway frequency. The nodal planes for X and Z displacements occurred at different levels, but the mean rotation showed nodal planes between levels 4 and 5 and levels 7 and 8, and the mode was classed as the third torsion mode.

4.5.3 Other Global Modes

Another five global modes were found in the frequency range of interest. These modes did not exhibit useful sensitivity to the kind of structural damage simulated in this work, but as some of them can be confused with the second and third mode groups it was considered necessary that they be studied. The first of the five modes was found at 84.18Hz and the mode shape is contained in Table 4.25. The layout of the table is similar to that used for the sway modes except for the addition of four corner joints from the lower deck (Figure 4.5). The vertical displacement of these four joints was important in identifying the five mode shapes. From Table 4.25 it was found that the mode exhibited a strong content of vertical displacement as well as some displacement in the global X-direction, but negligible displacement in the Z-direction. The pattern of vertical displacement suggested the mode to be the fundamental vertical mode with rotation of each level about the global Z-axis due to the mass asymmetry on the lower deck. This also gave rise to the X-displacements. The mode shape in Table 4.25 showed that for the X-displacements there were three horizontal node planes - between levels 6 and 7, 7 and 8 and 8 and 9, and if horizontal displacements only were measured the mode might be mistaken as a higher X-mode.

The next global mode was found at 90.60 Hz and the mode shape is given in Table 4.26. It is also characterised by rotation of the deck structure about an axis parallel to the global Z-axis together with vertical displacements at each level. The axis of rotation was between the two shakers but was closest to the offset one. The vertical mode (Table 4.25) exhibited similar rotation of the decks, but the axis of rotation was on the opposite side of the global ZY plane and both shakers were moving in phase. The X displacements of the mode at 90.6 Hz were similar to those of

the vertical mode and from measurement of X and Z displacements at locations at levels 3, 7 and 9 the two modes would appear very similar. However, they could be distinguished by measurement of vertical displacements of one of the two decks. Thus the mode at 90.60 Hz (Table 4.26) is referred to as a "deck pitch" mode, because rotation of the deck occurs about an axis parallel to the global Z-axis (the shorter side of the deck) and the position of this axis of rotation is between the two shaker masses.

The third of the additional global modes was found at 101.35 Hz, and the mode shape is given in Table 4.27. There were considerable displacements in the Z-direction and three node planes were found; between levels 4 and 5, 7 and 8 and 8 and 9. The calculated mean vertical displacements were small and not useful for interpretation of the mode shape. However, from the vertical displacements it was clear that legs on opposite sides of the global XY-plane were moving in antiphase and that the decks were rotating about an axis parallel to the global X-axis. This was parallel with the longer side of the deck and the mode was thus named a "deck roll" mode. It was clear that identification of this mode shape would also require measurement of vertical displacements at one of the decks. The mode might be confused with a second sway mode if horizontal measurements only were made at levels 3, 7 and 9.

Another mode was found at 127.44 Hz and Table 4.28 gives the mode shape. It was also identified by the vertical movement of the legs and corner joints of the decks. Diagonally opposite legs moved in phase resulting in a twist movement of the decks, and the mode was named a "deck twist" mode. The pattern of mean

displacements in the Z-direction were similar to that of a third sway mode.

The last of the five additional modes occurred at 159.73 Hz and the mode shape is given in Table 4.29. The mode was again characterised by the movement of the decks and, from the vertical displacements of level 8, the deck was found to bend about an axis parallel to the global Z-axis. The mode was therefore named "deck bending" and the maximum displacement was at the centre shaker (joint 90) which moved in anti-phase with the vertical displacements of the decks. The horizontal displacements in the X and Z directions were small compared to the vertical displacements of the decks but the mean X displacements showed a node plane between levels 4 and 5, and between levels 8 and 9. The mode might therefore be mistaken for a third sway mode in the X-direction if horizontal measurements only were made.

4.5.4 Ovalising Modes

The fourteen modes so far discussed were global modes and the remaining six were local modes which mainly involved a small group of members. These modes resulted from horizontal vibration of level 2 to 7 and the mode shape at each level is plotted in Figure 4.7. The mode was termed an "ovalising" mode because parallel sides of the level were moving in anti-phase to create an impression of alternating expansion and contraction. There was no lateral displacement of the corner joints, but some rotation about the global Y axis. The first ovalising mode occurred at 39.60 Hz and

the mode shape can be deduced from Table 4.19 which shows levels 3 to 7 to have a shape similar to that at level 2 but with reducing amplitude.

In the second ovalising mode at 46.39 Hz the maximum displacement occurred at level 3 and levels 4 to 7 moved in phase with level 3 (Table 4.20). Level 2, however, moved in anti-phase, thus there was an imaginary node plane between levels 2 and 3.

Table 4.21 gives the mode shape for the third ovalising mode at 57.99 Hz. The maximum displacements were now at level 4 with the node plane between levels 3 and 4. In the three remaining ovalising modes at 79.15 Hz (Table 4.22), 101.75 Hz (Table 4.23) and 155.47 Hz (Table 4.24) the maximum displacements occurred at levels 5, 6 and 7 respectively, with a phase change below these levels.

4.6 DISCUSSION OF NORMAL MODE SENSITIVITY

TO MEMBER SEVERANCE

4.6.1 Sway and Torsion Modes

The effect on natural frequencies of removing five members in turn from one face of the structure (Figure 4.4) can be seen from Table 4.6 and 4.7. The six sway and three torsion frequencies are given in Table 4.6 and the frequencies for the other eleven modes are listed in Table 4.7. The percentage changes from the frequencies of the undamaged structure are also included in the Tables. For all the main sway or torsion modes the natural frequencies were either reduced or remained unchanged. The largest reduction was 29.6% for the sway mode Z,2 when member 84 (in the lowest panel between levels 2 and 3) was removed. Apart from a drop of 8.7% in the second torsion frequency all the other reductions were less than 3%. Frequency changes less than 1% are regarded as insignificant for the present purpose and are marked N.C. (no change) in the Tables.

Three Tables of mode shapes were also compiled for member 84 removed and Table 4.30 contains the joint displacements for the fundamental sway Z,1 mode. The layout is the same as that used previously for sway modes but there is an additional column giving percentage differences between the mean displacement at each level for the damaged and undamaged structure. The mean mode shape of the damaged structure (Table 4.30) was normalised such that this mean displacement of level 7 was the same for both undamaged and damaged mode shapes. Level 7 was chosen because it was close to an antinode of the important higher modes. From Table 4.30 it

was clear that the maximum distortion of the mode shape occurred at level 3. An increase of 67% in normalised displacement was calculated for this level, and for level 2 an increase of 39%. These figures suggest that the location of a failed member could be detected from mode shape measurements. However, this is unlikely to be practicable because of the large number of underwater transducers that would be required to monitor the mode shape in sufficient detail.

The second sway mode in the Z-direction with member 84 removed is given in Table 4.31. The maximum distortion was 139% at level 3 with 126% at level 9, and this did not seem unreasonable for a frequency reduction of 29.6%. Table 4.32 shows the third sway mode in the Z-direction. The largest distortion was 41% at level 8 with -32% at level 2. These distortions were higher than anticipated for a natural frequency reduction of only 1.9%

Acceleration receptances were computed and plotted with and without member 84 removed and Figures 4.8 and 4.9 show the receptances at joints 49Z and 52Z, both at level 7 (Figure 4.4). The excitation was applied at the offset shaker position, joint 82Z. From these receptance plots the change in the second mode at 62.59 Hz before to 44.09 Hz after member 84 was removed is clear. It can also be seen from Figure 4.8 that the response magnitude at joint 49Z of the second torsion mode dropped by more than one order of magnitude. Receptances were also plotted for the response at joints 49X and 50X, both at level 7 (Figure 4.4), for excitation at joint 82X and these plots are given in Figure 4.10 and 4.11.

Both plots are identical and they show a small change ($<+1\%$) in the third sway mode at 143.9 Hz (Table 4.6).

Removal of member 104, a K-brace between levels 5 and 6, produced the next largest frequency reduction; 24.1% in the third sway mode. There was also a reduction of 8.1% in the third torsion frequency but the changes in the other frequencies were again less than 3%. The fundamental sway mode shape with member 104 removed is given in Table 4.39; at level 2 the normalised displacement dropped by 8.3% and at levels 3 and 4 it decreased by 10%. The shape of the sway mode Z,2, contained in Table 4.40, shows the maximum reduction in normalised mean displacement to be 11% at levels 4 and 5. The corresponding reduction in natural frequency was less than 1% (Table 4.6). In the third Z-direction sway mode (Table 4.41) the nodes of the mean mode shape moved from below to above level 5 (-232%) and from above to below level 8 (-220%) for a change of 24.1% in natural frequency.

The largest reduction in a fundamental sway frequency occurred when member 102 was removed. This was a K-brace between levels 6 and 7, and it contributed mainly to stiffness in the global ZY plane. The reduction was 9.6% compared with less than 3.4% in the other eight natural frequencies listed in Table 4.6. The fundamental sway mode shape in Table 4.42 showed reductions of about 20% in the mean normalised displacements below level 7. The second sway mode shape in Table 4.43 showed generally larger displacements than the undamaged mode shape, with the exception of level 9 (-21%). The frequency reduction was 3.4%. The third sway mode shape is contained in Table 4.44. All levels showed a reduction in the mean

normalised displacements and the maximum reduction , 56% , occurred at level 8. The corresponding frequency reduction was less than 1%.

Removal of members 92 and 100 produced similar effects to those already discussed; the largest frequency reductions were 15.1% in the mode Z,2 for member 92, and 20.6% in mode Z,3 for member 100. The sway modes for member 92 are given in Tables 4.33 to 4.35, and for member 100 in Tables 4.36 to 4.38.

The sixth K-brace removed was member 135 between levels 5 and 6 and it contributed to structural stiffness in the global XY-plane (Figure 4.4). The effect of removing this member was similar to removing member 104 but the reductions occurred in the X mode frequencies. There was a 20.9% reduction in the third sway frequency X,3 but only small changes in the other frequencies (Table 4.8). The distortion of the fundamental (Table 4.45) and second (Table 4.46) sway modes was small. The third sway mode shape (Table 4.47) showed a node movement from below to above level 5 (-443%), and a considerable relative increase of the displacement at level 8 (336%).

Finally, the effect of the removal of member 118 on the nine global modes was found to be negligible (Table 4.8). The member is part of the horizontal rhombic bracing at level 5 and would not be expected to contribute significantly to the global modes.

4.6.2 Ovalising and Other Global Modes

The frequency tables for the six ovalising and the remaining five global modes are given in Tables 4.7 and 4.9. The five global modes did not exhibit useful sensitivity to removal of any of the

six shear braces and the largest frequency reduction was 5.7% in the "deck roll" mode when member 102 was removed.

The overall effect on the ovalising modes was even less and what changes did occur were increases in natural frequency indicating that the member removed contributed to the mode by its mass more than by its stiffness. The effect on the fourth ovalising mode with member 118 removed was small considering that this member was part of the rhombic bracing of level 5, and it is conceivable that the change in mass and stiffness are comparable.

4.6.3 Deck Load Changes

There may be several changes in the deck load of an offshore platform during its operational life and, to obtain some information on the sensitivity of normal modes to deck mass changes, Tables 4.48 and 4.49 were compiled. For a mass increase of 5% in an offset position (joint 99, level 8) there was a small reduction (<3%) in the fundamental group of frequencies. The change in the fundamental sway mode shapes was negligible as shown by Tables 4.50 and 4.51.

The trend for a substantial mass increase (100%) distributed equally between the four deck leg joints of levels 8 and 9 is evident from Tables 4.48 and 4.49. The frequencies of both the fundamental sway modes dropped by approximately 25% and there was a reduction of about 20% in the first torsion frequency. In the second group the largest reduction was 3.1% (Table 4.48) and in the third group the two sway frequencies dropped by 3.4% and 1%. A large reduction of 18.5% was indicated for the third torsion

frequency. The changes in the mean mode shape for this mode are contained in Table 4.60 and the values suggest that either the torsion mode shape has been fundamentally changed or a new mode has preceded the third torsion mode in the first twenty modes computed. The latter is the most likely explanation. The changes in the mode shapes for the fundamental group (Tables 4.52 to 4.54) were small but in the second mode group (Tables 4.55 to 4.57) the sway mode shapes showed reductions in the normalised displacements at most levels consistent with movement of the nodal plane towards level 8. The same trend was apparent for the third sway modes (Tables 4.58 and 4.59), and it was because the deck was near a nodal plane in the second and third mode groups that the frequencies were relatively insensitive to increases in deck mass.

Of the other five global modes (Table 4.49) the deck bending mode showed no change with a mass increase. This is explained by the fact that the mass increase was applied to the deck legs and this mode was governed mainly by the vertical movement of the centre shaker (joint 90, Figure 4.5, Table 4.29). The other four modes showed frequency reduction between 14.8% and 18%.

4.6.4 Support Stiffness Changes

The support stiffness is also an important parameter in an offshore structure. The results in Table 4.61 and 4.62 are for rigid support (zero displacements in the Y-direction at joints 1 to 4 as well as in the X-andZ-directions) and for a 10% reduction in the vertical stiffness coefficient. Reducing the vertical displacements at the supports to zero increased the frequency of the vertical

mode by 22.7% and the fundamental sway modes by 12% to 15%. For a 10% reduction in the vertical stiffness coefficient the largest reduction in frequency was 1.4% in the fundamental sway Z,1 mode.

These results suggest that while an assumption of rigid supports may lead to large errors in the estimates of natural frequencies, acceptable accuracy may be expected from reasonable engineering estimates of stiffness coefficients. Any further study of the effect of structural changes on natural frequencies should include changes in lateral support stiffness. Removal of a brace in a bottom panel produced a large change in a second sway mode, and reduction in lateral support stiffness may have a similar effect.

4.6.5 The Shear Structure

The computer experiments on the model platform predict that failures of inclined members in the K-braced panels produce reductions of up to about 30% in natural frequencies. The frequencies most affected by damage depend on the plane and the level of the plane in which the damage has occurred. For example, when members 84 and 100 are damaged, the sway frequencies in the XY-plane are not affected. The largest changes in the second sway frequencies occur when the bottom panel is damaged while the third sway frequencies are most affected by damage to middle panels. The fundamental sway frequencies are not much affected (2 to 10%) by damage to any of the panels. This result was surprising at first sight and it was investigated further.

Much of the deformation in the sway modes comes from shear displacements in the panels. If one of the inclined K-braces fails, the companion brace cannot transmit direct load without primary

bending of the horizontal member to which it is attached. Thus the second inclined member is virtually inactive and the transverse shear force transmitted by the panel must then be carried by the legs. As bending deformation in legs replaces axial deformation of panel members, the stiffness of panel in shear is substantially reduced. If reduced to zero, the panel on opposite face of structure must transmit twice the shear force; and the shear displacement of panels (relative displacement of levels at top and bottom) will be doubled.

For example the ratio of mean displacement in the fundamental sway mode (Table 4.10) between levels 2 and 3 was 3.5, and after member 84 was removed (Table 4.30) the ratio increased to 4.22, ie. 72%. There is a **smaller** reduction in panel stiffness if a horizontal member in a panel fails. Another feature of the structure is that the top panel (below the deck) does not have inclined braces and its shear stiffness is much less than the other panels. Also the mass at deck level is about half the total mass of the structure. A simple shear model shown in Figure 4.12 can be used to illustrate some of the more important effects. For an applied load W the displacement at deck level is given by

$$\delta = \delta_1 + \delta_2 + \dots + \delta_5 \dots\dots\dots(4.13)$$

and stiffness K at this level is given by

$$K = \frac{W}{\delta} = \frac{W}{\delta_1 + \delta_2 + \delta_3 + \delta_4 + \delta_5}$$

$$= \frac{W}{\delta_1} \times \frac{1}{(1 + \delta_2/\delta_1 + \delta_3/\delta_1 + \delta_4/\delta_1 + \delta_5/\delta_1)}$$

or

$$K = k_1 \times \frac{1}{(1 + \delta_2/\delta_1 + \delta_3/\delta_1 + \delta_4/\delta_1 + \delta_5/\delta_1)} \dots\dots(4.14)$$

where k_1 is shear stiffness of top panel remaining unchanged and small compared to the shear stiffness of the other panels. The terms δ_2/δ_1 , δ_3/δ_1 , etc. are obtained from centre line displacements (normalised to unity at deck). $\delta_2 = u_2 - u_3$ etc. where u_2 is displacement of level 2 etc. From Equation (4.14) it can be deduced that the shear stiffness of the structure at deck level is proportional to the shear stiffness of panel 1 and that the stiffness of the other panels only have a secondary effect on K . Thus the fundamental sway frequencies are largely controlled by the low stiffness of the top panel. However, if the stiffness of the top panel had been braced with similar stiffness to the other panels it becomes apparent from Equation (4.14) that the shear stiffness of the platform is governed equally by **all** panel stiffnesses.

Deformation associated with bending (legs in axial tension and compression) and kinematics of tapered panels in shear (counteracts displacements at deck from bending of structure) make the displacement pattern complex and a simple sketch in Figure 4.13 was drawn to clarify this point. A model with five dynamic degrees of freedom can also be used to illustrate effects of reduced panel stiffness on higher sway modes and one account of this is given in paper [13].

The changes in torsion frequencies produced by damage are smaller than the changes in sway frequencies, but the trends are similar. For sway in one plane there are only two panels between level contributing to shear stiffness; in torsion all four panels contribute.

CHAPTER 5EXPERIMENTS ON MODEL PLATFORM5.1 INTRODUCTION

The frequency shifts calculated in chapters 3 and 4 for the full scale and model platforms were considered large enough to justify construction and testing of the model platform. The objects of experiments on the model platform were:

- (a) to measure and identify natural frequencies and mode shapes;
- (b) to confirm some of the predicted frequency shifts when members were removed;
- (c) to confirm that the main natural frequencies and mode shapes could be obtained with broad band random excitation.

5.2 EXPERIMENTAL RESULTS

5.2.1 Method of Test

Figure 5.1 shows the model platform and associated test equipment. The method of test was essentially the same as that described in chapter 2 section 2.2.6, and it included two electromagnetic shakers which were attached to the lower deck, with the shaker power cables suspended from the centre of the deck. The accelerometer preamplifiers and their co-axial leads were also attached to this central cable and were thus clear of the structure. An accelerometer can be seen attached to a leg between levels 3 and 4 by a magnetic base, and a light weight co-axial cable connects it to the preamplifier on the adjacent stool. A 75Ω co-axial cable runs from the preamplifier to a signal amplifier in the instrumentation rack. This rack includes other equipment described in chapter 2, a Transfer Function Analyser (TFA), two channel Power Amplifier, two Oscilloscopes and an Ultra-Violet Recorder.

A Brüel & Kjaer Sweep Sine Generator and Level Recorder was used for plotting the frequency response to constant force input, as for the plane frames.

5.2.2 Determination of Natural Frequencies and Mode Shapes

A typical response plot at joint 49X (Figure 4.4) is shown in Figure 5.2. The excitation was from the offset shaker (joint 82X, Figure 4.5) with a force of 2.6 Newtons RMS over the frequency range 12 Hz to 200 Hz. The plot (Figure 5.2) which has logarithmic scales on both axes shows that the maximum acceleration exceeded

0.1 g RMS for the fundamental sway X,1 mode.

A number of frequency response plots was recorded at different locations for inputs from one or other of the shakers as listed below.

EXCITATION AT JOINT	RESPONSE AT JOINT	FREQUENCY RANGE (Hz)	FIGURE NUMBER
82X	49X	12-200	5.2
82Z	49Z	12-200	5.3
90Z	49Z	12-200	5.4
90X	49X	100-130	5.5
90X	40X	100-130	5.6
90X	32X	100-130	5.7
90X	24X	100-130	5.8
90X	16X	100-130	5.9
82X	53Y	50-130	5.10

One of the features of Figures 5.3 and 5.4 is the reduced response at 19.5 Hz and 67.8 Hz when the excitation is changed from the offset shaker to the centre shaker. Figures 5.5 to 5.9 show the response in the X-direction at 5 joints down one leg (levels 7 to 3 inclusive) for the frequency range 100 Hz to 130 Hz. It is apparent that in the mode group at about 120 Hz there is a node close to level 4 (Figure 5.8).

The vertical response at the lower deck (joint 53Y, Figure 4.5) for excitation from the offset shaker at joint 82X is shown in Figure 5.10. The peaks in this plot include the fundamental vertical

mode and the deck pitch mode predicted by the computation.

The frequencies of resonant peaks in Figures 5.2 and 5.3 were taken to be the natural frequencies of the structure and they were determined accurately with the Transfer Function Analyser.

When a natural frequency had been accurately determined the input force was adjusted to a convenient level (2.6 Newtons or 4.3 Newtons RMS) and response measurements were then taken. One accelerometer was used, and the measurements were taken in the X,Z and Y directions at the four corner joints of the two decks, (levels 8 and 9), and in the X and Z directions at the four corner joints of levels 3 and 7 on the jacket.

The response amplitude and phase angle (in or out-of-phase) at these locations were recorded and used to determine the mode shapes given in Tables 5.1 to 5.8 as detailed below. At a fixed frequency the measured accelerations are proportional to displacements and to obtain normalised displacements the accelerations were divided by the magnitude of the largest value measured in the test for a particular mode.

MODE	EXCITATION AT JOINT	EXCITATION FORCE (N) RMS	TABLE NO.
Sway Z,1	90Z	4.3N	5.1
Sway X,1	90X	4.3N	5.2
Torsion 1	82Y	2.6N	5.3
Sway Z,2	90X	4.3N	5.4
Sway X,2	90Z	4.3N	5.5
Torsion 2	82Z	2.6N	5.6
Sway X,3	82X	2.6N	5.7
Sway Z,3	82Z	2.6N	5.8

A convenient way of comparing measured with computed mode shapes was needed and Tables 5.1 to 5.8 also contain computed mode shapes. A diagram with explanation of mode shape table layout and the way mode shapes were normalised is given in Table 5.1B.

5.2.3 Removal of Members

Member 84 (Figure 4.4) was removed and the sweep sine tests were repeated to obtain the new natural frequencies. Before number 135 was removed, tests were carried out again with member 84 replaced to ensure that the original frequency response had been restored.

The response plots recorded at joint 49 in the X- and Z- directions for excitation at joint 82 are listed below.

	FIGURE NUMBER	EXCITATION AT JOINT	RESPONSE AT JOINT	FREQUENCY RANGE (Hz)
Base Line 84 removed	5.11 5.12	82Z	49Z	12- 24
Base Line 84 removed	5.13 5.14	82Z	49Z	30- 90
Base Line 84 removed	5.15 5.16	82Z	49Z	115-130
Member 84 replaced	5.17 5.18 5.19	82Z	49Z	12- 24 30- 90 115-130
Base Line 135 removed	5.20 5.21	82X	49X	12- 30
Base Line 135 removed	5.22 5.23	82X	49X	35-110 35-100
Base Line 135 removed 135 removed	5.24 5.15 5.26	82X 82X	49X 49X	115-130 90-100

Mode shapes were also measured for those natural frequencies which exhibited large changes, and Tables 5.9 and 5.10 contain the modified sway Z,2 and sway X,3 modes respectively.

5.3 DISCUSSION OF MEASURED AND COMPUTED NATURAL FREQUENCIES AND MODE SHAPES, AND THE EFFECT OF MEMBER REMOVAL

5.3.1 Fundamental Mode Group

From the measured frequency response at level 7 joint 49, shown in Figures 5.2 and 5.3, two groups of peaks are easily identified, and the three peaks in the first group are the fundamental modes. In Figure 5.2 there is a dominant peak at 16 Hz and two other peaks at 14.2 Hz and 19.5 Hz, and, as the excitation was in a plane of symmetry of the structure (XY-plane) and in the X-direction, it followed that the peak at 16 Hz was the fundamental sway mode in the X-direction (Table 5.2). The fact that two other modes at 14.2 Hz and 19.5 Hz were also excited indicates that the structure was not perfectly symmetric or that the excitation was not applied exactly in the plane of symmetry.

The response plot of Figure 5.3 was recorded for excitation in a plane perpendicular to the XY-plane at joint 82Z (Figure 4.5, offset shaker). The two peaks at 14.2 Hz and 19.5 Hz are both larger than the peak at 16 Hz and they were identified as the fundamental sway mode in the Z-direction (Table 5.1) and the fundamental torsion mode (Table 5.3). The torsion mode can be distinguished from the sway mode by the out of phase displacements, for example at joints 73X and 74X (Table 5.3). The peak at 16 Hz should theoretically not have been excited and its presence is a further indication of a slight asymmetry in the structure. Higher modes were similarly identified from Tables 5.4 to 5.8 and Table

5.11 gives a summary of measured and computed natural frequencies and percent difference between them.

The frequencies in the fundamental group were computed with good accuracy; the difference being 6.1%, 2.9% and -0.3% for sway Z,1, sway X,1 and torsion 1 respectively. Tables 5.1, 5.2 and 5.3 give the measured mode shapes and a plot of sway Z,1 mode is given in Figure 5.27. A comparison of the normalised mean displacements at levels 9, 8, 7 and 3 with the corresponding computed displacements (Tables 5.1, 5.2 and 5.3) shows generally good agreement. The main discrepancy is in the sway Z,1 mode at level 3 where the measured and computed normalised displacements were 0.04 and 0.12 respectively, and in the torsion mode in which the normalised mean rotations of level 8 and 9 were 1.0 measured, compared with .7 computed.

Table 5.13 shows percent reductions in measured and computed natural frequencies with members 84 and 135 removed in turn. The predicted reductions in the fundamental group for removal of either of these members were relatively small, ie less than 3.6%, and the measured reductions confirmed this; for example the computed reduction with member 84 removed was 2.7% and measurement of the natural frequency of this sway Z,1 mode gave a reduction less than 1%.

An expanded plot of the fundamental group with excitation in the Z-direction is shown in Figure 5.11, and a similar plot recorded after member 84 was removed is given in Figure 5.12. Comparison of the two plots confirm that no significant change in the frequency response has taken place in the fundamental mode group. The spikes

in Figure 5.12 (and Figures 5.5 to 5.8) are due to background laboratory noise and whenever possible the sweep sine tests were carried out in the evenings. Finally, the computed fundamental sway Z,1 mode shapes indicate that an increase in response can be expected at joint 49Z when member 84 is removed (Tables 4.10 and 4.30). This is confirmed by the measured response in Figures 5.11 and 5.12.

5.3.2 Second Mode Group

The second group of modes in Figures 5.2 and 5.3 was found between 55 Hz and 80 Hz. Figure 5.2 for central excitation in the X-direction shows a distinct peak at 56.4 Hz, and from the measured results given in Table 5.5 this peak was identified as the second sway mode in the XY-plane. In Figure 5.3 for offset excitation in the Z-direction there are three distinct peaks at 60.3 Hz, 67.8 Hz and 80.3 Hz.

The first peak was the second sway mode in the ZY-plane (Table 5.4) followed by the second torsion mode at 67.8 Hz (Table 5.6). The third peak at 80.3 Hz was found to be the deck roll mode suggested by the computer model. Table 5.11 shows that the sway Z,2 mode was predicted with good accuracy, (3.8% difference). However, the sway X,2 and torsion 2 modes were not predicted with the same accuracy, the difference being 14.3% and 20.1% respectively. No explanation is apparent for these differences.

The main difference between the measured and computed sway Z,2 mode shape of Table 5.4 was in the relative displacement of levels 3 and 7. In the computed results the same displacement

occurred at both these levels; in the measured mode shape the displacement at level 7 was 18% less than that at level 3. The ratio of mean displacement between levels 9 and 7 was 0.29 and 0.27 for measured and computed results. There was considerable difference in the vertical displacements at the deck corner joints; for example 0.04 was measured and 0.14 was computed at joint 53Y. The mean sway Z,2 mode shape is plotted in Figure 5.27.

The 14.3% error in the computed natural frequency of the sway X,2 mode was reflected in the measured and computed mode shapes (Table 5.5). The ratio of modal displacement at levels 9 and 7 was 0.26 measured and 0.19 computed and at levels 3 and 7 it was 1.01 measured and 0.71 computed.

The 20.1% error in the predicted second torsion mode also corresponded to relatively large differences between the ratios of measured and computed rotations (Table 5.6); 0.42 measured and 0.13 computed for levels 9 and 7, and 0.77 measured and 0.58 computed for levels 3 and 7.

Despite the errors in the values of the computed frequencies, the computed reductions agreed well with the measured ones for members 84 and 135 removed. Table 5.13 shows these reductions to be less than 1% for all modes in the second group when member 135 near the top of the structure was removed. However, when member 84 was removed the frequency of the sway Z,2 mode dropped by 35.1% compared with the computed drop of 29.6%. The sway X,2 natural frequency changed by less than 1% and the second torsion dropped by 4%.

The measured mode shape for the sway Z,2 mode with member 84 removed is given in Table 5.9, and a comparison with Table 5.4 shows that major changes have taken place in this mode. The ratios of mean modal displacements between levels 9 and 7 were 0.29 before and 0.46 after member removal. Between levels 3 and 7 they were 1.22 before and 4.05 after. The comparison also shows that jacket was now subjected to increased shear displacement in horizontal planes. The distortion of this mode shape was more severe than calculated in Table 4.31 which predicted an increase of 139% in mean modal displacement of level 3 compared with a measured increase of 232% (Table 5.9). The measured change at levels 8 and 9 however, was less than the computed change.

The frequency response recorded at joint 49Z before and after member 84 was removed is shown in Figure 5.13 (before) and Figure 5.14 (after). There is a dramatic change in the second mode group. Not only did the second sway Z,2 mode frequency drop by 35.1%, but the response of the second torsion mode was lost at joint 49Z. The deck roll mode at 80.3 Hz however, was not affected by removal of member 84. A receptance plot was generated for the first and second mode groups, Figure 5.28, and it agreed well with the measured frequency responses in Figures 5.11 to 5.14.

5.3.3 Third Mode Group

The third mode group occurred between 100 Hz and 130 Hz approximately. Figures 5.2 and 5.3 show a considerable number of peaks in this frequency range, but many of them are secondary peaks from the vibration of individual members and groups of members.

Identification of the third mode group is made more difficult by this increase in modal density.

The third sway mode in the X-direction was found from the measured shape (Table 5.7) to be that at 118.4 Hz, and can be seen in Figure 5.2 grouped with two other peaks at 105.4 Hz and 122.4 Hz. The measured and computed mode shapes (Table 5.7) were compared and the mean displacement ratios between levels 9 and 7 were 0.31 measured and 0.17 computed, and, between levels 3 and 7, 0.54 and 0.78. As expected both the measured and computed mode shapes were symmetric about the XY-plane.

The modes at 105.4 Hz and 122.4 Hz were investigated further. The first was identified as the deck pitch mode (predicted by computation and given in Table 4.26) and the mean modal displacements for the second (122.4 Hz) are given in Table 5.15. They are similar to those of mode X,3 but measurements at levels 3 and 7 show that the mode was not symmetric about the XY-plane. It was not predicted by the finite element computation and its existence is likely to be due to structural asymmetry, including a slight twist known to have been introduced into the structure during welding. It was because of the asymmetry of the mode shape that the lower frequency (118.4 Hz) was taken as the sway X,3 mode.

Figures 5.5 to 5.9 show the frequency response at five levels for excitation by the central shaker (joint 90X). The response at both 118.4 Hz and 122.4 Hz can be seen and that at 118.4 Hz dominates. From these five plots (levels 7, 6, 5, 4, 3) the response can also be seen to be a minimum at level 4, which infers a

node between levels 5 and 3. This is confirmed in the mode shape Tables 5.7 and 5.15.

The third natural frequency in the Z-direction was taken to be that at 119.4 Hz and can be seen in Figure 5.3. The measured mode shape is given in Table 5.8 and a comparison with the computed mode shape shows that the ratio of the mean displacements at levels 9 and 7 was 0.8 measured and 0.38 computed, and for levels 3 and 7 0.68 measured and 0.77 computed. The measured mode shape was plotted and is given in Figure 5.27.

The sway Z,3 mode at 119.4 Hz in Figure 5.3 is followed by a group of distinct peaks. The first of these at 126 Hz was investigated and the mode shape is given in Table 5.16. It shows that there is another mode similar to the sway Z,3 mode at this higher frequency. This is a similar observation to that already made for the X-direction, and the modes were not predicted by finite element computation. A comparison of Tables 5.8 and 5.16 reveals little difference in the mean mode shapes at 119.4 Hz and 126 Hz. There was some difference in the vertical displacements of the corner joints of the decks. For example, the ratio of vertical displacement at joints 53 and 97 on level 8 was 0.91 (119.4 Hz) and 0.78 (126 Hz) and between joints 54 and 97 at level 8 it was 0.93 (119.4 Hz) and 0.81 (126 Hz).

Measured and computed frequency changes for removal of members are given in Tables 5.13. Removal of member 84 has little effect on any of the modes in the third group. Figures 5.15 and 5.16 show the measured frequency response before and after the member was removed and there was no significant shift of any of the peaks.

Removal of member 135 was predicted by the computations to have a considerable effect on the sway X,3 mode and the results of Table 5.13 confirm this; there is good agreement between the measured (-18.1%) and computed (-20.9%) changes in frequency. The measured mode shape with member 135 removed is given in Table 5.10. The mean displacements did not change significantly, but removal of the member left the mode asymmetric about the XY-plane with large out of plane movements.

The change in frequency response is clear from Figures 5.22 to 5.26, the peaks at 118.4 Hz and 122.4 Hz (Figures 5.24 and 5.25) being lost. Comparison of Figures 5.22 and 5.23, however, shows that two new peaks appear in the range 90 Hz to 100 Hz. The first peak at 92.6 Hz was found to be the deck pitch mode and the second peak at 96.9 Hz. was that given as the sway X,3 mode with member 135 removed in Table 5.10. It cannot be said with certainty that the mode at 118.4 Hz. and not 122.4 Hz reappeared at 96.9 Hz, but it is likely that removal of member 135 would have the greatest effect on the more symmetric mode.

The remaining mode to be identified in the third group is torsion. The mode that was at first taken to be torsion at 130 Hz (Table 5.17) was found on closer examination to be very different from the computed mode shape, and closer to the computed deck twist mode. A third torsion mode was thus not satisfactorily identified and the reason may be that the point of excitation was not favourable for this mode although the third sway modes were excited.

5.3.4 Ovalising and Other Global Modes

In addition to the modes discussed so far six ovalising and the fundamental vertical modes were identified and a comparison with computed frequencies is given in Table 5.12. There was good agreement between measured and computed results for all the ovalising modes with less than 5% difference in frequencies. The frequency of the computed fundamental vertical mode was within 11.2% of the measured frequency and a frequency response plot was recorded at 53Y for excitation at 82X (offset shaker). This plot in Figure 5.10 includes the sway X,2 mode and the deck roll mode. These modes are little effected by removal of members 84 and 135 (Table 5.14).

5.4 RANDOM VIBRATION

5.4.1 Introduction

The main part of this research work has been concerned with the sensitivity of natural frequencies to failure of primary load-carrying members, and it has been shown that substantial changes can be expected in certain normal modes. Sine and sweep sine wave excitation was used to verify the computed results. It is not practical to employ artificial excitation on full scale platforms and certainly not on the latest generation of deep water structures. However, an alternative type of excitation exists. All structures are constantly subjected to natural excitation and in the case of offshore structures the wave, current and wind loadings are reliable sources of excitation.

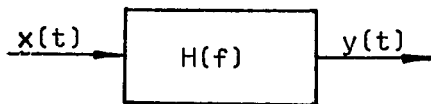
Natural sea state excitation however is random and a different analysis technique is required to determine the natural frequencies and mode shapes. The theory of frequency analysis of random vibration is well documented in the literature [26, 27, 28], and dedicated digital computer systems have been developed commercially for this analysis. Such a computer was made available towards the end of the research work, and a number of tests were carried out with random excitation in order to compare with results obtained by sinusoidal excitation.

5.4.2 Frequency Analysis of Random Vibration

The computer system was a Time Series Analyser manufactured by Time/Data [29] and it included a Programmable Data Processor (PDP - 11/05) with 24K memory, two channel analogue to digital converter (12 bits) with programmable anti-aliasing filters, storage oscilloscope, high speed paper tape punch/reader, and a Tele-type terminal. A further description of the system is available in reference [29]. The computer language is described in reference [30] and it is designed such that little prior knowledge of programming is required to write application programmes. For example, fundamental time series operations such as Fast Fourier Transform and Auto and Cross-spectrum computations can be executed with a single instruction. Auto and Cross-spectrum computations are fundamental to the analysis of the response of an offshore platform and a brief description of some basic equations and the computational approach implemented on the Time Series Analyser is outlined below.

5.4.3 Basic Equations and Computational Approach

For the single input/output system shown below



the following equations apply,

$$G_y(f) = |H(f)|^2 G_x(f) \dots\dots\dots(5.1)$$

$$G_{xy}(f) = H(f) G_x(f) \dots\dots\dots(5.2)$$

where $G_x(f)$ and $G_y(f)$ are mean square auto spectra of $x(t)$ and

$y(t)$ respectively, and $G_{xy}(f)$ is the mean square cross-spectrum between $x(t)$ and $y(t)$. It is assumed that $x(t)$ is stationary and that the system is a constant parameter linear system described by a frequency response function $H(f)$ which may be similar to the receptance function derived in 2.2, Equation (2.57). The frequency response function is complex,

$$H(f) = |H(f)| e^{-i\theta(f)} \quad \dots\dots\dots(5.3)$$

and it can be shown that the cross-spectrum $G_{xy}(f)$ defined by Equation (5.2) is also complex with a phase angle equal to the phase angle of the frequency response function $H(f)$.

The ordinary coherence function between $x(t)$ and $y(t)$ is defined by

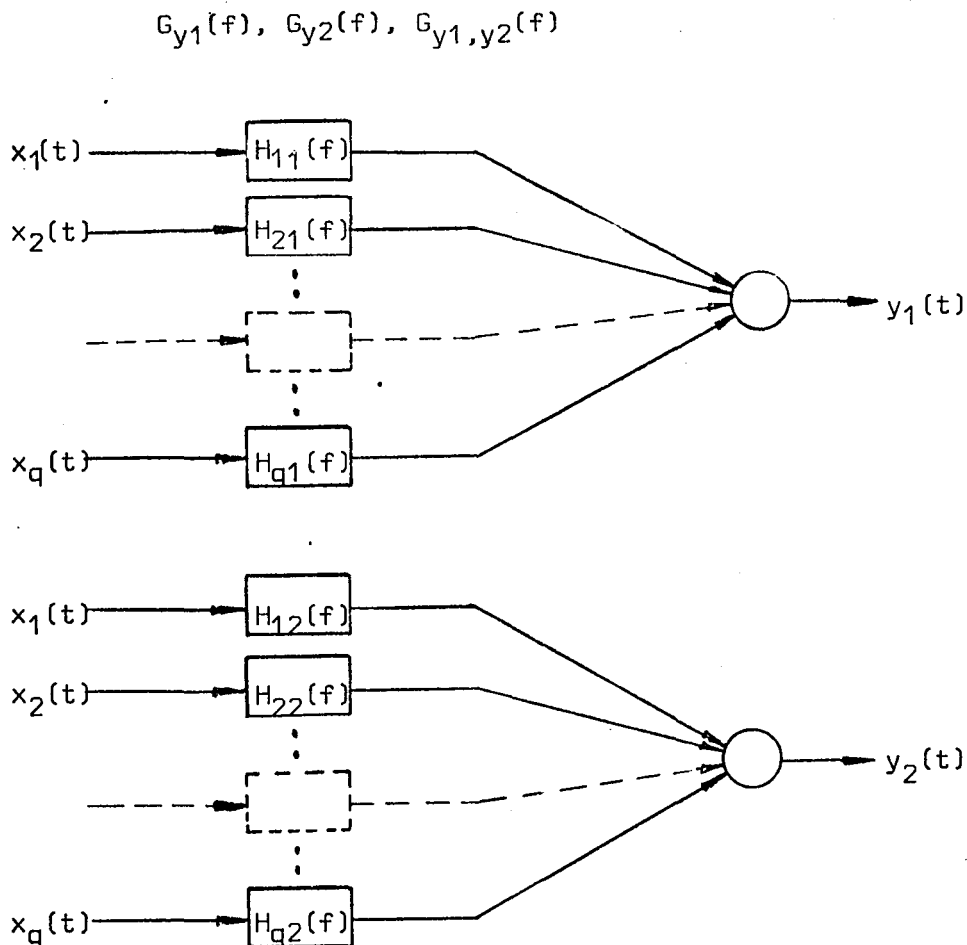
$$\gamma_{xy}^2(f) = \frac{|G_{xy}(f)|^2}{G_x(f) G_y(f)} \quad \dots\dots\dots(5.4)$$

and is bounded by

$$0 \leq \gamma_{xy}^2 \leq 1 \quad \dots\dots\dots(5.5)$$

Measurement noise at either the input or output point, non-linearities in the system, or a non-stationary input will cause the coherence function to be less than unity. A measured coherence function will nearly always be less than unity and coherence considerations are important in determining the accuracy of frequency response function measurements.

For the multiple input/two output system shown below (which arises in the determination of the natural frequencies and mode shapes of offshore structures) the following spectra are used:



Here $G_{y1}(f)$ and $G_{y2}(f)$ are the auto-spectra of the responses measured at station 1 and station 2 respectively and $G_{y1,y2}(f)$ is the cross-spectrum between these responses.

A coherence function between $y_1(t)$ and $y_2(t)$ is defined by

$$\gamma_{y1,y2}^2(f) = \frac{|G_{y1,y2}(f)|^2}{G_{y1}(f) G_{y2}(f)} \dots\dots\dots(5.6)$$

and is again bounded by

$$0 \leq \gamma_{y1,y2}^2 \leq 1 \dots\dots\dots(5.7)$$

As for the coherence function between input and output, the measured coherence function between two responses will nearly always be less than unity.

For the experiments on the model platform sinusoidal excitation was replaced by a band limited noise signal. The excitation was applied at joint 82Z (offset shaker) and the response was measured at joints 49Z and 52Z.

In order to compute spectra, frequency response and coherence functions a number of analysis parameters had to be decided. The Time Series Analyser uses segment averaging to obtain spectral estimates with acceptable statistical accuracy. For example a total record length of T_r seconds is divided into n equal time slices such that

$$T_r = nT \quad \dots\dots\dots(5.8)$$

and the spectral estimate is given by

$$\hat{G}(f) = \frac{1}{n} (\hat{G}_1(f) + \hat{G}_2(f) + \dots + \hat{G}_n(f)) \quad \dots\dots\dots(5.9)$$

where $\hat{G}_n(f)$ is the raw spectral estimate of the n^{th} time slice. The variance of the estimate $\hat{G}(f)$, Equation (5.9), is given by

$$\text{Var} [\hat{G}(f)] \approx \frac{G(f)^2}{n} \quad \dots\dots\dots(5.10)$$

where $G(f)$ is the true spectrum.

A normalised expression for the variance is obtained if Equation (5.10) is divided by $G(f)^2$.

$$\frac{\text{Var} [\hat{G}(f)]}{G(f)^2} \approx \frac{1}{n} \quad \dots\dots\dots(5.11)$$

and a random error is defined by'

$$\epsilon_r = \frac{1}{\sqrt{n}} \dots\dots\dots(5.12)$$

which can be used to calculate confidence intervals (Section 6.7 and 6.8 of reference 27), for the unknown true spectrum.

The sampling frequency (f_s) and number of sampled points (N) determines the length of each time slice

$$T = \frac{N}{f_s} \dots\dots\dots(5.13)$$

and the effective resolution bandwidth is

$$B_e = \frac{1}{T} \dots\dots\dots(5.14)$$

To obtain a satisfactory description of spectral peaks it is desirable to choose the resolution bandwidth

$$B_e < \frac{B_r}{4} \dots\dots\dots(5.15)$$

where B_r is the bandwidth at the half power points (Chapter 2, Section 2.7).

The spectral estimates given in Tables 5.18 to 5.20 were computed with the following parameters

$$\begin{aligned} f_s &= 409.6 \text{ Hz} \\ N &= 1024 \text{ pts} \\ n &= 350 \text{ time slices} \end{aligned}$$

hence

$$\begin{aligned} T &= 2.5 \text{ secs} \\ T_r &= 875 \text{ secs} \\ B_e &= 0.4 \text{ Hz} \\ \epsilon_r &= 0.054 \text{ or } 5.4\% \end{aligned}$$

5.4.4 Results

The force excitation spectrum is plotted in Figure 5.29 and it is not a white noise (flat) spectrum. The shape is mainly determined by the electro-magnetic shaker which has a natural frequency between 30 and 40 Hz. The response spectrum recorded at joint 49Z is shown in Figure 5.30 and is not unlike the frequency response plot given in Figure 5.3. This also applies to the cross-spectrum magnitude plotted in Figure 5.31. The cross-spectrum phase angle plotted in Figure 5.32 alternates between 0 degrees and ± 180 degrees and is difficult to interpret from the Figure. The coherence function, Equation (5.4), is plotted in Figure 5.33 and was found to be generally low at the natural frequencies. The frequency response function was computed from the cross-spectrum and the input spectrum, Equation (5.2), and plotted on logarithmic and linear scales in Figures 5.34 and 5.35.

A computer print-out of Figures 5.29 to 5.35 is given in Table 5.18 and the seven columns from left to right are:

- Frequency incremented at 0.4 Hz intervals;
- Excitation auto-spectrum (Figure 5.29);
- Response auto-spectrum (Figure 5.30);
- Frequency response function magnitude (Figure 5.35);
- Cross-spectrum magnitude (Figure 5.31);
- Cross-spectrum phase angle (Figure 5.32);
- Coherence function (Figure 5.33).

The cross-spectrum phase angle is the phase angle between output and input and a phase angle of ± 90 degrees indicates a

natural frequency. Three frequency bands at which there is a peak and a phase angle change through ± 90 degrees can be found. They are at:

14.0 Hz to 14.4 Hz,

60.0 Hz to 60.4 Hz,

119.2 Hz to 119.6 Hz,

which agree with the natural frequencies of the first three sway modes given in Table 5.11. The low coherence between output and input is of some concern. Table 5.18 reads 0.344 at 14 Hz, 0.615 at 60 Hz and 0.288 at 119.2 Hz. The effect of noise in the electronics, used to make the measurements will reduce the coherence. Another contributing factor to the reduction in coherence was considered to be background noise in the laboratory. This was the conclusion drawn after it was found that well-defined spectra could be computed without any form of artificial excitation. The frequency response function in the frequency band between the fundamental and the second group of natural frequencies was highly coherent compared with the response in the two groups (Figure 5.3D), and this may be the result of low structural damping coupled with short time slice length ($T = 2.5$ secs), ie. response to an input during a time slice continues to affect the response in the subsequent time slice and will not be coherent with the input during that time slice.

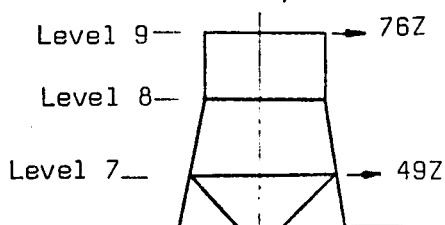
Theoretical receptance magnitude (Figure 5.36) and phase angle plots (Figure 5.37) were generated and compared well with the results of the random vibration tests (Figures 5.38 and 5.39).

Single point artificial excitation of large offshore structures is not practical and natural frequency/mode shape interpretation must depend on response measurements only; the responses being the result of natural sea state excitation.

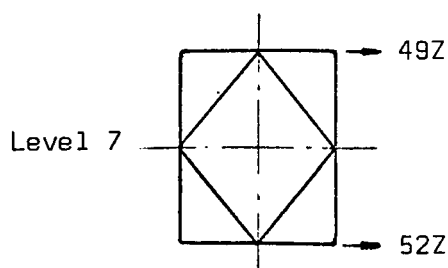
The model structure was tested with this point in mind and a number of plots of response spectra recorded at joints 76Z/49Z and 52Z/49Z are given in Figures 5.40 to 5.51. A computer print-out of the frequency spectra, measured at joints 76Z/49Z (level 9 and 7, Figure 4.4) is given in Table 5.19 and another print-out of the response measured at level 7 joints 52Z/49Z is given in Table 5.20. Natural frequencies measured this way will normally be characterised by peaks in the auto and cross-spectra and the phase angle between two points on the structure will be close to 0 or ± 180 degrees (a phase angle of 185 degrees, for example, will be printed/plotted as -175 degrees).

The common mean square response as a function of frequency between two locations on the structure is expressed by the coherence estimate, Equation (5.6). High coherence is normally found when a distinct normal mode is detected, and for high coherence an accurate estimate of the relative movement of two points on a structure can be made. From Table 5.20 the fundamental sway Z,1 and torsion 1 modes can be distinguished by the relative phase angle of joints 52Z/49Z which is close to 0 degrees for the sway mode and 180 degrees for the torsion mode. The second sway in the Z-direction is characterised by 180 degrees phase angle between levels 9 and 7 (joints 76Z/49Z) and in phase movement of joints

52Z/49Z (level 7). The peak at 60.4 Hz in Table 5.19 and 5.20 exhibits these characteristics



FREQ	MODE	F.R.F.	PHASE	COHER.
14.4	Sway Z,1	1.59	0.71	0.982
19.6	Torsion 1	3.48	1.0	0.995
60.4	Sway Z,2	0.27	169	0.952



FREQ	MODE	F.R.F.	PHASE	COHER.
14.4	Sway Z,1	0.81	0.23	0.99
19.6	Torsion 1	2.41	-179	1.
60.4	Sway Z,2	0.89	-1.44	0.997

Natural frequency and mode shape characteristics can thus be found and identified when a structure is subjected to random excitation. There are, however, several practical problems that will make natural frequency/mode shape interpretations difficult. They include: insufficient excitation, limited stationary record length, structural non-linearities and high modal density. The practical implementation of the method is discussed in the appendix.

A random vibration test was carried out for an increase in deck mass of 10 kg (about 4%). The mass was a shaker base (Figure 2.2) and it was attached to joint 99 level 8 (Figure 4.5, second offset shaker position). A comparative response plot is shown in Figure 5.52 and the frequency reductions in the fundamental group were calculated from Tables 5.21 and 5.22 and are summarised over.

	NO MASS CHANGE	4% MASS INCREASE	
MODE	FREQUENCY (Hz)	FREQUENCY (Hz)	Δ %
Sway Z,1	14.25	14.1	-1.05%
Sway X,1	16.0	15.8	-1.25%
Torsion 1	19.5	19.0	-2.56%

The trend of these frequency reductions agrees well with those computed in Chapter 4 (Table 4.4B) for a 5% mass increase.

CONCLUSIONS

- 1) In the tests on simple structures there was generally good agreement between measured natural frequencies and mode shapes and those predicted by computation with a finite element model.
- 2) Computations on the full scale oil production platform predicted substantial reductions in natural frequencies when inclined members of K-frames were severed.
- 3) The frequency changes were due to the large reduction in shear stiffness of a K-frame when an inclined member is removed.
- 4) The pattern of the changes gave an indication of the location of the failure.
- 5) Computations on the model platform showed similar sets of sway and torsion modes to those computed for the full scale structure.
- 6) The frequencies computed for the model were in reasonable agreement with the measured values but there were some difficulties with identification in the third mode group.
- 7) Cutting of two inclined members in the model gave frequency changes close to the computed changes.
- 8) The first two mode groups were readily identified when random force excitation was applied to the model to simulate wind and wave loading.
- 9) Severance of those members which carry the main shear loads in offshore structures can be detected from changes in global natural frequencies of the structure.

REFERENCES

1. NELSON, E.M., Jr. 'Offshore Structures, Past, Present,
Future and Design Considerations'.
Offshore Conference, Stavanger, June 1971.

2. KOEHLER, A.M., 'Development of the North Sea Forties
HRUSKA, S.J., Field Platform Concept'.
WALKER, R.C. Offshore Technology Conference, Paper 2245,
Houston, Texas, May 1975.

3. GRAY, R.M., 'Dynamic Analysis of the North Sea
BERGE, B., Forties Field Platforms'.
KOEHLER, A.M. Offshore Technology Conference, Paper 2250,
Houston, Texas, May 1975.

4. LOFTIN, T.D. 'Feasibility of a Fixed Platform for
1300 Feet of Water'.
Offshore Technology Conference, Paper 2689,
Houston, Texas, May 1976.

5. 'Gas platforms - how designers
underestimated North Sea'.
Offshore Engineer (ICE periodical),
June 1975.

6. Provisional requirements for instrumentation of fixed installations
for the exploitation of petroleum in the seabed and substrata
of the Norwegian inner coastal waters, in Norwegian territorial
waters and on that part of the continental shelf which is subject
to Norwegian sovereignty, but not in areas subject to private
property rights, issued by the Norwegian Petroleum Directorate
22nd December 1975.(Unofficial translation).

7. OSTROFSKY, B. 'Permanently Installed Ultrasonic Testing System for Offshore Platforms'.
Offshore Technology Conference, Paper 1253,
Houston, Texas, May 1970.
8. GLEW, C.A.W. 'The Effectiveness of Vibration Analysis as a Maintenance Tool'.
The Institute of Marine Engineers,
Transactions: Vol. 86, Series A, Part 2,
1974.
9. BLUMBERG, R.,
STRADER II, N.R. 'Dynamic Analyses of Offshore Structures'.
Offshore Technology Conference, Paper 1009,
Houston, Texas, May 1969.
10. TIEDEMANN, H.M. 'Shortcomings of Offshore Subsurface Engineering Inspections'.
Marine Technology (Periodical),
January 1974.
11. HUDSON, D.E. 'Dynamic Properties of Full-Scale Structures Determined from Natural Excitation'.
Dynamic Response of Structures,
Herrmann, G., & Perrone, N., Eds,
Pergamon Press. Inc., New York, 1972.
12. LOLAND, O.,
MACKENZIE, A.C. 'On the Natural Frequencies of Damaged Offshore Oil Platforms'.
Mechanics Research Comm., Vol.1, No.5/6,
Pergamon Press. Inc., 1974.

13. LOLAND, O.,
MACKENZIE, A.C.,
BEGG, R.D. 'Integrity Monitoring of Fixed, Steel
Offshore Oil Platforms'.
Measurement in the Offshore Industry.
BSSM/RINA Joint Conference,
Edinburgh, September 1975.
14. LOLAND, O.,
BEGG, R.D.,
MACKENZIE, A.C. 'The Dynamic Response of a Fixed Steel
Offshore Oil Platform'.
Measurement in the Offshore Industry.
BSSM/RINA Joint Conference,
Edinburgh, September 1975.
15. VANDIVER, J.K. 'Detection of Structural Failure on Fixed
Platforms by Measurement of Dynamic
Response'.
Offshore Technology Conference, Paper 2267,
Houston, Texas, May 1975.
16. 'ICES STRUDL-II, Engineering User's Manual'.
Department of Civil Engineering,
Massachusetts Institute of Technology,
Cambridge, Massachusetts, June 1972.
17. ROSEN, R.,
RUBINSTEIN, M.F. 'Dynamic Analysis by Matrix Decomposition'.
Journal of the Engineering Mechanics
Division, ASCE, 94, April 1968.
18. WILKINSON, J.H. 'The Algebraic Eigenvalue Problem'.
Clarendon Press, Oxford, 1965.

19. WITTRICK, W.H. 'Rates of Change of Eigenvalues, With Reference to Buckling and Vibration Problems'.
Journal of the Royal Aeronautical Society,
Vol. 66, September 1962
20. FOX, R.L., 'Rates of Change of Eigenvalues and
KAPoor, M.P. Eigenvectors'.
AIAA Journal, Vol.6, December 1968.
21. ARCHER, J.S. 'Consistent Mass Matrix for Distributed
Mass Systems'.
Journal of the Structural Division,
ASCE,89, August 1963.
22. PRZEMIENIECKI, J.S. 'Theory of Matrix Structural Analysis'.
McGraw-Hill 1968.
23. BISHOP, R.E.D. 'The Mechanics of Vibration'.
Cambridge at the University Press, 1960.
24. VOLTERRA, E., 'Dynamics of Vibrations'.
ZACHMANOGLOIE, E.C. Charles E. Merrill Books, Inc.,
Columbus, Ohio, 1965.
25. AMEY, H.B., Jr., 'Added Mass and Damping of Submerged Bodies
POMONIK, G. Oscillating Near the Surface'.
Offshore Technology Conference, Paper 1557,
Houston, Texas, May 1972.
26. ROBSON, J.D. 'Introduction to Random Vibration'.
Edinburgh University Press 1963.

27. BENDAT, J.S.,
PIERSOL, A.G. 'Random Data: Analysis and Measurement
Procedures '.
Wiley-Interscience 1971.
28. OTNES, R.K.,
ENOCHSON, L.D. 'Digital Time Series Analysis '.
Wiley-Interscience 1972.
29. 'TDA 31 Time Series Analyser System '.
Brief system description by Time/Data,
a General Radio Company, Palo Alto, USA.
30. 'TSL - Time Series Language '.
Brief description of solving problems
with TSL by Time/Data, a General Radio
Company, Palo Alto, CA 94303, USA.
31. WALKER, A.,
SIBLY, P. 'When Will an Oil Platform Fail '?
New Scientist, February 1976.
32. EARLE, E.N.,
MANDERY, W.L. 'Determination of Dynamic Characteristics
of Offshore Platforms from Random
Vibrations '.
Offshore Technology Conference, Paper 1840,
Houston, Texas, May 1973.
33. MARSHALL, P.W. 'Philosophy of Monitoring, Inspection, and
Repair for Fixed Offshore Platforms '.
European Offshore Petroleum Conference,
London 1978.
34. BUCKENHAM, L.G.,
ALLIS, G. 'Techniques and Developments in Underwater
Structural Inspection '.
Offshore Europe Conference, Aberdeen 1977.

APPENDIXPRACTICAL IMPLEMENTATION OF THE METHOD

The research work described in the preceding chapters was completed in the autumn of 1975. Since then the author has had an opportunity of applying the method to a number of offshore structures. The method and philosophy are described in three papers included in this appendix. Others are in references 31 to 34.

OFFSHORE TECHNOLOGY CONFERENCE
6200 North Central Expressway
Dallas, Texas 75206

PAPER OTC 2549
NUMBER

Structural Integrity Monitoring Using Digital Processing of Vibration Signals

Robert D. Begg, Alexander C. Mackenzie, U. of Glasgow, Colin J. Dodds, and Olaf Loland
Structural Monitoring Ltd.

THIS PAPER IS SUBJECT TO CORRECTION

©Copyright 1976

Offshore Technology Conference on behalf of the American Institute of Mining, Metallurgical, and Petroleum Engineers, Inc. (Society of Mining Engineers, The Metallurgical Society and Society of Petroleum Engineers), American Association of Petroleum Geologists, American Institute of Chemical Engineers, American Society of Civil Engineers, American Society of Mechanical Engineers, Institute of Electrical and Electronics Engineers, Marine Technology Society, Society of Exploration Geophysicists, and Society of Naval Architects and Marine Engineers.

This paper was prepared for presentation at the Eighth Annual Offshore Technology Conference, Houston, Tex., May 3-6, 1976. Permission to copy is restricted to an abstract of not more than 300 words. Illustrations may not be copied. Such use of an abstract should contain conspicuous acknowledgment of where and by whom the paper is presented.

INTRODUCTION

THE NEED FOR STRUCTURAL MONITORING

As the search for offshore gas and oil is pursued into deeper and deeper water, the environment in which the necessary structures must exist becomes increasingly hostile. Because of these more arduous conditions there is a higher probability of structural failure and, because of the increased capital cost of each structure and the difficulty of repair, there is a much higher penalty for catastrophic failure.

In parallel with the increased inspection requirement there is a major increase in the difficulties of subsea diving. Not only does the cost rise steeply with depth, but the available weather windows diminish, the productivity per diver drops and the danger to human life, though all precautions are taken, must inevitably rise.

References and illustrations at end of paper

Although diving expertise and equipment are continually improving, many are convinced that it will be impossible to inspect platforms in deeper water, such as the northern North Sea, with anything approaching the same thoroughness and detail that is now afforded these platforms in the southern half of that sea.

In addition to these factors, the large capital cost of each structure increases the cost level at which undersea repairs are profitable, and, as undersea welding technology improves, it cannot be long before major undersea repairs are undertaken. Quite obviously such repairs will be greatly assisted and cheapened if structural damage can be detected at an early stage, before the primary failure can induce secondary damage.

The preceding arguments lead inevitably to the conclusion that increased and more frequent comprehensive inspection is required and, moreover, that either diving

inspection should be made easier and quicker or else an alternative method developed.

This paper describes just such an alternative method for overall assessment of platform structural integrity with the possibility that, in the future, it may be upgraded to provide more detailed information about the condition of individual members and joints.

The new monitoring technique is based on the fact that, whereas a structure has a series of natural frequencies or resonances which are continually excited by the motion of the sea and wind, these natural frequencies are appreciably changed if a load-carrying member, such as a brace or pile, breaks or loosens materially. Using vibration analysis techniques it is possible to measure the appropriate natural frequencies of such a structure from relatively few measurements taken at selected positions above the water level so that monitoring may proceed whatever the weather. The amount and distribution of the change in the natural frequencies due to a member failure varies depending on the position of the member within the structure and on the topology and degree of redundancy.

The research and development of this project was carried out over a period of three years in the Department of Mechanical Engineering of the University of Glasgow, Scotland, followed by one year of measurement and development in the North Sea by Structural Monitoring Ltd. on three steel platforms belonging to B.P. CO., Ltd. with financial support from B. P. and Comex Diving (U. K.) Ltd.

The programme has been channelled along two main avenues.

1. The final stages have been reached in the development of techniques for overall structural monitoring by vibration analysis. Initially this will detect only complete member severance or pile failure.
2. Development is continuing of

ways of using vibration analysis as a technique for accelerated diving inspection routines. These will not require structural cleaning and will require access to each member at only one axial position. It is hoped that this method will detect relatively large cracks anywhere along a member or in the nodes at its extremities.

Advantages claimed for the method of overall monitoring include speed, cheapness, safety, independence from weather and sea state, and much increased frequency of inspection.

VIBRATION OF OFFSHORE STRUCTURES

When a structure is acted upon by a time-varying set of exciting forces it vibrates over the same range of frequency as is contained in the excitation. All structures have a large number of resonances or natural frequencies (in fact an infinite number). If the range of the excitation contains natural frequencies, the structural response will be large at these particular frequencies and relatively small at all others. The ratio of response amplitude at resonance to the amplitude at other frequencies is governed by the structural damping and by the ratio of the input powers.

In general, vibration at the lower natural frequencies is associated with the motion of the entire structure whereas at the higher natural frequencies the motion is principally confined to small sub-structures or to individual members. The motion of a structure at a natural frequency is known as a mode shape, and the first two or three mode shapes for tall, slender towers, such as oil platforms, resemble those for a cantilever with a mass at the free end. Thereafter the modes are increasingly dissimilar.

These structural vibration characteristics were fully demonstrated and explored in a three year laboratory experimental programme using a sixteen foot high scale model of a four legged, K-braced platform (Reference 1). Tests included both sinusoidal sweep and random excitation inputs.

Structures standing in the sea experience forces over a very wide range of frequency so that the total structural motion is complex, containing components at many frequencies. The relative sizes of the individual components varies from place to place in the structure as does their phase. Although the frequency spectrum of the sea motion itself is wide, the nonlinear interaction of the waves with the structural members extends the spectrum upwards, by breaking large slow fluid movements into smaller and quicker eddies. This interaction increases the excitation at the lower end of the range of natural frequencies which is normally between 20 and 50 times the fundamental wave frequency. In general the fundamental (first) platform natural frequency is fixed at the design stage to be more than 5-10 times that of the expected large wave. Wind excitation is less periodic than that of the sea and most of the structural vibration appears to be associated with transient gusting rather than a steady blow. This too produces vibration over a wide spectrum and may contribute considerably to platform motion.

As a result of these inputs, offshore structures vibrate at all frequencies and, because of low damping, the amplitude at a natural frequency may be two orders of magnitude greater than at another adjacent frequency. The whole picture of vibration amplitude to a base of frequency is known as the vibration spectrum and a typical such spectrum is shown on Figure 1.

This spectrum is typical in that the fundamental wave frequency peak is well below the the first structural resonance and is the only excitation peak to appear in the measured vibration. The other major peaks represent structural resonances and, over the frequency band shown, can be separated into three groups which correspond approximately to the fundamental, second and third cantilever bending modes. The separation is achieved by determining the vibration mode shapes at each peak using modal

analysis cross correlation techniques which involve a comparison (vibration amplitude and phase) of signals from several transducers placed at appropriate points on the platform. This determines the mode shape above the waterline; the shape of the rest of the structure can be inferred from this, drawing on experience gained in model platform measurements and, possibly, from structural dynamics computation (discussed later).

Not all of the smaller peaks in the spectrum represent resonances and several of them are attributable to the effects of non-linear pile/structure interaction. This is particularly noticeable on platforms piled through the legs where the connection between pile and leg below the top of the leg is indeterminate due to the difficulties of grouting. It is thought that the same effect also causes the splitting of the peaks representing the higher modes.

Because of the low damping inherent in such structures, indicated by the sharpness of the peaks, and the absence of input peaks in the frequency ranges of interest, the measured vibration spectrum peak frequencies can be assumed to be purely a measure of structural characteristics and to be independent of the weather conditions. Measurements on offshore platforms have shown this to be the case, over a wide range of wind, wave and tidal conditions.

INTEGRITY MONITORING BY VIBRATION ANALYSIS

In an economical design of platform each member must contribute in some way to the structural stiffness. Integrity monitoring is based on the assumption that each load-carrying member is involved in the overall vibration modes. Since these overall modes are wholly dependent on the stiffness of the platform it follows that the more efficient the design the greater will be the effect on the spectrum of the failure of a member. The position of the member in the structural topology governs which

of the overall modes is most affected by the failure. In general, the more heavily loaded is the member, the bigger will be the effect of its failure on the spectrum. The fact that the more serious the damage suffered the bigger the indication given is a decided advantage in a monitoring arrangement.

The second important consideration is the magnitude of the changes caused by a failure. Reference 2 tabulates the effects of the failure of a series of members on the first three natural frequencies of a typical 4 legged North Sea platform. This indicates changes of up to 30% in some of the frequencies and these figures have been confirmed experimentally in tests on the 15 ft model, which was based on that platform. (Reference 3) Finally, measurements made in the North Sea on a 16 legged, highly redundant platform showed a 10% change in a fundamental mode after an extra bracing member was fixed in position.

Whether the position of a failure can be located through the changes in the spectrum depends on whether the structure's spectral sensitivity to failure is known. The sensitivity can be calculated approximately by computer analysis but a separate calculation has to be made for each member, which is expensive and time consuming. However, if the mode shapes corresponding to the overall structural resonances are known, even approximately, then some indication of the failure location can be inferred. Again, this has been demonstrated on the laboratory model.

It is to be noted that, at the lower frequencies, the mode shapes are such that the individual members deform primarily in tension and compression and not in bending. Since the introduction of a deep crack in a long member does not change the axial stiffness appreciably, the effect of cracks on the lower structural modes will be small.

More exact information regarding a failure is contained in the

upper frequency peaks of the spectrum where the peak corresponding to the natural frequency of the individual member concerned must be greatly changed by a failure, or even by a severe crack. This is because the individual member modes are controlled by bending stiffness and the bending stiffness of a beam is changed by the existence of a substantial crack. If the individual peaks in this region could be detected and identified then an exact diagnosis of failure could be made. However, experiment on the laboratory model and on three platforms in the North Sea have indicated the impossibility of doing this without many more transducers, positioned under water the length of the platform, and the problems of underwater instrumentation are considerable.

The alternative approach is to use vibration analysis as a tool to accelerate diving inspection. By placing a transducer anywhere on a member it is possible to obtain a spectrum in which the individual member frequencies can be easily distinguished. In this way, since bending is the primary mode for individual member modes, it is possible to identify structural failure and may be possible to detect partial failure - either through changes brought about by the weight of water filling the member if the crack is big enough to allow leakage, or by changes to the spectrum caused by decreased bending stiffness. This latter effect appears to be quite complex and experiments are in progress to examine it more closely. Cracking also affects the spectrum in other ways and accelerated diving inspection routines are being developed which, it is hoped, may be able to detect sizeable cracks in members or nodes.

DIGITAL VIBRATION ANALYSIS

Since the principal forms of excitation to offshore structures in the frequency ranges under consideration are stochastic in nature (waves, wind, etc.) the vibration response is also stochastic and analysis has to be carried out in

the frequency domain using statistical methods.

Relatively recent advances in computing technology have included the development of software packages which permit on-line real time analysis of vibration signals. These use the Fast Fourier Transform method and reduce both the computing time and the storage required. The process involves the frequency analysis of successive samples of signal, accumulating until sufficient statistical accuracy has been attained. As well as extracting individual spectra from single signals it is now possible to obtain cross-spectra between several simultaneous signals, from which relative coherency and phase can be obtained. This latter is used in the extraction of mode shapes since it is possible to determine both the sense and statistical interdependence of the motions at various points at the resonance frequencies. As acknowledged before in this paper, once the mode shapes are approximately known, changes in the spectrum due to damage can be interpreted to locate the damage.

Because of the immense size of offshore platforms, the lower frequencies are within the range 0.4-10 Herz, which is much lower than normally encountered in vibration problems. This causes slight difficulty in instrumentation, being outwith normal frequency ranges, but has a decided advantage in that very large signal-to-noise ratios can be obtained due to the lack of electrical noise and other extraneous inputs at these frequencies. Similarly the relatively low speeds are suited to multi-channel on-line processing using quite modest computing systems.

On such systems it is possible to detect frequency changes down to 0.1% of the frequency in question, which allows very fine changes in spectra to be detected. Since changes associated with structural damage are of the order of 5-30%, the accuracy of the data processing is more than adequate.

As has been mentioned previously, the pile/jacket interaction and

the piles themselves introduce non-linear effects which cause spurious peaks to appear in certain parts of the spectrum, in particular in the fundamental region. Whereas very little can be done to eliminate these peaks in the analytical process they can be identified when several spectra, obtained under differing weather conditions, are compared. The exact mechanism of the non-linearity has still to be defined mathematically, although a small experimental rig with an inbuilt similar nonlinearity has exhibited the same spectral peculiarities. Work is continuing on this important aspect.

STRUCTURAL DYNAMIC ANALYSIS

There are now a number of structural analysis programmes capable of a dynamic analysis of offshore platforms. These model the various structural members in terms of equivalent mass, inertia and stiffness and solve the resulting matrix equation to predict natural frequencies and mode shapes. Unfortunately the nonlinearity inherent in the pile/jacket connection and the problems of modelling dynamic pile behaviour reduce the usefulness of such computation and there appears to be a considerable gulf between calculated and measured natural frequencies. The authors have no experience as yet in applying such computation to platforms whose spectra has been measured.

Similar calculations were carried out on the laboratory model platform and the first 13 natural frequencies were predicted to within 20%, the first 6 within 5%. However this model had well defined linear elastic base supports so that non-linear effects were not encountered.

Experience gained in even these relatively small scale calculations has shown that dynamic analysis costs can be high. Figures of between \$20 and \$50 per single natural frequency appear to be the correct order of magnitude for the basic computation, but to this must be added the cost of modelling the structure (plus trial runs) preparing the data describing the structural topology and finally interpret-

ing the results. What could be a major further addition is the extra analysis necessary to model the nonlinearities of the pile behaviour and fixing.

To produce say the first ten natural frequencies and modes for the undamaged platform is probably a normal design procedure, but to produce a similar spectrum to show the effect of losing each structural member in turn would be an extremely expensive operation. At the present state of the art it is doubtful if appreciably more accurate failure location could be obtained by calculating such a table of failure sensitivity coefficients.

THE STATE OF THE ART

This paper has dealt with the theoretical ideas and assumptions from which structural monitoring using vibration analysis has been developed. From these considerations it can be seen clearly that the method is founded on principles and ideas which are already well-established in other fields. Although troublesome, the effect of the pile nonlinearity is being overcome and the remaining doubts are in the domain of practicability.

Four main questions have to be answered.

1. Can spectra with sufficient information for monitoring be measured consistently on platforms?
2. Are these spectra stable and are natural variations due to scour, weed growth, weather, tide, etc. small enough to allow a failure change to be detected unambiguously?

3. Can it be demonstrated directly that the method works?

4. Using the method in conjunction with diving inspection, is there an appreciable saving in overall cost or a substantial improvement in safety?

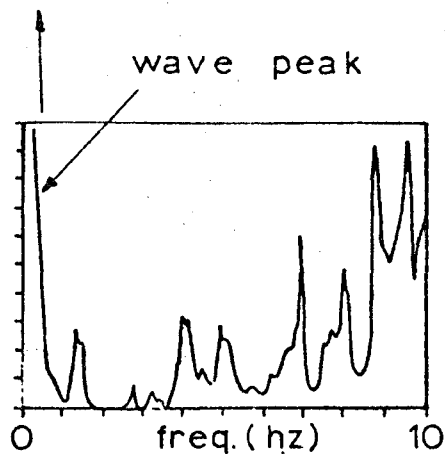
A later paper at this conference (No. 2551) answers these questions in the affirmative, based on a year of operational experience offshore.

ACKNOWLEDGEMENT

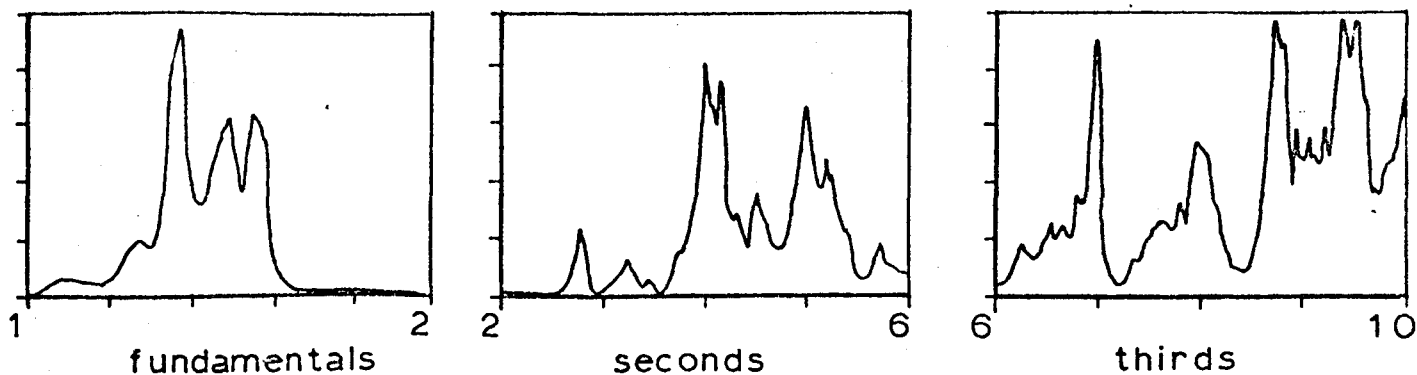
The authors would like to record their appreciation of the help and encouragement they have received from B. P., Comex Diving (U.K.) Ltd., and many others.

REFERENCES

1. Loland, Begg, Mackenzie, "The dynamic response of a fixed, steel offshore oil platform", BSSM/RINA Joint Conference "Measurement in the Offshore Industry", Edinburgh, September 1975.
2. Loland and Mackenzie, "On the natural frequencies of damaged offshore oil platforms", Mechanics Research Communications. Vol. 1. 1974.
3. Loland, Mackenzie, Begg, "Integrity monitoring of fixed, steel offshore oil platforms", BSSM/RINA Joint Conference "Measurement in the Offshore Industry", Edinburgh, September 1975.



1.a. $(\text{Acceleration})^2$ spectrum, 0 - 10 hertz, showing wave frequency peak.



1.b. Expanded spectrum in three ranges.

Fig. 1 - $(\text{Acceleration})^2$ spectrum from North Sea platform.

OFFSHORE TECHNOLOGY CONFERENCE
6200 North Central Expressway
Dallas, Texas 75206

PAPER NUMBER OTC 2551

Experiences in Developing and Operating Integrity Monitoring Systems in the North Sea

By

Olaf Loland and Colin J. Dodds, Structural Monitoring Ltd.

THIS PAPER IS SUBJECT TO CORRECTION

©Copyright 1976

Offshore Technology Conference on behalf of the American Institute of Mining, Metallurgical, and Petroleum Engineers, Inc. (Society of Mining Engineers, The Metallurgical Society and Society of Petroleum Engineers), American Association of Petroleum Geologists, American Institute of Chemical Engineers, American Society of Civil Engineers, American Society of Mechanical Engineers, Institute of Electrical and Electronics Engineers, Marine Technology Society, Society of Exploration Geophysicists, and Society of Naval Architects and Marine Engineers.

This paper was prepared for presentation at the Eighth Annual Offshore Technology Conference, Houston, Tex., May 3-6, 1976. Permission to copy is restricted to an abstract of not more than 300 words. Illustrations may not be copied. Such use of an abstract should contain conspicuous acknowledgment of where and by whom the paper is presented.

ASSTRACT

Offshore structures vibrate under the action of the sea, wind and on board machinery. The response is most marked at the natural frequencies of these structures which are dependent on the geometry, stiffness and mass of the structure and are independent of the excitation. Measurements of the responses of three platforms in the North Sea have been made over a period of nine months. Each platform has produced a unique signature which has remained constant within prescribed limits.

Failure of any structural member in the platform will produce a change in the signature and changes of greater than 15% have been measured when minor modifications were made to one of the test platforms.

This vibration analysis technique for the monitoring of offshore structures as a primary inspection aid is both technically feasible and practically possible.

References and illustrations at end of paper

INTRODUCTION

At the present time there are approximately 80 offshore fixed steel structures installed in the coastal waters of the United Kingdom and it has been predicted that by 1980 there will be around 150 steel structures in water depths varying from 30m to 300m. Underwater inspection is a requirement for these platforms to ensure their structural integrity.

The Offshore Installations (Construction and Survey) Regulations which came into operation in May 1974 called for a Certificate of Fitness to be obtained for each platform by August 1975. When the certificates are granted they remain valid for a period of 5 years, renewal being conditional on a satisfactory survey of the entire installation. Periodic surveys are required between each of the main surveys. The suggested format for a main survey of steel structures is given in the guidance to the UK Offshore Installation Regulations and contains the following:

"Visual examination of the whole

structure above and below water to assess its general conditions, to detect obvious damage

If this inspection routine has to be carried out by divers operating in water depths up to 300m and over possibly 150 platforms, then even allowing for a percentage inspection each year, there exists an immense problem if a guarantee as to the structural integrity of each platform must be given (1). It must be borne in mind here, that this inspection forms only a small part of the total underwater commitment required to fulfil these regulations.

However, alternative techniques are available to aid this primary inspection process and one such method relies on the changes which occur in the natural frequencies of a structure when load-carrying members are damaged. The principle and application of this technique to offshore structures is not new - indeed laboratory and computer studies were carried out two to three years ago and much useful data obtained (2, 3, 4). The technique has also been used to verify the absence of damage in a small US Coastguard Tower (5). However, the technique had yet to be proved operationally offshore. Many environmental problems which do not exist in the laboratory could render the technique impractical for the reliable identification of primary structural damage over long periods of time.

A steel offshore platform, located on the sea bed by a number of independent piles will vibrate under the forcing excitation of its environment. It will behave like any dynamic system and vibrate at its natural frequencies which are dependent only on the geometry, stiffness and mass of the structure and the nature of its foundations. At each natural frequency there is a particular mode shape associated with that frequency which distinguishes it from all others.

If any load-bearing member fractures, this will produce a change in some of the natural frequencies, and detection and identification of this change is the basis of this vibration monitoring technique. An earlier paper at this conference (6) has described in some detail the analytical principles of this method together with the computational requirements for the analysis of the platform response data.

It is the object of this paper to discuss operating experiences and present some of the results obtained from a structural integrity monitoring system of this type which has been in use for a period of 6-9 months on three

platforms in the North Sea. The aim of this project was to extend the laboratory and computational studies of Loland et al (4) to full scale platforms in the North Sea and present to the offshore industry a reliable and unambiguous inspection method, which can be used for primary inspection of fixed offshore structures.

SYSTEM REQUIREMENTS

The conclusions from the laboratory work carried out by Loland et al (4) made it abundantly clear that a successful integrity monitoring system for fixed steel offshore platforms had to fulfil certain requirements. If the laboratory results were to be extended and used in field case studies then the following requirements had to be met:

1. It must be possible to measure the vibration response of the platform under environmental excitation and from this response extract the natural frequencies with sufficient accuracy and reliability. Only transducers located above the water line could be used for this purpose and at least 9 vibrational nodes (i.e. the fundamental group plus 2nd and 3rd harmonics) would be required to enable the possible identification of the failure area.
2. The vibration spectra, containing these frequencies, must remain stable in frequency over long periods in time and be independent, in the frequency axis, of tide, sea and wind conditions. The long term frequency stability will be affected by changes in platform deck mass, build up of marine growth on the structure and such like occurrences.
3. The instrumentation package must withstand the rigours of the environment and ensure accurate recording of information with signal-to-noise ratios compatible with the response spectrum (i.e. signal-to-noise ratios greater than 50 dB)
4. It must be possible to infer the mode shapes for the complete structure from the measurements taken from transducers located above the water line. Sufficient information must be obtained from transducers in this region to remove any ambiguity from mode shape identification.
5. The installation and operating costs of the monitoring system must enable obvious savings to be made over existing diver orientated inspection methods and be competitive with other monitoring techniques which are available such as underwater

television.

PLATFORM TOPOGRAPHY AND ENVIRONMENT

The three platforms on which the monitoring system has been developed are owned and operated by British Petroleum Company Ltd. and are situated in the southern sector of the North Sea. They are of widely different design:

- o Platform Number 1 is the most complex and contains two 4 x 2 leg jackets fixed together on the longer side at deck level.
- o Platform Number 2 contains one 3 x 2 leg jacket attached on the shorter side at deck level to a 4 x 2 jacket.
- o Platform Number 3 is a single 4 leg jacket structure.

All platforms are constructed of mild steel and piled into the sea bed in approximately 30m of water.

During the period measurements were taken (from April 1975 to date), wave heights have varied from a flat calm to around 10m with wind speeds up to 100 knots. Vibration spectra have been recorded in various sea states up to 3m high waves and a range of wind speeds from 2-3 knots to a maximum wind speed of 50 knots. Tidal variations in the area are around 4m and measurements have been made at both high and low tide states.

On platform number 1 a small percentage change in deck mass was recorded during the test period.

INSTRUMENTATION AND RECORDING

The first measurements of platform vibration response were made in April 1975 using Endevco piezo-resistive type accelerometers coupled through a strain-gauge bridge and high gain amplifier to a FM tape recorder. These accelerometers are extremely fragile and cannot withstand shock loading greater than 20g. Locations were chosen on each platform at main deck level and at "spider-deck" (jacket-deck interface) level in two mutually perpendicular directions.

On each platform, the data from a selected number of transducers was recorded on FM tape for a period of 3 hours. The environmental conditions were noted for future reference. Analysis of this first data set provided sufficient encouragement for the project to continue with a high probability of success.

The next few visits were carried out using the same instrumentation. During this period

a new transducer was designed and manufactured which contains not only the accelerometer but the amplification and filter circuits required to ensure optimum signal-to-noise recording ratios.

This single transducer now replaces the accelerometer and amplifier units. They have been designed to S&L specifications and are completely self-contained in a watertight case. Excitation for the amplifier and filter circuits is provided by any dc source in the range $\pm 9V$ to $\pm 18V$. The nominal output of these transducers is $\pm 10V/g$.

The accelerometers terminate in a water-sealed plug and are connected to the recording medium through cable lengths varying from 30m to 150m. These cable runs have proved to be the weakest part of the system in this temporary installation. This has been due to the fact that the cables were run along handrails and vertically up the jacket legs on the outside of the platform. Damage to the handrails under severe weather conditions resulted in loss and damage to the cables. However, for a permanent installation, secure cable runs present no major problem.

The signals are pre-whitened prior to recording on FM tape. The result of this pre-whitening process and the fact that the frequency band containing the data is restricted to 0-20 Hz, has produced signal-to-noise ratios in excess of 60 dB on a standard commercial FM tape recorder at a recording speed of $7\frac{1}{2}$ ips.

At the present time, each platform contains four or five permanently mounted transducers which are used for the continued monitoring of the frequency spectra. A further four transducers are used for temporary installation when mode shape identification is required.

Each transducer is contained in a mild steel box which is fixed to one of the main jacket legs using plastic-padding cement and a stainless steel tensioned band. Welding of the boxes was impractical and in some cases impossible and this method of attachment has to date proved extremely reliable, as no damage has yet been noted.

ANALYSIS

Since the excitation is random, i.e. the sea and wind, then the structural response data recorded is also random and hence statistical analysis techniques must be employed to extract the natural frequencies from the response data. It is outwith the

scope of this paper to present the analysis techniques employed and the reader is referred to one of the many books on the general topic of random data analysis (7). However, one important consideration in the analysis of random data is the estimation of the statistical error inherent in the estimation of the frequency spectrum. This error is a function of the analysis bandwidth and data length. High statistical accuracy requires long data lengths and wide analysis bandwidths:

$$\text{Accuracy} \propto \text{Data length} \times \text{bandwidth.}$$

Unfortunately, resolution bandwidths of between 0.2 and 2% of the fundamental frequency of 1 Hz are required to ensure the tracking of the natural frequencies and this results in long data lengths being required to minimise the statistical error. However, long data lengths of over 3 hours become impractical under the winter conditions in the North Sea when sudden changes in weather conditions can drastically alter the excitation forces. These changes have a practical bearing on the amplifier gains which are pre-set during any recording period and from an analytical viewpoint introduce a non-stationarity (7) into the response data which casts doubts on the validity of the analysis techniques.

Analysis of the data was performed on shore on a Time-Data computer analysis system which is based on a PDP11/05 computer to obtain, in the first instance, the frequency spectra for each recording in the frequency band 0-20 Hz.

Figure 1 shows a typical set of spectra from one of the platforms. They are displayed in 5 bands, with each band containing a characteristic set of frequencies:

- 0-1 Hz Platform rigid body motion.
- 1-2 Hz Fundamental group of frequencies.
- 2-6 Hz 2nd harmonic group.
- 6-10 Hz 3rd harmonic group.
- 10-20 Hz Individual member frequencies.

Mode shapes were confirmed using other transducers suitably located and a cross-spectral analysis to obtain gain and phase information. A more sophisticated modal analysis technique which utilises a residual spectral analysis routine has been developed from work reported by Dodds and Robson (8) and has been successfully employed to interpret modal information from data recorded on one of the three platforms.

RESULTS

Throughout the period of measurement

(from April 1975 to date) the spectra on all platforms were found to be stable in frequency to within 3%. The variations that were encountered within this limit were generally attributable to known changes in deck mass or to tidal effects. No evidence of the effect of weed growth or foundation scour were found. It is worth noting here that the ultimate resolution of the computer analysis of the measured data was 0.2% of the fundamental frequencies on all three platforms although for normal analysis a bandwidth of 0.025 Hz was used which represents some 2% of the fundamental.

Examination of the spectra obtained from two of the platforms shows effects which, it is now fairly certain, can be explained by a non-linear dynamic behaviour of the platform. Figures 2 and 1(ii) and (iii) compare spectra analysed from data recorded on one of the three platforms in the North Sea with data analysed from a simple dynamic model containing a non-linearity of the type suspected to be inherent in the offshore platform. Although modal coupling is not obtained in the model which results in only a single mode being obtained in each band compared with at least two on the real structure and the frequency ranges are different, the agreement is remarkably good especially in the reproduction of the double peak effect. This finding will make structural computer modelling of these platforms more complex and expensive and increase the complexity of any technique used to extract damping information from the response data.

During the period of the investigation platform 1 underwent minor structural modifications and figure 3 shows the spectra obtained from this platform before and after this modification. The effects of this modification which can be taken as typical of a splash-zone failure, resulted in frequency changes of 10 to 15%. Tracking of these frequencies was made possible by identifying the mode shapes.

The operational cost of a manually run system with onshore analysis has worked out at about £10,000 - £15,000 per platform per visit with a low initial capital cost. Visits would be recommended at least once per month in the initial stages. However, a completely automatic system can be installed in which a computer on board the platform handles all housekeeping operations as well as the data analysis. Tapes can then be sent to shore once every 2-3 months for back-up analysis and storage. This will involve a high capital cost depending on the computer used,

but low running costs can be envisaged which will be dependent mainly on the maintenance costs of the computer hardware.

CONCLUSIONS

1. Spectra can be obtained with sufficient information for monitoring purposes.
2. Spectra are stable enough for monitoring purposes.
3. Instrumentation techniques have been developed which are capable of measuring the platform response spectra with sufficient accuracy and reliability for monitoring purposes.
4. Analysis techniques are available and have been developed which enable the determination of the platform mode shape above the water line, the accuracy limitation being on the measurement side. From these measurements the overall mode shape can be successfully inferred.
5. Changes in this response spectrum due to minor structural modifications are clearly observed and confirm the validity of this technique as a means of platform inspection for primary structural damage.

ACKNOWLEDGEMENT

The authors wish to express their gratitude to British Petroleum Company Ltd. for their kind permission to publish this paper.

REFERENCES

1. SLETTEN, R. "Underwater Inspection" Veritas(85) 12-16 Sept. 1975
2. LOLAND, O
MACKENZIE, A.C. "On the natural frequencies of damaged offshore oil platforms" Mech.Res.Comm, 1, 353-354 (1974)
3. LOLAND, O
BEGG, R.D.
MACKENZIE, A.C. "The dynamic response of a fixed steel offshore oil platform" BSSM/RINA Conference, Edinburgh, Sept. 1975
4. LOLAND, O
MACKENZIE, A.C.
BEGG, R.D. "Integrity monitoring of fixed steel offshore oil platforms" BSSM/RINA Conference, Edinburgh, Sept. 1975
5. VANDIVER, J.K. "Detection of structural failure on fixed platforms by measurement of the dynamic response" OTC 2267, 1975.
6. BEGG, R.D.
MACKENZIE, A.C.
DODDS, C.J.
LOLAND, O. "Structural integrity monitoring using dynamic processing of vibration signals" OTC 2549, 1976.
7. BENDAT, J
PIERSOL, A. "Random Data: Analysis and Measurement Procedures" Wylie Interscience 1971
8. DODDS, C.J.
ROBSON, J.D. "Partial coherence in multivariate random processes" J. Sound Vib (1975) 42(2) 243-249

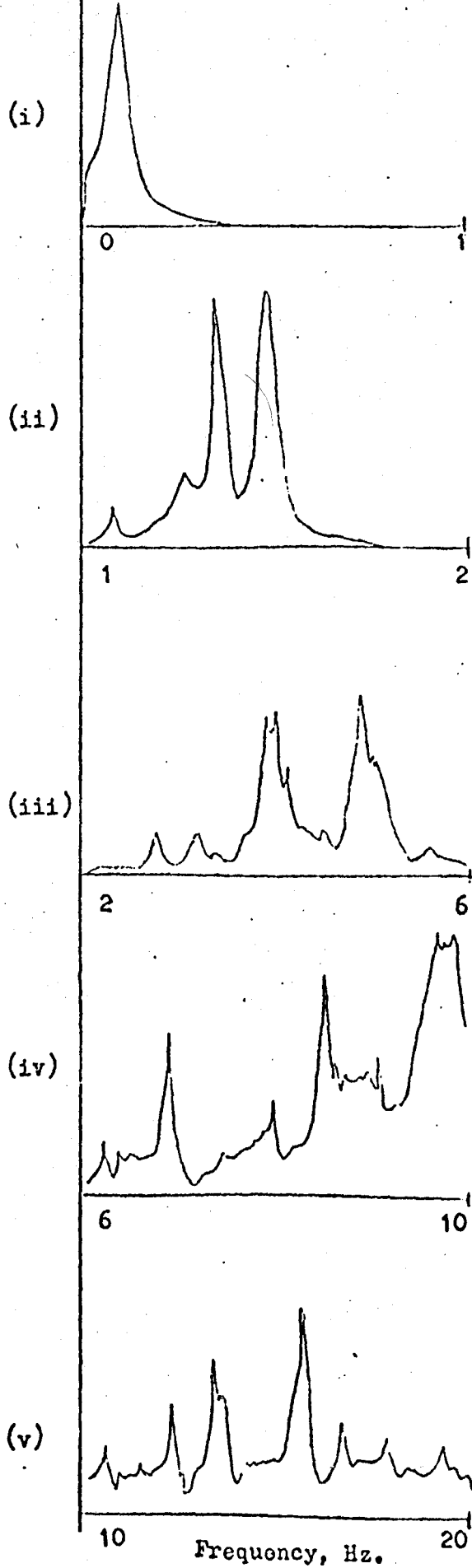


FIGURE 1: Platform Response Spectra.

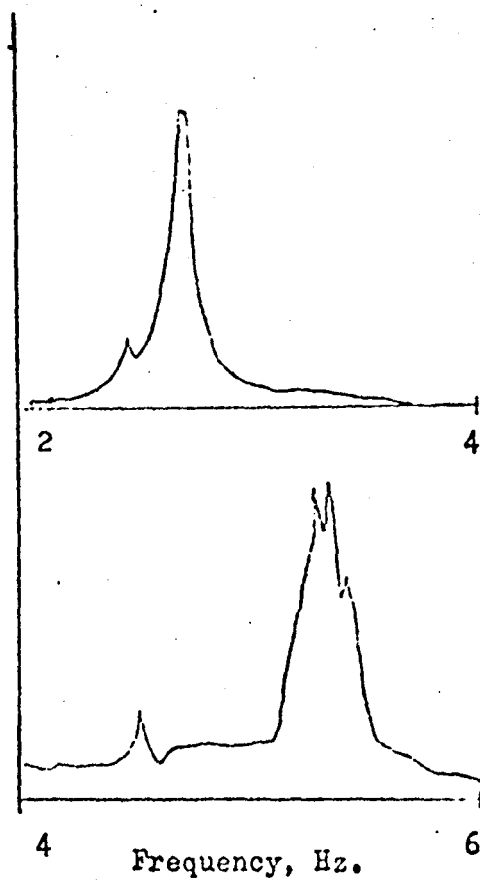


FIGURE 2: Model Response Spectra

Note: In both figures the vertical scales have units of g^2 and the amplitudes have been normalised in each band. All scales are linear.

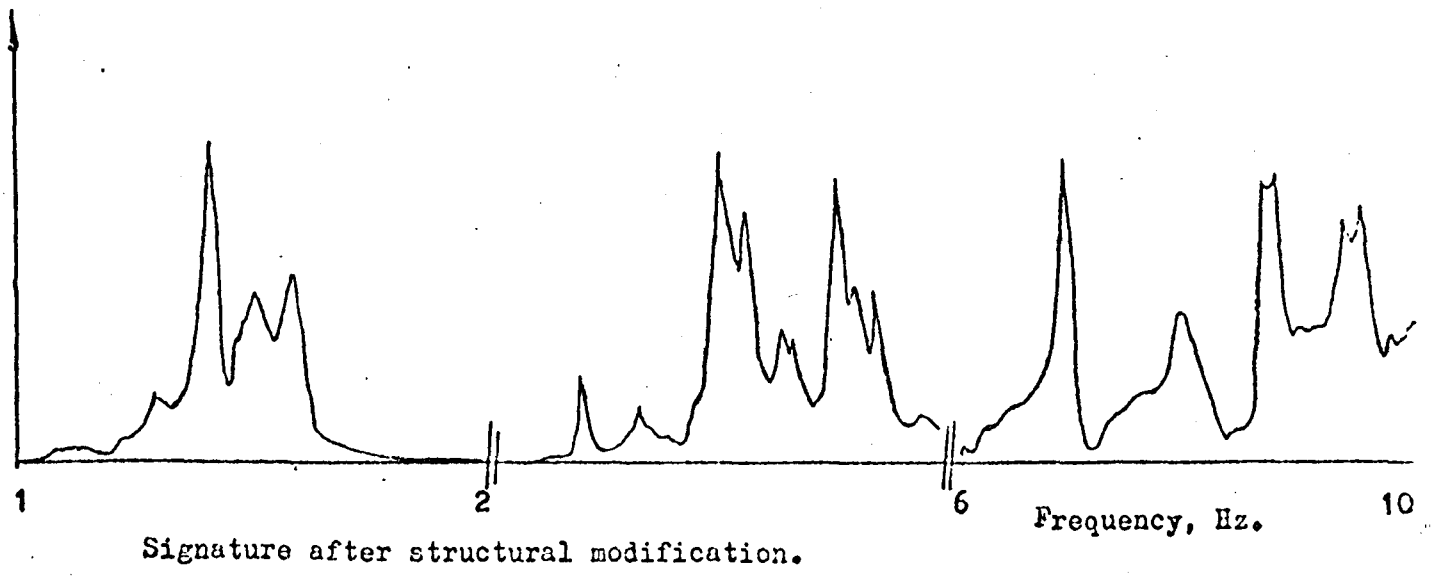
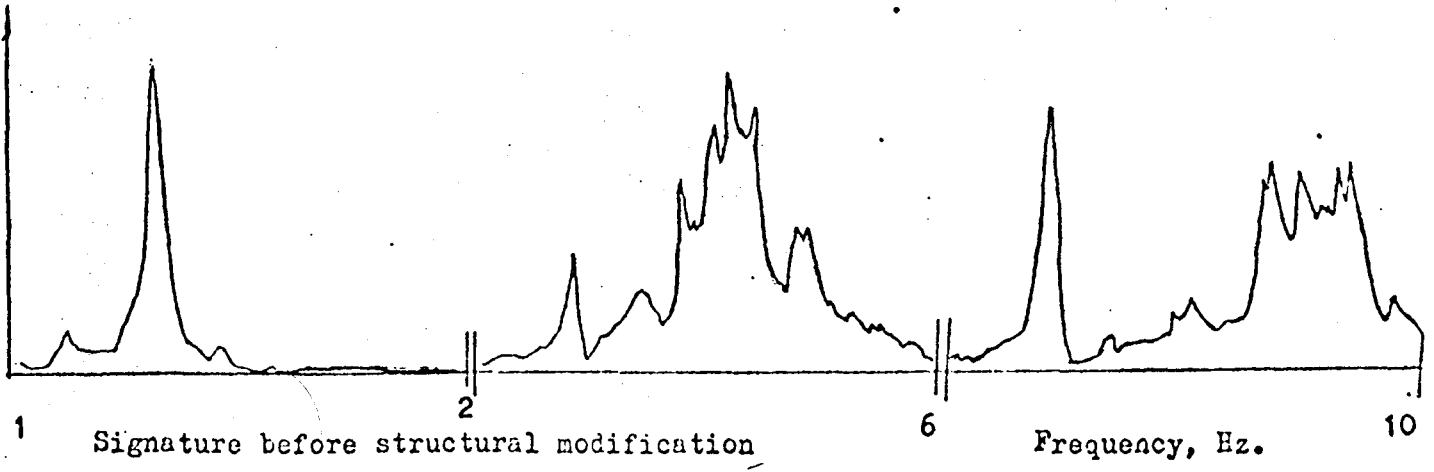


FIGURE 3: Platform signatures before and after minor structural modifications.

Note : All graphs linear scaling with vertical scale normalised in each frequency band and units of g^2 .

MONITORING OF OFFSHORE STRUCTURES USING VIBRATION ANALYSIS

R. D. Begg and A. C. Mackenzie
Structural Monitoring Ltd. Glasgow.

1 INTRODUCTION

All offshore platforms must be inspected to ensure that the risk to human life and to the environment is at an acceptably low level. In structural terms the inspection is intended to establish that the platform retains sufficient strength to withstand the largest wave forces envisaged. The inspection is normally carried out by divers, and attention is focussed on the inclined members which provide the shear connection between the legs. This shear connection is essential if wind and wave loads are to be resisted mainly by axial tension and compression forces in the legs and bracing members, and not by bending of the legs. Only a small percentage of such members can be examined annually, and it is usual to concentrate on those welds which have been calculated to be most susceptible to fatigue.

Unfortunately, as platforms are positioned in deeper water where the environment is more extreme, the problems of diver inspection become more severe, and the cost and danger of such work rise sharply. The point has now been reached at which inspection programmes in deep water cover only a fraction of the members which would be inspected in shallower waters; the risk of loss of load-carrying capability of a member going undetected has risen appreciably.

As well as this increased risk, there are other problems associated with the

operation of any platform on which serious damage has been detected in a diving inspection programme, or is suspected as a result of a collision or some other accident. Normal practice is to restrict operation of such a platform until repairs are complete and to insist on shut-down and evacuation when waves greater than a stipulated height are forecast. Although this reduces any immediate risk to personnel, it does nothing to check that the platform is fit for re-occupation after the storm. To some extent, the operating limit is imposed as a result of known damage, but the decision is also influenced by the thought that the damage may have spread to other members from redistribution of loading, or that there may be other damage that has not been detected. If continuous assurance can be given that the condition of the structure has not seriously deteriorated, the operational restriction can be relaxed.

These requirements for a back-up inspection of primary load-carrying members and for damage surveillance can be met by vibration monitoring.

2 VIBRATION MONITORING

Platforms in the sea vibrate continually under the action of wind and waves with some additional excitation from onboard activity. They are also lightly damped so that almost all of the energy is concentrated either at the wave frequency or at the natural or resonant frequencies of the structure. In an efficient structure, a member failure will cause a change in stiffness; it follows that such a change will affect the magnitude of the responses and, in the case of the responses at the natural frequencies, the frequencies will also be affected. In all cases, the more structurally important the member that has failed, the bigger will be the changes in response. It is to be noted that all of the quantities involved, such as wave input forces and response amplitudes, are stochastic, and the relationships between cause and effect can only be described in statistical terms.

The response to direct wave action occurs at a frequency determined by the wave period, so that the information to be gained is from the measurement of response amplitude relative to input wave excitation. The potential accuracy of such a comparison is limited because of the difficulties of measuring the response magnitude accurately, and even more so, the difficulty of describing the wave input forces.

However, the responses at the platform resonances are at frequencies governed by platform stiffness (including foundation stiffness) and mass. If a

shear member in a braced panel is severed at one end, the forces and deformations in other members are increased. This local loss of stiffness leads to reductions in some of the natural frequencies of the structure; these reductions can be measured. In most platforms, the first and second groups of natural frequencies are easily obtained from measurements made with only natural excitation. Failure of a particular member produces larger changes in some of these frequencies than in others, and the location of the failed member can be deduced approximately from the pattern of these changes. In some structures, the frequencies of the third mode group can also be obtained and provide further confirmation of a failure and increased confidence in its location. Changes in mode shapes also assist in failure location. More details of the effects of damage on natural frequencies are given elsewhere, (1,2,3) and the first three sway mode shapes for a typical steel platform are shown on Fig. 1.

Thus, in this instance, it is the natural frequencies which contain the information about structural integrity. The amplitudes give additional information about changes in the vibration mode shapes which assists the location of a stiffness change. In such lightly damped structures, the accuracy with which the frequencies can be measured is very high, so that considerable sensitivity can be achieved.

Based on these considerations, accurate techniques have now been developed for the measurement of structural vibration on steel platforms and for the deduction of vibration mode shapes and foundation characteristics. Offshore measurements made on 18 different structures have shown that on many steel platforms the changes in the natural frequencies caused by the failure of a single, structurally important member are large enough to be detected unambiguously.

Structures to which the method is less well suited include squat platforms with base dimensions comparable to height. In such platforms, it may not be possible to identify any more than the fundamental modes; this reduces the detection sensitivity. Also, platforms which have strong non-linearities due to pile/soil or pile/leg interactions may not be suitable. However, if the non-linearities develop at only relatively large amplitudes, the calibration and subsequent monitoring can be done during smaller amplitude vibrations.

3 PLATFORM BACK-UP INSPECTION

Under normal circumstances, vibration monitoring provides a back-up assurance

of the platform's ability to withstand major wave loading. In order that the assurance is given with the maximum possible degree of accuracy, it is necessary that the dynamics of the particular platform are completely understood and that a good base line for comparison is obtained. For the same reason, it is necessary to calculate the sensitivity of the platform to damage at various locations in order to provide a basis for identifying the damage from changes in the vibration spectra.

Thus the stages in implementing such a back-up inspection are as follows:

1. Computational (beam element) analysis of platform response.
2. Comprehensive measurements to establish the base line for future comparisons.
3. Analysis of measurements and 'tuning' of the computational model.
4. Use of tuned model to study effects of damage.

Any changes in platform strength will then be detected, and located approximately, by subsequent measurement and analysis.

The frequency of inspection visits depends on the degree of assurance required. To retain maximum accuracy of detection at least two measurements per year are required to update the base line records. Any significant changes in mass or known changes in support stiffness (due to scouring, for example) would be logged and included in an assessment of changes in natural frequencies. On platforms which have not settled to their final operating configuration (deck mass, number of conductors and risers etc.) it may be necessary to make more frequent measurements.

It is suggested that one of these sets of measurements (and the initial base line measurements) should be made at the end of a diving inspection period when information on the integrity of the platform is at a maximum.

4 PLATFORM DAMAGE MONITORING

When damage is known to have occurred to a platform, or when there has been an incident which might have caused damage, a more intensive inspection may be required to ensure that adequate strength is retained, and possibly to reduce any restrictions placed on operations by the certifying authorities.

If there has been sufficient damage to affect the vibration spectrum appreciably, or if the platform has not been previously calibrated, then a base line must be established as quickly as possible (by beam-element analysis and a measurement visit). Only when this has been done can further damage be identified.

Once a base line for monitoring has been obtained, the approach chosen depends on the conditions imposed by the certifying authority. If the monitoring is regarded simply as a more frequent periodic check on platform strength, than measurement/recording visits with on-shore processing of data is the cheapest method in the short-to-medium term. However, if a report on structural condition has to be made before the platform can be brought back into service, then on-board instrumentation is necessary so that the data can be processed in real time and assessments of integrity can be made on the spot.

There is portable equipment now available for performing this work, but as yet its use, and especially the interpretation of the results, is a highly skilled operation in which experience of platform vibration analysis is essential. Experience has shown that it should be possible to reach preliminary but fairly definite conclusions after 6 hours of measurement and analysis, but final confirmation would take about 72 hours. The approach is thus potentially capable of providing temporary clearance within 6 hours and full clearance within 72 hours, and would be used where the additional expense of on-board instrumentation was justified.

5 UNDERWATER INSPECTION FOR NODE WELD CRACKING

With vibration monitoring, severance of primary members can be detected from changes in the first few natural modes of a platform (Fig. 1) without the need for underwater measurements. For the detection of partial failures, such as cracking of node welds, it is necessary to use some of the higher modes in which the vibration is concentrated in small groups of members, or even in single members. Typical modes involving in-plane vibration of a K-braced frame are shown in Fig. 2. To identify the modes by cross-spectral analysis techniques, acceleration measurements must be made on all the members simultaneously.

When a crack penetrates the wall of one of the members, there will be an increase in mass and a reduction in natural frequencies from flow of water into the member. There will also be a loss of stiffness, but the effect on frequencies when the crack first penetrates the wall will generally be too small to be detected. The amount of water that enters, and its rate of entry, depend on the depth at which the member is located, its angle of inclination, and the position and size of the crack. A member at 100m depth will fill to about 90% of its volume without any escape or absorption of air, and a typical bracing member with

a crack 10mm long and 0.1mm wide will fill in a matter of weeks. The filling time will be less than the period between annual inspections even if the crack is open for only 10% of the time. By comparison, a similar horizontal member in 10m water depth may take in only 50% of its volume of water in several months, even if the crack is open all of the time.

The mode shapes before and after one of the inclined members of the K-frame is flooded are shown in Fig. 3, and a typical reduction in frequency is 5-10%. Such changes are large enough to be attributed positively to flooding of the inclined member and not to be confused with an increase in mass from other causes such as marine growth. There are similar changes in mode shape and frequency when the length of a through-thickness crack at the end of an inclined member exceeds about 50% of the circumference, and the changes due to flooding and cracking are cumulative.

This method of inspection is at an advanced stage of development; its main advantage is that, in a typical platform in 150m water depth, all the primary members can be inspected for coarse defects in 1-2 weeks. Thus it is feasible for all these members to be inspected annually instead of perhaps every four to five years by other, currently available inspection methods which can detect smaller defects. Inspection for small defects can be concentrated on those welds which have the highest expected stress levels, with the vibration method providing a check that gross cracking has not occurred unexpectedly elsewhere.

6 CONCRETE PLATFORMS

The discussion so far has related to steel platforms, but there is much debate about the inspection of concrete structures both as regards cost and effectiveness. What is certain is that the inspection procedures now available do not assess the platform strength directly; rather, strength is inferred from the lack of local damage.

Recent measurements made on a multileg platform have shown that many vibration modes associated with overall sway and with vibration of individual legs can be measured and identified by adapting the instrumentation developed for steel jackets. From the results it seems likely that such measurements can be used to monitor some aspects of foundation conditions and of the integrity of the legs and their attachment to the base. Further tests are planned to determine how stable the measurements are, and to assess their sensitivity to

structural change.

Other tests on a single tower type of concrete platform have shown that modes can be found which provide information about foundation stiffness, but which give little information about the integrity of the central structure. It may be possible, however, to use the vibration approach to check on the condition of the Jarlan wall, and work on this is planned for the near future.

The sensitivity and diagnostic power of vibration monitoring on concrete structures may always be less than on steel jackets. Nevertheless, other inspection techniques do not give a direct assessment of strength and this enhances the value of a method which does, however non-specific it may be. Future developments are likely to result in more information from the same measurements.

7 METHODS OF VIBRATION RESPONSE MEASUREMENT AND TYPICAL RESULTS

The methods of vibration response measurement for overall monitoring have been described elsewhere (4,5). Sets of orthogonal accelerometers are positioned at two levels of the platform; one near the top of the legs, and the other as close as possible to water level. Sets of accelerations are recorded simultaneously with inputs from wind and wave excitation; a typical acceleration/time record for a steel platform is shown in Fig. 4. Spectral analyses are then performed to give auto and cross-spectra; an autospectrum is shown in Fig. 5 and Fig. 6 shows a cross-spectrum from accelerometers at two levels of a platform. The way in which the phase angle between the two levels varies with frequency is shown in Fig. 6. In the first two groups of peaks (wave excitation and fundamental groups), the two levels are in phase; in the next group, they are out of phase. From information such as this, the relative motion of the two levels can be deduced and the natural modes of vibration identified. An acceleration autospectrum for a concrete platform is shown in Fig. 7.

The underwater measurements for node weld inspection are also made with accelerometers, attached temporarily to members with magnetic clamps; a typical autospectrum is shown in Fig. 8. There is sufficient excitation to give good spectra even under the relatively calm conditions necessary for diving.

8 FATIGUE LIFE PREDICTION

After nearly ten years of operations in the North Sea, fatigue is now acknowledged to be of major concern to platform operators, and strenuous efforts have been made to improve this aspect of design.

From the instrumentation programmes that have been carried out, and from a study of failures which have occurred so far, it appears that fatigue can be induced by

- (a) primary forces in members from response of the structure at the wave period and at its lower natural frequencies;
- (b) localised forces on members due, for example, to wave slam or vortex shedding and vibration at higher natural frequencies.

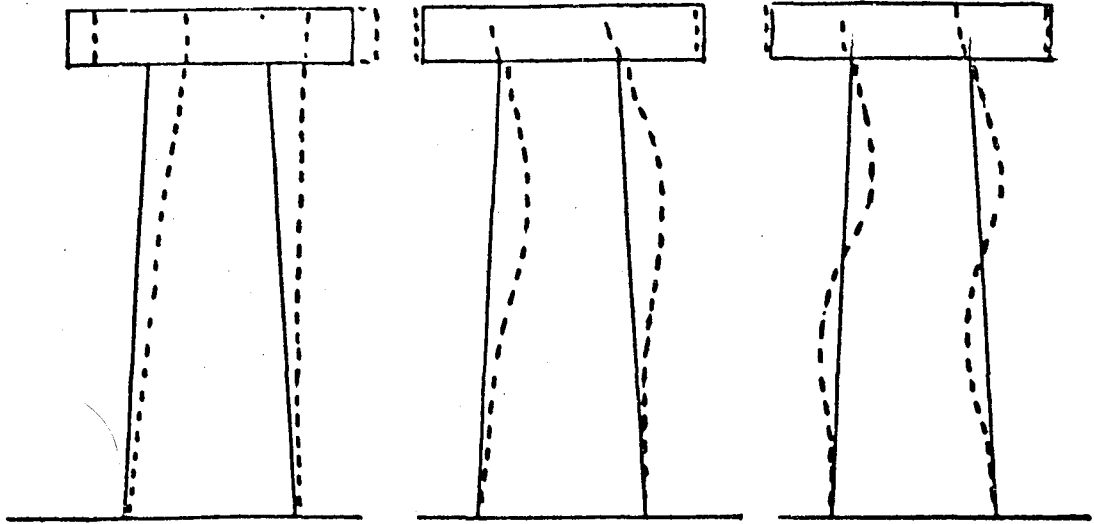
By suitable response analysis the primary forces in the members at the significant frequencies can be related to platform displacements. Thus a history of these displacements expressed in appropriate statistical terms will give a good indication of the stress history of a joint in any primary member, and allow an assessment to be made of the residual life of a platform. It should also lead to improved procedures for design against fatigue.

The information on platform displacements can be obtained from the measurements made in vibration monitoring, and a combined system for integrity monitoring and fatigue life assessment of primary members is feasible. Even though there is not yet agreement on a suitable model for initiation and propagation of fatigue cracks under random loading, the essential data on platform displacements can be collected and used with any improved model that may be developed in the future.

Platform displacements are not useful for monitoring fatigue due to wave slam or vortex shedding. Sensors on individual members or groups of members are necessary for this.

REFERENCES

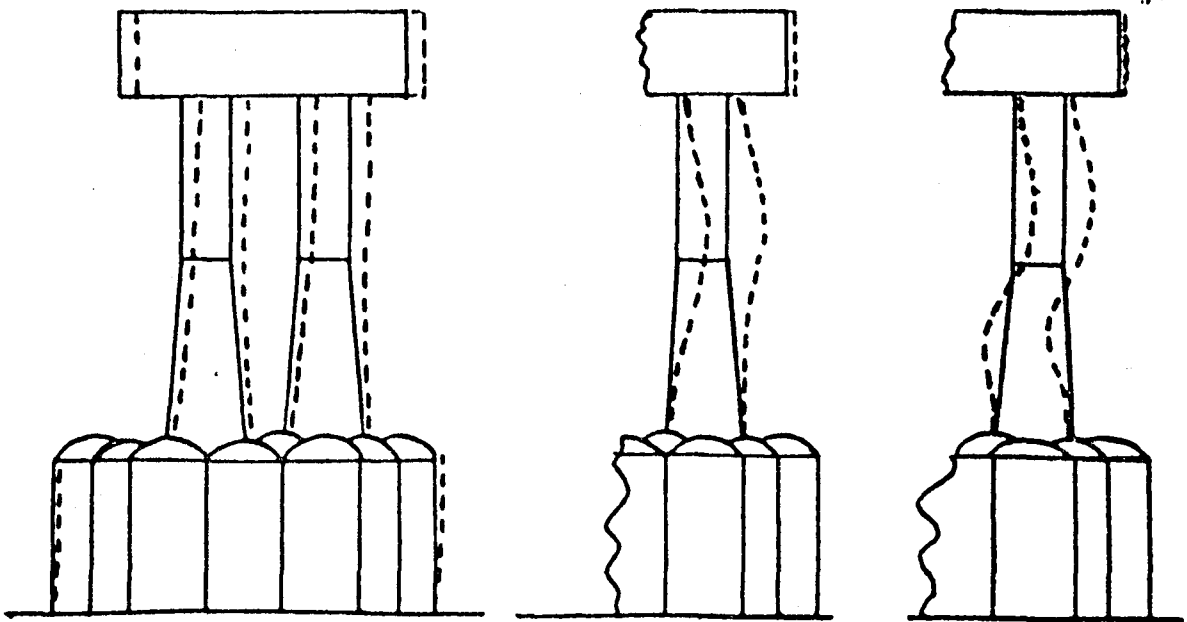
1. Loland, O. and Mackenzie, A.C. "On the natural frequencies of damaged offshore oil platforms" *Mechanics Research Comm.*, 1, 353-354, 1974.
2. Vandiver, J.K. "Detection of Structural failure on fixed platforms by measurement of the dynamic response". OTC 2267, 1975.
3. Loland, O., Mackenzie, A.C. and Begg, R.D. "Integrity monitoring of fixed steel offshore oil platforms". BSSM/RINA Conference, Edinburgh, Sept 1975.
4. Loland, O. and Dodds, C.J. "Experiences in developing and operating integrity monitoring systems in the North Sea". OTC 2551, 1976.
5. Begg, R.D., Mackenzie, A.C., Dodds, C.J. and Loland, O. "Structural integrity monitoring using digital processing of vibration signals". OTC 2549, 1976.
6. Begg, R.D. "Analysis for deep North Sea Installations". *Petroleum Engineer* 106 - 115, October 1977.
7. Begg, R.D. and Bendat, J.S. "Instrumentation and analysis techniques for the monitoring of offshore structures". *Petroleum Times*, October, 29,30, 1976.



1st Sway Mode

2nd Sway Mode

3rd Sway Mode



Overall Sway Mode

1st Independent Leg Mode

2nd Independent Leg Mode

FIGURE 1

OVERALL SWAY MODES FOR STEEL AND CONCRETE PLATFORMS

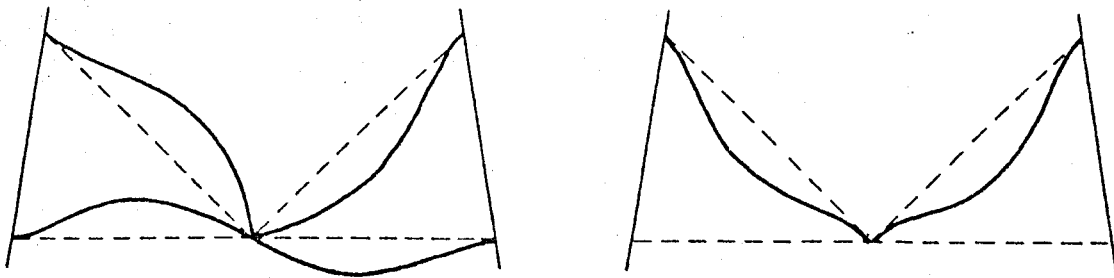


FIGURE 2. VIBRATION MODES OF A K-FRAME.

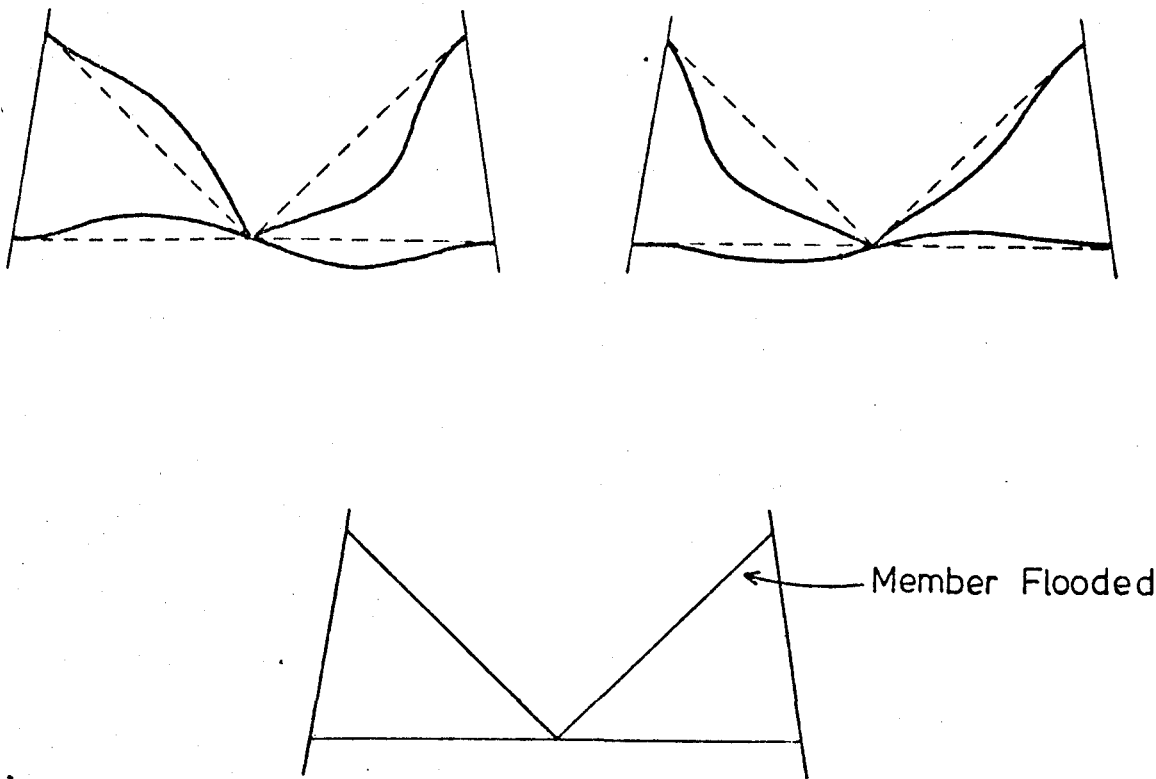


FIGURE 3. VIBRATION MODES OF A K-FRAME WITH FLOODED MEMBER.

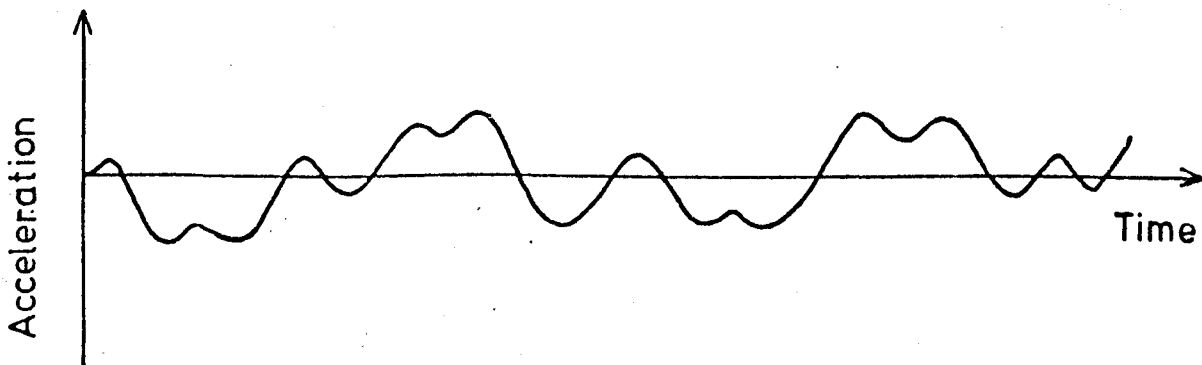


FIGURE 4. ACCELERATION-TIME RECORD.

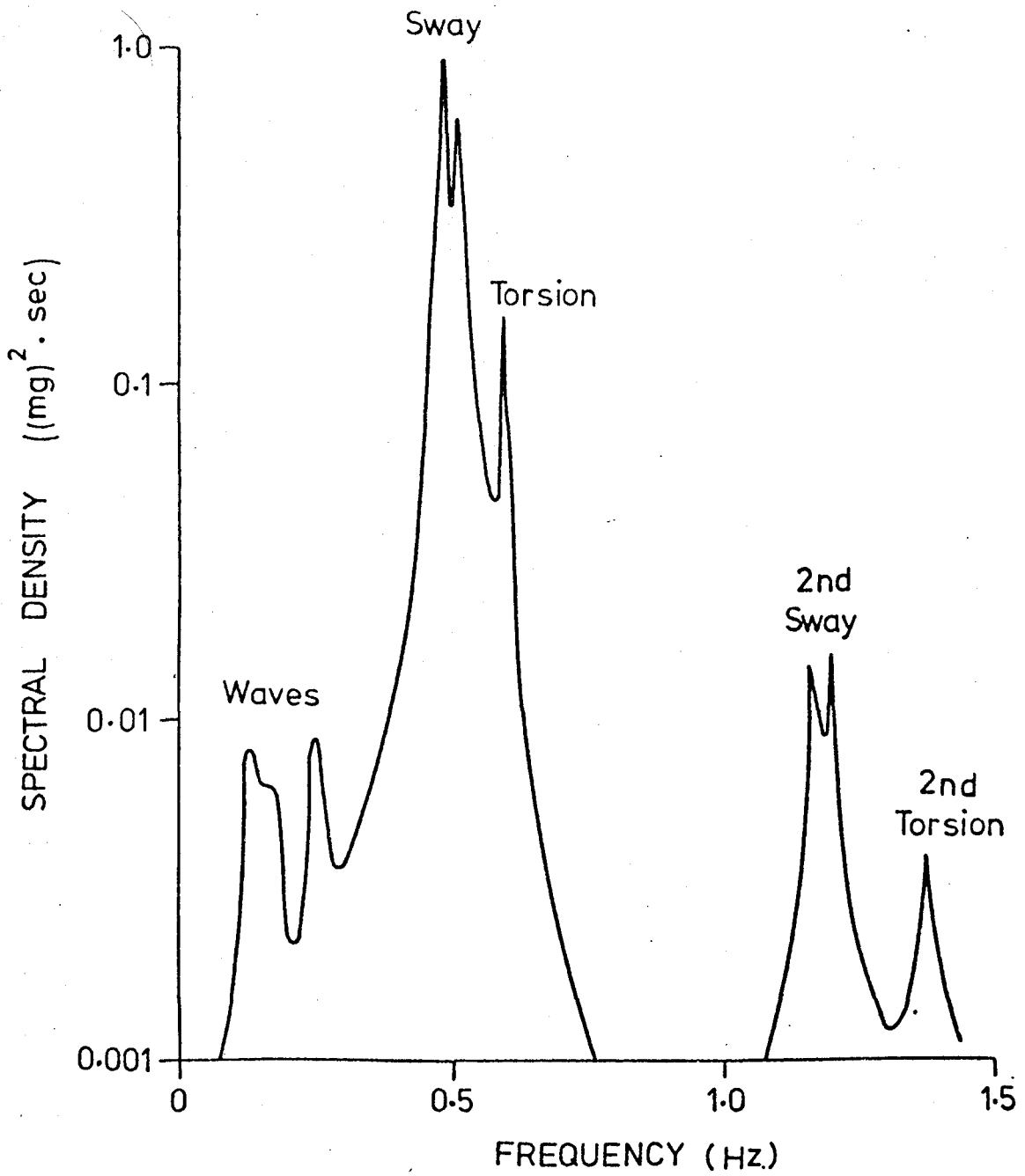


FIGURE 5. AUTO-SPECTRUM FROM DECK OF STEEL PLATFORM.

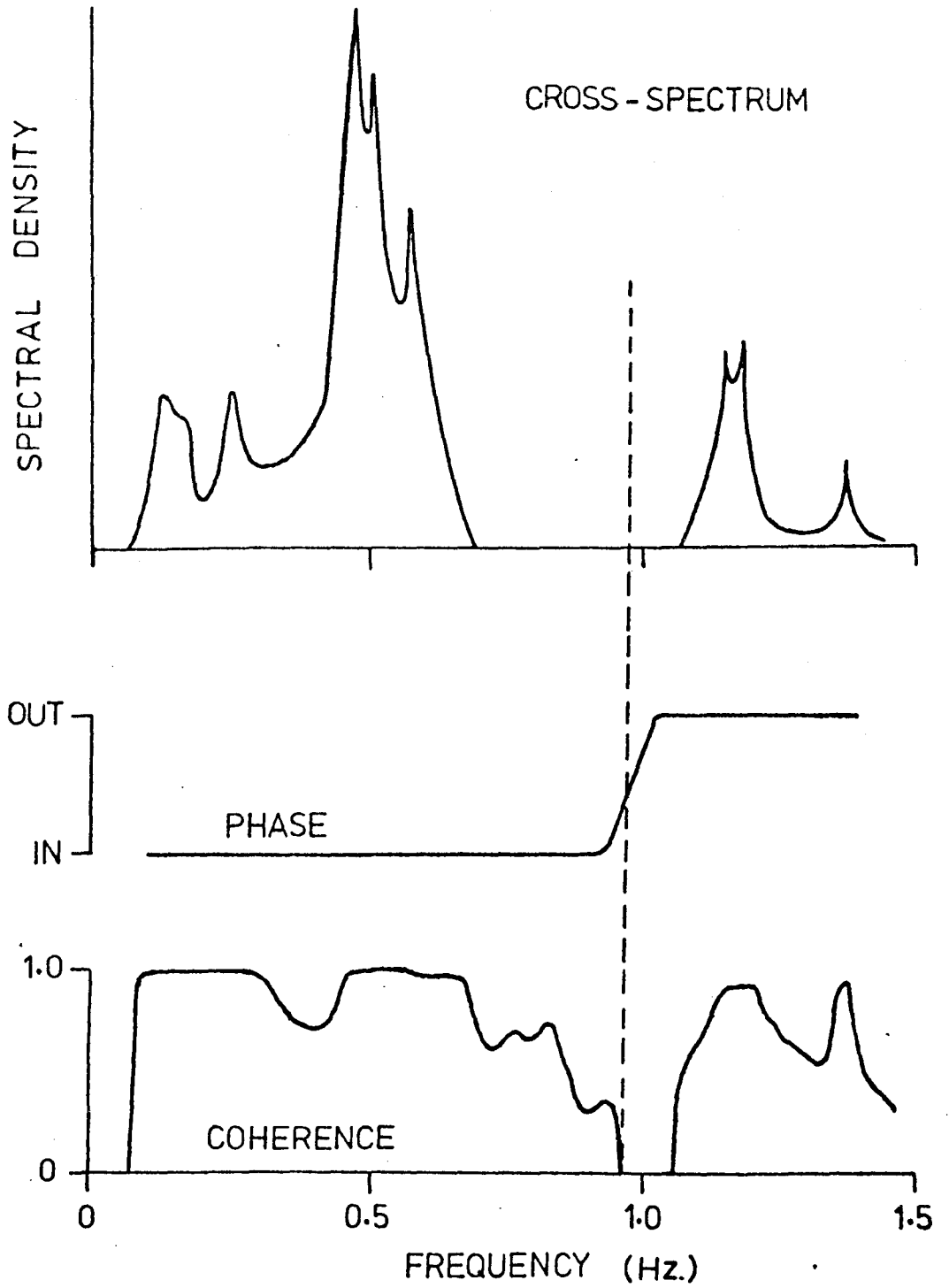


FIGURE 6. CROSS-SPECTRUM BETWEEN TWO LEVELS OF STEEL PLATFORM.

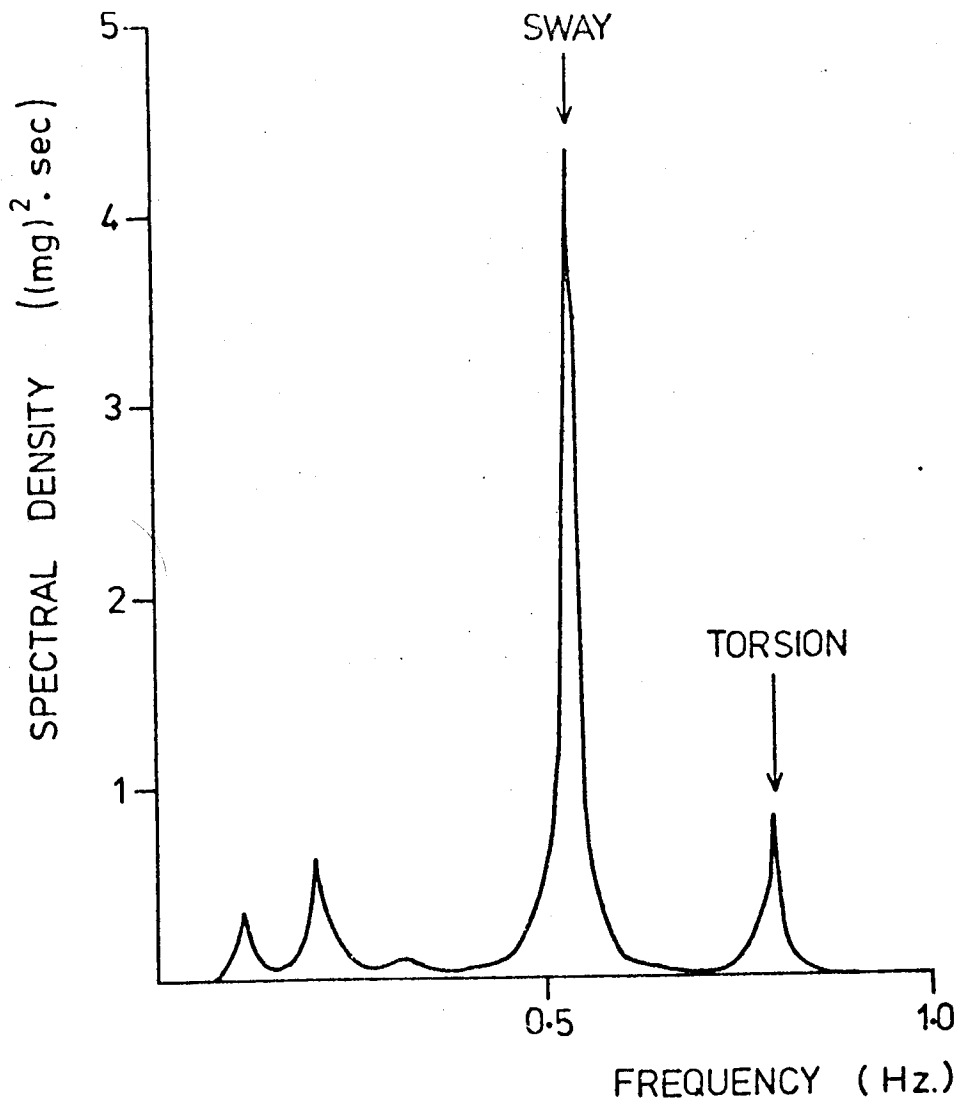


FIGURE 7. AUTO-SPECTRUM FROM CONCRETE PLATFORM.

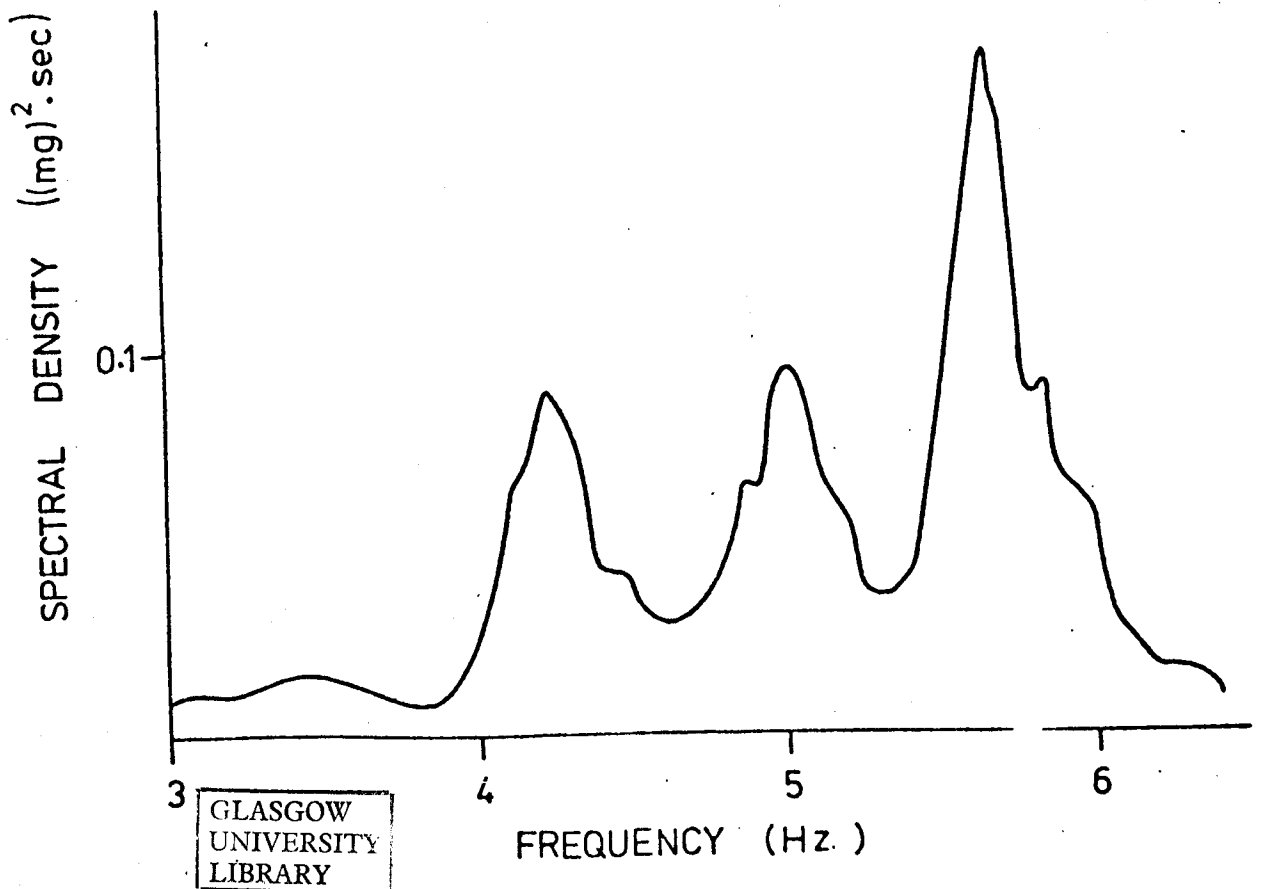


FIGURE 8. AUTO-SPECTRUM FROM UNDERWATER MEMBER OF STEEL PLATFORM.